Report to BSEE:

Deepwater Horizon Lessons Learned Studies: Detection of Oil Thickness and Emulsion Mixtures using Remote Sensing Platforms

(3 Phase Project)

Work Performed Under Contract
E16PG00023

Submitted by:
George Graettinger
NOAA, National Ocean Service
Office of Response and Restoration
7600 Sand Point Way NE
Seattle, WA 98115
(206) 526-4660
george.graettinger@noaa.gov

Submitted to:
Bureau of Safety and Environmental Enforcement (BSEE)
Oil Spill Response Research Branch
June 12, 2018

Open Ocean Oil Spill Response: Methods for Estimating Oil Slick Coverage

Submitted to:

National Oceanic and Atmospheric Administration
1305 East West Highway
Silver Spring, MD 20910
Attn: Lisa DiPinto

7600 Sand Point Way N
Seattle, WA 98115
Attn: George Graettinger

Submitted by:

Abt Associates
1881 Ninth Street, Suite 201
Boulder, CO 80302

Contacts:

Jamie Holmes
Jeff Morris
Heather Forth

This effort was funded in part by the U.S. Department of the Interior, Bureau of Safety and Environmental Enforcement, Oil Spill Preparedness Division through Interagency Agreement E16PG00023 with the U.S. Department of Commerce, National Oceanic and Atmospheric Administration.

December 6, 2018
14450

Contents

1. Introduction

The *Deepwater Horizon* (DWH) oil spill lasted 87 days, discharged millions of barrels of oil 40 miles offshore at a depth of 5,200 feet, and covered about 43,300 square miles in oil slicks (DWH Trustees, 2016). The spill presented oil spill responders and natural resource trustees with many new challenges, including how to quantify the amount of oil spilled, how and where to respond to the oil spill, and how to determine and quantify exposure and injury to natural resources.

As part of the Natural Resource Damage Assessment (NRDA), natural resource trustees quantified the amount and extent of oil using the best available data, primarily satellite-based remote sensing data, in the Programmatic Damage Assessment and Restoration Plan (PDARP; DWH Trustees, 2016). The "oil on water" group of remote sensing experts examining the DWH data identified notable data gaps and methodology needs that would have greatly helped the effort to quantify the DWH spill. In particular, they noted the desirability to collect data on the water, in the air, and from space, at approximately the same time (i.e., synoptic sampling). This would allow for the cross-comparison of data and ground-truthing to support the analyses of the remote sensing data.

After the settlement, the National Oceanic and Atmospheric Administration (NOAA) worked with Abt Associates (Abt) and others to verify the methods used to quantify oil in the PDARP, as well as to develop and improve methods for quantifying oil slicks in open ocean. This report summarizes much of the data from those efforts.

The research summarized in this report includes funding from multiple sources. The majority of the remote sensing verification work was funded by the U.S. Department of the Interior, the Bureau of Safety and Environmental Enforcement (BSEE), and the Oil Spill Preparedness Division through Interagency Agreement E16PG00023 with the U.S. Department of Commerce, NOAA. Additional funding came from NOAA to support the collection and analysis of supplemental data, including air quality, water quality, and subsurface oil sampling. The U.S. Environmental Protection Agency (EPA), the National Aeronautical and Space Administration (NASA) Jet Propulsion Laboratory (JPL), the University of North Texas (UNT), and the Woods Hole Oceanographic Institute (WHOI) collaborated on this research with separate funding or in-kind contributions.

1.1 Objectives

For oil spill responders and NRDA practitioners, the primary goals of oil slick data collection in the open ocean are:

- Quantification of the volume of oil discharged (for which Clean Water Act penalties may apply)
- Identification of "actionable" oil at the surface (i.e., oil of sufficient quantity that responders can feasibly collect, burn, disperse, or otherwise reduce the amount of oil in the oil slick)
- Estimation of the nature and extent of exposure of natural resources to petroleum, both at and below the ocean surface.

The primary objective of this research was to compare the ability of multiple remote sensing platforms to detect and quantify surface oil, and verify that anomalies identified in remote sensing images corresponded with oil slick features that could be observed and quantified on a boat. The specific objectives of the field and laboratory studies conducted as a part of this effort to verify DWH methods included:

- To what extent can remote sensing data from satellites, airplanes, and unmanned aircraft systems (UAS, or drones) detect and quantify oil on the ocean surface?
- To what extent can data collected from a boat help with the quantification of oil slicks and the verification of remote sensing data?
- To what extent can field data collection methods be improved if tested in a controlled laboratory environment?
- Can data be collected under the ocean surface that can quantify the extent of subsurface oil droplets and dissolved oil plumes?

The NOAA and Abt Team (the Team) addressed these questions using multiple methods. These included data collection methods development at the Oil and Hazardous Materials Simulated Environmental Test Tank (Ohmsett) at the National Oil Spill Response Research & Renewable Energy Test Facility in Leonardo, New Jersey. At Ohmsett, a known quantity of oil was placed into an outdoor water tank and subsequently emulsified using a wave generator to simulate the open ocean. The Team subsequently tested the accuracy and precision of oil slick measurement methods in a controlled laboratory experiment in St. Petersburg, Florida. In addition, the Team developed methods for synoptic collection of satellite imagery, airborne imagery, surface oil characterization, oil and water chemistry, and subsurface oil slick data at Mississippi Canyon lease block #20 (MC20), which has an ongoing chronic oil discharge.

As will be discussed in this report, we conclude that synoptic collection of remote sensing and surface data provides a wealth of useful information that can form the basis of oil spill response and natural resource exposure and injury decisions in future oil spills. However, because of the heterogeneity of oil slicks and the presence of subsurface oil droplets, any quantification of the volume of oil in an oil slick will have a substantial degree of uncertainty.

1.2 Timeline

This report summarizes data from multiple field sampling events as well as two controlled laboratory experiments. Specifically:

- July 14–23, 2016: Controlled experiments in the outdoor tank at Ohmsett in Leonardo, New Jersey
- November 15–17, 2016: Field data collection at MC20
- February 27–March 3, 2017: Controlled laboratory experiments at the University of South Florida (USF), St. Petersburg, Florida
- April 25–26, 2017: Field data collection at MC20
- August 15–17, 2017: Field data collection at MC20.

1.3 Team

The Team included multiple researchers from Abt and from NOAA, as well as researchers from Ocean Imaging Corp. (Ocean Imaging), Water Mapping LLC (Water Mapping), UNT, EPA, WHOI, and others. Researchers from Fototerra Aerial Survey LLC (Fototerra) collected remote sensing data concurrently with the Team.

1.3.1 NOAA Team Members

Numerous individuals from NOAA's Ocean Service, Office of Response and Restoration (ORR) led and participated in all phases of these studies:

- Mr. George Graettinger, a senior environmental scientist in the Assessment and Restoration Division (ARD), Spatial Data Branch of ORR and co-lead of the Gulf of Mexico Environmental Response Management Application (ERMA), NOAA's Common Operational Picture (COP), participated in all aspects of the studies and served as the project Principle Investigator
- Dr. Lisa DiPinto, senior scientist at ORR, participated in all aspects of the studies and served as a team leader
- Dr. Daniel Hahn, a natural resources specialist from the Southeast Branch of ARD in St. Petersburg, Florida, participated in all field activities as well as the laboratory data collection in St. Petersburg
- Dr. Kevin Kirsch, the ARD Southeast Branch Chief, participated in field data collection activities
- Mr. Jeff Lankford, a physical scientist in ORR's Environmental Response Division (ERD), collected observational data and photographs from an airplane above the oil slick
- Mr. Steven Wall, a commissioned officer (NOAA CORPS) in ERD, also collected observational data and photographs from an airplane above the oil slick
- Mr. Adam Davis, an ERD Scientific Support Coordinator from Mobile, Alabama, participated in field activities.

1.3.2 Abt Team Members

Abt led many of the studies and had several staff members who participated in this research effort:

- Dr. Heather Forth led the controlled studies at Ohmsett and the USF laboratory, and she served as the Field Team Leader (FTL) for the November 2016 field work at MC20. She was the lead author of the sampling and analysis plans (SAPs) and health and safety plans (HSPs); and led much of the logistical planning, data management, and analysis.
- Dr. Jeff Morris served as FTL for the April 2017 and August 2017 MC20 field work. He was co-lead of the SAP and HSP development, and led the logistical planning for the 2017

trips. In addition, Dr. Morris assisted with data management and analysis, and designed and managed the toxicology work at UNT.

- Mr. Jamie Holmes served as an overall project manager. In addition, he coordinated remote sensing data collection, and led the data services and dissemination effort onboard the boat in April 2017.
- Dr. Michelle Krasnec assisted with SAP and HSP development and logistical planning.
- Mr. Andrew McFadden also assisted with SAP and HSP development and logistical planning, and led much of the data management and analysis work.

1.3.3 Other Abt Team Members

The research team also included:

- Water Mapping: Dr. Oscar Garcia helped with the overall project design, collected and analyzed remote sensing from UAS, and led the analysis of synthetic aperture radar (SAR) data. In addition, Dr. Garcia developed new methods of collecting oil slicks in the field and precisely measuring the thickness of those slicks. Dr. Garcia's team included Ms. Diana Garcia, who assisted with the data analysis.
- Ocean Imaging: Mr. Mark Hess collected and analyzed visible and thermal infrared data from a helicopter at Ohmsett and a fixed-wing aircraft over MC20, using Ocean Imaging's proprietary sensor. In addition, Mr. Hess worked with the Marine Spill Response Corporation (MSRC) to develop and field-test a communications system that allowed direct data transmission from an airplane to a boat in the open ocean. Mr. Hess' team at Ocean Imaging included Dr. Jan Svejkovsky, Mr. James White, and Ms. Jennifer McCall.
- UNT: Dr. Aaron Roberts designed a light attenuation measurement method and conducted laboratory toxicity tests using MC20 oil-contaminated water. Dr. Kristin Bridges provided assistance with field work and logistics at MC20, and also conducted the laboratory toxicity tests.
- On Wings of Care: Ms. Bonnie Schumaker piloted a Cessna 182 over MC20 and provided oil-spotting services.

1.3.4 Other Team Members

Several researchers participated in these data collection and analysis efforts with funding sources that were not part of BSEE's interagency agreement with NOAA. These other researchers and organizations included:

- EPA: Dr. Robyn Conmy collected fluorometry and water chemistry data, as well as collaborated on study design and data analysis
- WHOI: Ms. Amy Kukulya piloted an autonomous underwater vehicle (AUV) at MC20 (WHOI received logistics and travel support from NOAA and EPA and provided in-kind contributions for the research)

- NASA JPL: Drs. Ben Holt and Cathleen Jones collected remote sensing data using their proprietary sensor during the November 2016 field effort at MC20.
- Fototerra: Mr. Alessandro Vagata led Fototerra's remote sensing data collection at Ohmsett and MC20.

1.4 Report Organization

The remainder of this report provides the details of these studies. Chapter 2 presents the laboratory, Ohmsett tank, and MC20 field methods. Chapter 3 summarizes the results; and Chapter 4 presents a summary and conclusions, including recommendations for additional studies.

2. Methods

This chapter first introduces the NOAA and Abt Team that conducted the field and laboratory studies. It then presents an overview of the methodologies that were developed and tested. More detailed SAPs, HSPs, and standard operating procedures (SOPs) are included as attachments.

In this chapter, we briefly summarize activities at Ohmsett (Section 2.1) and USF (Section 2.2). The remainder of the chapter discusses in more detail the methods developed and used in the field at MC20.

2.1 Ohmsett

In July 2016, we conducted a simulated oil spill in a controlled environment to develop methods for oil slick detection and characterization. This included synoptic collection of remote sensing data (from satellite, helicopter, fixed wing aircraft, and UAS), oil slick samples, and underlying oil-contaminated water.

We conducted these tests in an open-air tank at the Ohmsett in Leonardo, New Jersey. Ohmsett has an oil slick testing tank that is 203 meters long by 20 meters wide by 2.4 meters deep, holding 9.8 million liters (2.6 million gallons) of saltwater.

On July 14, 2016, the Ohmsett team added 1,500 liters (400 gallons) of fresh Hoover Offshore Oil Pipeline System (HOOPS) oil to the tank. For four days, the oil weathered on the surface of the tank. On the morning of July 18, the Ohmsett team activated wave generators. The resulting waves mixed the surface slick into the water column and created oil-water emulsions at the surface.

The Abt and NOAA Team collected in situ surface oil thickness data and water column samples starting on July 16, 2016 before the wave generators were turned on, and we continued collecting these data through July 22, 2016. Ocean Imaging synoptically collected visible and thermal infrared (IR) data from a helicopter. Fototerra collected data using their sensor suite, including sensors mounted on the bridge over the slick, and sensors mounted on a fixed wing aircraft that they flew overhead. Dr. Garcia of Water Mapping collected visible thermal IR data from a UAS, and also collected slick thickness data from an early prototype of a remote sample collector.

Additional information is provided in subsequent sections.

Details of the Ohmsett research are summarized in Attachments A through D.

2.2 USF

From February 27 to March 3, 2017, personnel from Abt, NOAA, and Water Mapping conducted laboratory studies at USF to test three methods of surface slick thickness measurement. We prepared oil slicks of known volumes that could be reasonably replicated, with the oil spread across a small measurement area. This allowed us to replicate slicks with a known average thickness. We then used three different methods to measure that thickness, allowing us to determine the accuracy and precision of each measurement method.

The three different slick thickness measurement methods that we tested in this laboratory study included (1) the sorbent pad method, (2) the dip plate method, and (3) the Water Mapping Sampler method. We report method performance parameters for these three methods using different oil types across a range of thicknesses.

Details on methods used in the USF laboratory experiments are included in Attachment E.

2.3 Remote Sensing

The primary objective of synoptic sampling is to provide data and observations on the ground that can verify (ground-truth) remote sensing data. For this research at MC20, we attempted to collect as much remote sensing data as was practicable. We scheduled field sampling events to occur when satellites were collecting data. We also collected remote sensing data from a UAS and as many as four separate fixed-wing aircraft.

Abt and NOAA coordinated the UAS flights as well as the oblique aerial imagery from On Wings of Care and the Ocean Imaging data collection. Separately, NASA collected remote sensing data during the November 2016 field sampling at MC20, and Fototerra collected remote sensing data at each of the field sampling events.

This section provides an overview of methods for the remote sensing data collection. More details on the Ocean Imaging and Water Mapping data collected at MC20 are included in Attachments F and G, respectively. NASA and Fototerra were not part of the NOAA/Abt Team and did not produce reports under our direction. Therefore, their methods are only briefly summarized. Additional details of the Fototerra missions to MC20 in November 2016, April 2017, and August 2017 are provided in Attachments H through J, respectively.

2.3.1 Aerial Imagery: Digital Camera from Cessna

For each of the field sampling efforts at MC20, the On Wings of Care Cessna 182 flew over the sampling site while the boat and crew were preparing to sample. Oil spotters from NOAA ORR Emergency Response Division (ERD; Mr. Lankford and/or Mr. Wall) were on the plane with Ms. Schumacher, collecting oblique aerial imagery with a high-resolution digital camera. The boat captain and sampling crew had direct communications with the Cessna via handheld aviation radio. The flight crew ensured that the boat was positioned over the most heavily oiled areas, allowing the boat crew to sample a range of oil thicknesses. In addition, the flight crew provided an overview of the spatial extent and morphology of the slick.

2.3.2 UAS

For the UAS (drone) data collection at Ohmsett and MC20, Dr. Garcia flew multiple DJI drones, including the S1000, Inspire, and Phantom-4 Pro models. Drones collecting visible imagery were fitted with a high definition (HD) video camera with Lightbridge data communications, providing a live video feed to the operator (Figure 2.1). Drones collecting thermal IR imagery were fitted with a FLIR camera.

Figure 2.1. Dr. Garcia observing the HD video from the overhead drone, on a monitor mounted in the wheel house of the boat.

The real-time UAS video was used to observe the oil slick from above and position the boat over the target oil slick (Figure 2.1). In addition, the camera collected still imagery at regular intervals, with time, elevation, aspect, angle off nadir, and other data saved with the image file.

At Ohmsett, Dr. Garcia collected visible and thermal IR imagery simultaneously using the DJI S1000 octocopter (Figure 2.2), which has a payload sufficient for carrying both the HD and the FLIR cameras. In post-processing, he could correct for the angle off nadir and stitch multiple images collected on a flight line to create a high-resolution orthomosaic of the entire tank.

Figure 2.2. DJI S1000 drone over Ohmsett.

Photo source: George Graettinger, NOAA.

The FLIR provides 8-bit uncalibrated emissivity, with 256 shades where dark is cool and bright is warm. These data show changes in emissivity with increasing oil thickness. When post-processing the data, Dr. Garcia overlaid the visible and IR images and classified approximate thickness categories of the oil in the tank. Examples of these data are included in Chapter 3.

Additional details of the Ohmsett data collection methods and analysis are provided in Attachment B.

2.3.3 TRACS

Ocean Imaging collected aerial multispectral and thermal IR imagery using their Tactical Response Airborne Classification System (TRACS) at Ohmsett and MC20. At Ohmsett, TRACS was mounted to a Robinson R44 helicopter, allowing for multiple passes at different altitudes over the tank (Figure 2.3). At MC20, TRACS was mounted to a fixed-wing aircraft (Piper PA-23 Aztec or King Air, as described below).

Figure 2.3. TRACS sensors mounted to a vertical pole on a Robinson R44 helicopter.

Source: Ocean Imaging (see Attachment C).

Ohmsett

The Ohmsett testing allowed Ocean Imaging to build a spectral library of oil thicknesses and emulsions in the visible and thermal IR data. To build the library, the TRACS data were first converted from their native format to GeoTIFF format for compatibility with ESRI's ArcGIS software and other geographic information system (GIS) applications. Select scenes were then projected to a geographic WGS-1984 coordinate system and georeferenced to an ESRI base layer. Ocean Imaging then compared the remote sensing data to data collected in the tank, including oil thickness, water:oil ratio, tank water temperature, oil and water spectroscopy, and photographs. Ocean Imaging ultimately classified oil thicknesses and emulsions based primarily on the red and thermal IR bands.

Details of Ocean Imaging's data collection and processing at Ohmsett are included in Attachment C.

MC20

Ocean Imaging collected TRACS data at MC20 in November 2016 and April 2017. In November 2016, TRACS was mounted to a Piper PA-23. Visible multispectral and thermal IR data were collected at altitudes of 1,000 and 6,000 feet. The Piper pilot communicated with the Cessna (On Wings of Care) and the boat crew when flying the flight lines. Each flight was coordinated with a satellite data collection, allowing for comparison of satellite, airborne, and ground-based data.

In April 2016, Ocean Imaging and MSRC collaborated to test a newly developed direct airplane to boat data communications (see Section 2.5). They shared the cost of renting a King Air, which is substantially larger than the Piper PA-23. Ocean Imaging and MSRC coordinated

flight times to ensure synoptic data collection with satellite and ground-based data collection. TRACS visible and thermal IR data were again collected at altitudes of 1,000 and 6,000 feet.

Ocean Imaging produced two separate data products from the MC20 data. In both November and April, Ocean Imaging personnel created mosaics of visible and IR imagery that were provided to the NOAA COP (ERMA) within four hours of the completion of the flight. Later, after the satellite data were available and ground-based data on oil thickness and emulsions were provided, Ocean Imaging classified the data into bins of average oil thickness/emulsions. In addition, during the April 2017 field effort, Ocean Imaging provided draft visible and thermal IR mosaics to researchers on the boat approximately 15 minutes after the data were collected, while the plane and the boat were both positioned over the oil (see Section 2.5).

Details of Ocean Imaging's data collection and processing at MC20 are included in Attachment F.

2.3.4 Fototerra Poseidon

Fototerra collected airborne remote sensing data at Ohmsett and at all three field efforts at MC20. As mentioned previously, Fototerra was not part of the NOAA-led team; the information included herein is summarized from preliminary reports produced after the Ohmsett research (Fototerra, 2016a) and after MC20 activities in November 2016 (Fototerra, 2016b), April 2017 (Fototerra, 2017a) and August 2017 (Fototerra, 2017b). The Fototerra reports are included as Attachment D and Attachments H through J.

Fototerra collected aerial remote sensing data from a dedicated fixed-wing Embraer EMB-110 aircraft. Fototerra's Poseidon Platform is equipped with a Multispectral Environmental Data Unit for Surveillance Applications (MEDUSA) system originally developed in Europe in 2006 (Robbe and Hengstermann, 2006). MEDUSA includes a Laser Fluorosensor (LFS), a Microwave Radiometer (MWR), as well as ultraviolet (UV), visible, IR, and bi-spectral ultraviolet/infrared (UV/IR) sensors.

At Ohmsett, Fototerra mounted the LFS and MWR on the bridge over the tank, and they mounted the other sensors on the plane (Fototerra, 2016a). For the MC20 flights, Fototerra mounted the LFS and MWR sensors on the plane, and they included an Electro-Optical Infrared (EO/IR) sensor and Side-Looking Airborne Radar (SLAR).

Fototerra flew flight lines over MC20 at altitudes ranging from 1,000 to 3,500 feet, collecting data from the suite of sensors.

2.3.5 UAVSAR

Staff at the NASA JPL have developed the Uninhibited Aerial Vehicle Synthetic Aperture Radar (UAVSAR) platform for identifying oil slicks from a high-altitude fixed wing aircraft. UAVSAR data were collected at MC20 on November 15 and 17, 2016. They collected data at an altitude of approximately 40,000 feet. As mentioned previously, the NASA JPL was not part of the NOAA-led team. JPL did not provide a report for the November 2016 flights.

The methods that JPL has developed for detecting and quantifying oil with UAVSAR have been published (Minchew et al. 2012, Jones & Holt, 2018). Those methods were used to analyze the UAVSAR data to obtain relative thickness classification of oil within the slick.

2.3.6 SAR

SAR is well-established as a platform for identifying the presence/absence of oil slicks (e.g., Garcia-Pineda et al., 2009; Leifer et al., 2012) and emulsified oil (Garcia-Pineda et al., 2014). Oil dampens capillary waves on the ocean surface, affecting the return of the microwaves sent from the sensor. This occurs even when the slick thickness is less than 1 µm. Some of the drawbacks of SAR include the lack of resolution, the lack of ability to differentiate slick thickness, and the lag time between image acquisition and image use for oil spill responders.

Mr. Gordon Staples of McDonald Dettwiler & Associates (MDA) in Vancouver, British Columbia, collaborated on this research and provided SAR imagery of Ohmsett and MC20 from MDA's RADARSAT-2 satellite. With a known target over a small area, MDA collected higher resolution quad-pole imagery. For the April 2017 sampling event, MDA tested a rapid-turnaround data service (see Section 2.5).

Water Mapping post-processed the SAR imagery using two semi-supervised classification methods. The overall slick extent was determined using the Textural Classifying Neural Network Algorithm (TCNNA; Garcia-Pineda et al., 2009), and areas of large oil emulsion (when present) were classified using the Oil Emulsion Detection Algorithm (OEDA; Garcia-Pineda et al., 2014).

2.3.7 Other Satellite Imagery

The NOAA National Environmental Satellite, Data, and Information Service (NESDIS) provided additional satellite imagery when available. These included DigitalGlobe Worldview 2 (WV-2) and WV-3, Aster, and Landsat data. No new analysis methods for these visible and near-IR data were developed for this research. Both Ocean Imaging and Water Mapping used the supplemental satellite imagery to help identify and classify oil slicks in their data.

2.4 Field Data Collection

Field data collections at MC20 included site characterization, oil sheen/slick thickness measurements, bulk oil sample collection, targeted discrete water sampling based on real-time fluorescence measurements, fluorescence monitoring, air monitoring, and UV and visible light attenuation measurements. Table 2.1 provides a summary of the total number of samples collected during the MC20 field work. The following sections provide an overview of the data collection methods.

Table 2.1. Number of samples collected during each MC20 sampling trip

Sample type	November 2016	April 2017	August 2017
Slick thickness by dip plate	48	25	8
Slick thickness by sorbent pad	30	16	18
Slick thickness by Water Mapping sampler	14	11	7
Water samples	20	14	24
Bulk oil samples	2	1	0
Air samples	18	0	0

We produced separate SAPs for each of the three MC20 trips summarized in this report (Attachments K through M). These SAPs provide detailed methods and SOPs for the MC20 field work.

2.4.1 Slick Thickness Characterization

We utilized three separate methods for characterizing slick thickness from a vessel: the dip plate method, the sorbent pad method, and the Water Mapping method.

Dip Plate Method

Svejkovsky and Muskat (2006) described the dip plate method of estimating oil thickness, where the slick thickness is measured using Plexiglass plates that are slowly lowered vertically through an oil slick, and the surrounding oil slick collects onto the plate (Figure 2.4). The slick thickness is then estimated by dividing the volume of oil collected on the dip plate by the surface area sampled.

Figure 2.4. Dip plate deployment at MC20.

Source: George Graettinger, NOAA.

Svejkovsky and Muskat (2006) indicated that the plates collect slick oil both as they are lowered into the water and being raised, and thus the surface area sampled is equal to four times the plate surface area (where the surface area is the plate width times the depth to which the plate was lowered, and oil adheres to both sides of the plate as it is lowered and raised).

Svejkovsky and Muskat (2006) determined oil volume on the plate by collecting the oil off the plate and transferring it to a graduated cylinder. To improve method sensitivity as well as decrease sample processing time, we modified the method at Ohmsett by measuring the weight of the oil collected and converting it to a volume using the oil density. For our modified method, we pre-weighed each dip plate in individual resealable plastic bags, and then reweighed the plate and its respective plastic bag following the sample collection, to determine the weight of the oil sampled. For the first field sampling trip, we used 10-cm-wide dip plates and dipped them to a depth of 15 cm (5.9 in; Figure 2.4). For the following two sampling trips, we used the same 10-cm-wide dip plates, but we submersed them fully (plates were 23-cm long) to reduce variability in the dipped depth.

Sorbent Pad Method

Daling and Leirvik (2002) described a method for measuring the slick thickness of floating oils using 3M T-151 sorbent pads (Figure 2.5). For this method, a sorbent pad of known size is placed onto the surface of the water, absorbing the floating oil from the area beneath the pad.

The pad is then chemically analyzed for total petroleum hydrocarbons (TPHs) or another set of oil constituents to determine the mass of oil collected by the pad. The oil mass is then converted to oil volume using the bulk oil density and the TPH concentration (or other oil constituents).

Figure 2.5. Sorbent pad deployment at MC20.

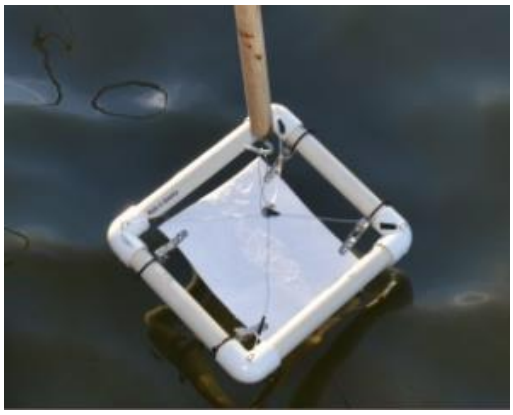

Source: George Graettinger, NOAA.

The thickness is then determined by dividing the oil volume by the area of the sorbent pad.

For our field studies, we used sorbent pads cut into 21.5 cm x 24 cm (8.5 in x 9.5 in) squares. We then rinsed the pads with methylene chloride, and let dry overnight in a fume hood to remove potential background contaminants from the pads. We deployed each pad onto the water using a plastic frame (Figure 2.5). While our aim was to deploy the sorbent pad sample for 30 seconds to permit adsorption of oil onto the pad, the drift of the boat often limited our deployment time to only a few seconds. We sent all of the sorbent pad samples to ALS Environmental (Kelso, Washington) for TPH analysis using EPA Method 8015.

Water Mapping Oil Sampler

Dr. Oscar Garcia of Water Mapping developed a new method of measuring oil thickness, which we call the Water Mapping sampler (Figure 2.6). In general, this sampler deploys a cylindrical plastic collection tube into the water so that the tube intersects the water surface. The sample tube is plugged to retain the slick oil captured within the tube. After the tube sits vertical for several hours to ensure that all the oil in the tube floats to the water surface, the thickness of the layer of oil in the tube is measured with a HD photograph. Using a calibration curve (discussed in Chapter 3), we relate the thickness of the oil layer in the sample tube to the slick thickness on the water.

Figure 2.6. Water Mapping sampler in August 2017 (patent pending).

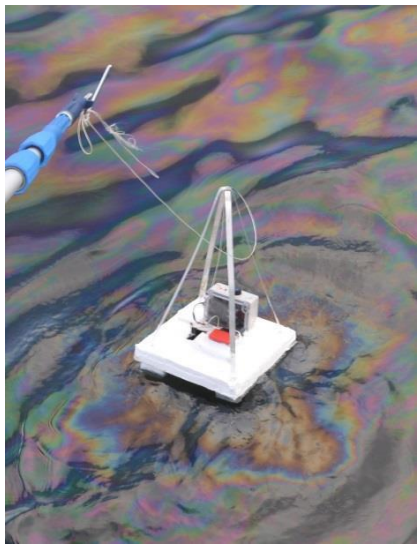

Source: George Graettinger, NOAA.

Dr. Garcia has made modifications to the sampler throughout the project. His modifications include deploying the tube vertically instead of horizontally to reduce loss of oil on the sides, changing the mechanism for plugging the tube, and altering the sampler structure to modify how it sits on the water surface. The most recent iteration of the Water Mapping sampler (Figure 2.6), from August 2017, has a patent pending.

2.4.2 Water Sampling

We collected water samples from multiple depths concurrently using a 4-line sampler with high-purity tubing and a peristaltic pump. For the first and second sampling trip (November 2016 and April 2017, respectively), we collected the samples by simply suspending the sample tubing off the side of the boat. The tubing was attached to a boom to ensure that samples were collected away from the boat. We modified the design for the third sampling trip (August 2017), attaching the sample tubing to an anchored cord that was attached to a floating buoy. This eliminated variability in the sample depth caused by boat movement and allowed the samples to be collected from a constant depth relative to the water surface. At each sampling depth, we collected a 250- mL whole water sample. We analyzed all water samples for TPH and a subset of samples for polycyclic aromatic hydrocarbons (PAHs).

To help interpret the water column results, we also collected wind intensity data using a handheld anemometer. In addition, we downloaded meteorological data, including wind speed and direction, collected by nearby buoys from NOAA's National Data Buoy Center (www.ndbc.noaa.gov/).

2.4.3 Oil Sampling

We collected bulk oil from the water surface using Plexiglas dip plates, scraping the slick oil collected on the dip plates into a sampling jar. The collection of bulk oil required the presence of thicker slicks, and thus we did not collect bulk oil during the August 2017 trip where the oil slicks were generally less than 50 µm (see Chapter 3). We sent all bulk oil samples to ALS Environmental in Kelso, Washington, for TPH and PAH analyses. After chemical analysis, we sent any remaining bulk oil to Triton Analytics in Houston, Texas, to determine water content and density.

During the August 2017 trip, we tested a hydrophilic oil scooper cloth that Dr. Myoung-Woon Moon (Korea Institute of Science and Technology, Seoul, Korea) designed to scoop oil off the water surface. We stitched the cloth samples onto a plastic frame to make a net that we attached to an extendable pole. We attempted to collect bulk oil samples using this net during the August 2017 trip but the lack of thicker oil precluded any meaningful collection. When we attempted to collect thin sheen oil using the net, the oil appeared to stick to the cloth but no liquid phase oil could be recovered for analysis.

2.4.4 REMUS 100 AUV

In August 2017, Ms. Kukulya (WHOI) brought a specially equipped AUV, the Remote Environmental Monitoring Units (REMUS) 100, to measure subsurface fluorescence and basic water quality conditions, and to collect subsurface images. Prior to that sampling trip, Ms. Kukulya and Dr. Conmy conducted controlled fluorometry calibration experiments at WHOI using the REMUS 100's fluorometry sensor and water accommodated fractions of oil generated using naturally weathered oil (Slick A; Forth et al., 2017a) collected from the surface during the DWH spill.

During the August 2017 field work, Ms. Kukulya deployed the REMUS 100 on several separate missions, at depths ranging from the surface to 100 meters below the surface. The REMUS collected data in grid patterns primarily under the oil slick. Dr. Conmy and her researchers at EPA conducted preliminary analyses of the data (see Chapter 3).

2.4.5 Cyclops Fluorometry

On the November 2016 and April 2017 sampling trips, we used a Turner Designs Cyclops fluorimeter to detect and quantify oil concentrations in the water column by fluorescence. During the water sampling events, we collected fluorescence measurements at each subsurface water sampling location and depth to relate the fluorescence signal to measured TPH concentrations. In addition, we conducted continuous fluorescence profiles to determine changes in oil concentrations with depth under an oil slick. We also conducted fluorescence transects, measuring fluorescence at a fixed depth (typically 1 m) as the boat drifted into and out of floating oil slicks.

2.4.6 UV and Visible Light Penetration

During the April 2017 MC20 trip, we used a Biospherical radiometer contained in a specially designed protective housing with a transparent plastic lid to measure subsurface light intensity. The radiometer collected several wavelengths of UV light (305, 313, 320, 340, 380, and 395 nm) as well as light within the spectrum of Photosynthetically Active Radiation (PAR) or visible light (400–700 nm). We collected one depth profile down to 3 m in a reference area outside the area containing visible surface oil to determine UV light attenuation. We also measured a transect with the radiometer at a fixed depth of about 1 m (attached to the side of the boat) and drifted from outside the slick back into the slick, taking measurements every 0.2 seconds.

During the August 2017 MC20 trip, we measured a broad spectrum of light (150–1,200 nm) using HOBO Pendant light sensors (Onset part #UA-002-08) that we attached to the top of our water sampling raft (out of water) and to two extended arms on either side of the raft at a submerged depth of about 15 cm (Figure 2.7).

We also used a Secchi disk to measure water clarity during the April 2017 trip. We lowered the disk off the side of the boat slowly and noted the depth where the disk was no longer visible, then we slowly raised the disk back up toward the surface and noted the depth where the disk became visible again. We calculated the Secchi depth by averaging these two depths.

Figure 2.7. HOBO light and temperature sensor/logger and water collection raft with GoPro camera and HOBO sensors attached to the submerged arms and air-exposed middle section (August 2017).

Source: George Graettinger, NOAA (right).

2.4.7 Air Sampling

Figure 2.8. Floating air sampler that collected samples at 0.1 m, 0.5 m, and 1.0 m off the surface of the oil slick.

Source: George Graettinger, NOAA.

During the November 2016 sampling trip, we collected air samples at approximately 0.1 m, 0.5 m, and 1.0 m above the oil slick (Figure 2.8; analyzing the samples for PAH and Volatile Organic Compounds (VOCs), including benzene, toluene, ethylbenzene, and xylenes (BTEX). We used Helium Diffusion Samplers (HDSs) to collect air samples for VOC analysis. For PAH analysis, we actively pumped air through Polyurethane Foam (PUF) sorbent tubes. At the last site sampled, we deployed the HDS and PUF samplers at approximately 0.5 m and 1 m off the front boat as well as suspended an HDS sampler from a drone at approximately 2 m above the water surface. We then used the maneuvering capabilities of the boat and the drone to keep the samplers within the slick area during sampling, which took at least 15 minutes to complete. We sent all air samples to ALS Environmental in Salt Lake City, Utah, for analysis.

For health and safety, we used an UltraRAE gas detector to continuously monitor the VOC concentrations in the air. While the primary purpose of the UltraRAE was to alert field staff on the research vessel when VOCs were sufficiently high to require a respirator, measurements from the detector also document locations with elevated VOC concentrations. In November 2016, the field team recorded spot measurements from the monitor throughout the day, along with Global Positioning System (GPS) waypoints showing when and where the spot readings were collected. During the April and August 2017 sampling trips, we set up the instrument to log the VOC concentration measurements every second.

2.4.8 Photographs/Videography

Mr. Graettinger documented the field sampling, including all in situ slick thickness measurements, with a digital camera. Dr. Garcia documented some field activities with a video camera. In April and August 2017, Dr. Morris collected subsurface video with an underwater GoPro camera.

2.4.9 Other Field Sampling Data

During each sampling trip, a GPS device logged coordinates every 30 seconds to track the position of the boat throughout the day. In addition, the field team collected waypoints to mark the location of each sampling event as well as other important events, such as when the boat drifted into or out of an oil slick during transects.

During the April and August 2017 trips, we deployed a YSI EXO1 water quality sonde to collect temperature, pH, conductivity, turbidity, and dissolved oxygen at various depths. These measurements generally coincided with water sample collection activities or surface oil collection activities. The autologging function on the multimeter was not working properly during the April trip, so data for the August trip are the only data available.

2.5 Data Services

In addition to slick characterization, our goals included establishment of near real time (NRT) data services, including providing aerial data to the sampling crew on the boat, and providing remote sensing and water quality data as quickly as possible to ERMA, NOAA's COP. Integral to providing NRT data services is the ability of researchers on the boat to be able to communicate with other researchers in the air, and the ability to transmit and receive data while in the field. This allows the field researchers to see the full extent of the slick and the areas where the oil is thickest, which ultimately guides the field sampling effort.

This section describes internet connectivity options on the boat, NRT data transmission, and efforts by Ocean Imaging, MSRC, and MDA to provide data services to the boat and to ERMA.

2.5.1 Shipboard Internet

Internet connectivity on the boat is essential for NRT data services. We investigated multiple options for data connectivity in the northern Gulf of Mexico near MC20. The options for onboard data services included satellite data transmission, cellular transmission via a proprietary network of cell towers mounted to oil rigs, and cellular transmission via onshore towers using a signal booster.

One of the industry leaders in satellite data transmission at sea is KVH, which has multiple TracFone models. We investigated the possibility of leasing a TracFone v3ip and v7ip. While this technology is reportedly reliable and data transmission rates are relatively fast, it is designed for larger ships that are at sea for long periods of time. It requires a large (close to 1-m diameter) radome antenna structure to be mounted on the wheelhouse or deck. The equipment costs thousands of dollars to rent (tens of thousands to purchase), and data throughput costs about $2 per MB. This is not a cost-effective solution for shorter-term, relatively nearshore data services.

In April 2017, we utilized a new northern Gulf of Mexico cellular technology that receives internet transmitted via a network of antennas on oil rigs. Blackhawk Datacomm provided the 4G LTE broadband technology, including installation of a large antenna on the boat and a wireless router in the wheelhouse. The technology worked well from MC20, but not from the mouth of the Mississippi River. The total cost was over $1,000 for a week of a field work.

For the August 2017 field trip, the boat captain utilized a Wilson Amplifiers weBoost cellular antenna booster. This $400 device allowed a regular smart phone to receive a cellular signal at MC20, approximately 30 miles from the nearest onshore cellular tower. The signal strength was sufficient to allow data transmission.

Together with an unlimited cell phone data plan, this is the most cost-effective solution for nearshore work.

2.5.2 Aircraft to Ship Communications

Researchers on the vessel communicated with researchers overhead in fixed-wing aircraft using a handheld aviation radio. On Wings of Care, with NOAA ERD personnel aboard, described the slick length and direction, and helped to position the vessel over the heaviest oil.

Ocean Imaging and MSRC developed a proprietary system of direct plane to vessel radio frequency (RF) communications, which we tested during the April 2017 sampling. They installed an antenna on the King Air and an antenna on the boat (Figure 2.9). Researchers on the plane and on the boat were able to communicate via instant message. After creating a draft mosaic of visible and thermal IR data from TRACS, the researchers on the plane used a command line file transfer protocol (FTP) application to transfer the data to a computer on the boat. The researchers on the boat had proprietary Ocean Imaging/MSRC software that allowed basic filtering of the imagery to clarify the nature and extent of the slick (see Chapter 3).

Figure 2.9. RF antenna that Ocean Imaging and MSRC installed on the boat for the April 2017 sampling. This allowed direct data communications between the King Air carrying TRACS and the boat at MC20.

Source: Ocean Imaging (see Attachment F).

After returning to the airport, the Ocean Imaging staff reprocessed the data and uploaded those data to the Ocean Imaging map server, which in turn provided the digital data service to ERMA.

2.5.3 SAR Dissemination

During the April 2017 sampling event, MDA successfully tested an in-house rapid data processing method to generate a compressed SAR image within 45 minutes of satellite acquisition. MDA researchers provided the compressed image of the slick extent to the researchers on the boat (which had internet connectivity, as described previously). MDA also provided a copy of the compressed image to ERMA.

2.6 Toxicity

The PAH composition of bulk oil collected at MC20 in November 2016 was very similar to the composition of oil skimmed from the surface during the DWH spill. During the DWH NRDA, Abt led a toxicology program for NOAA and other trustees that comprised over 650 aquatic bioassays and chemical characterizations to determine the toxicity of DWH oil at various weathering states and with other naturally variable parameters (e.g., temperature, dissolved oxygen, and UV light). To compare the relative toxicity of oil collected at the surface near MC20 to oil collected on the surface during the DWH spill, we conducted side-by-side bioassays with larval mysid shrimp at UNT, using surface oil collected at MC20 in April 2017 and DWH Slick A oil.

We prepared water accommodated fractions (WAFs) of both oils using a high-energy preparation method (HEWAF), which is described and characterized in detail in Forth et al. (2017a, 2017b). The exposure concentrations tested, reported as concentrations of total PAHs based on the sum of 50 separate PAHs (TPAH50), were:

- MC20 oil: 0.4 (control), 1.2, 3.6, 11, 33, and 101 µg/L TPAH50
- DWH Slick A oil: 0.4 (control), 1.3, 3.9, 12, 36, 110 µg/L TPAH50.

In some treatments, the mysids were also exposed to UV light using bulbs that produced UV light in primarily the 380-nm wavelength to determine the photo-induced toxicity of each oil. Mysids were exposed to each HEWAF solution for 4 hours in darkness, then the UV lights were turned on for 8 hours, then turned off for the remaining 12 hours of the 24-hour cycle and mortality was assessed. This light cycle was repeated and mortality was assessed again at 48 hours.

In addition to exposing mysids to all the HEWAF solutions with UV, we also conducted exposure without UV using the control solutions (0.4 µg/L TPAH50) and the highest HEWAF for each oil (101 and 110 µg/L TPAH50 for MC20 and DWH oils, respectively). We also exposed mysids to control treatments with no UV or oil, and treatments with the highest HEWAF concentration used in the UV test but with no UV. The general methods used to conduct these tests follow those described for similar tests we conducted for the DWH NRDA (e.g., Morris et al., 2015b; Nichols et al., in prep.).

We used Minitab statistical software (Version 16) to conduct analyses of variance (ANOVA) on the data. To fit dose-response curves, we used the drc package in R (Ritz and Streibig, 2005). We fit a 3-parameter log-logistic model for each endpoint of each test (Ritz, 2010). This produced estimates for the inflection point, the steepness of the line tangent to the curve at the inflection point, and the lower limit of the curve. This lower limit can be thought of as the modeled mortality when the dose is equal to zero.

To obtain effect concentrations and confidence intervals based on the profile-likelihood method (Venzon and Moolgavkar, 1988; Faraggi et al., 2003), we re-parameterized the log-logistic model for each desired effect level (U.S. EPA, 2013) and optimized the model using the bbmle package (Bolker and R Development Core Team, 2013). Effect concentrations calculated using these methods were adjusted for the modeled control mortality.

3. Results

Detailed data reports from Ohmsett and USF, as well as separate reports from Ocean Imaging, Water Mapping, Fototerra, and Abt are provided as attachments. This chapter summarizes those results and provides additional data not included in the separate data reports.

3.1 Slick Characterization: Remote Sensing

The primary goal of the BSEE-sponsored research was to ground-truth the remote sensing data that indicated the presence of oil slicks. As described in Chapter 2, the remote sensing data collected as part of this research includes visible and thermal IR data from UAS, multispectral and thermal IR data from Ocean Imaging's TRACS, and satellite data. In addition, Fototerra provided data from the MEDUSA system on their aircraft, and NASA JPL provided UAVSAR data from November 2016.

At MC20, we attempted to coordinate flight times and sampling from the boat with satellite passes, so we would have synoptic remote sensing and ground-truthing data. RADARSAT-2 passed over the site close to dawn on most sampling days; we needed to wait for the sun to be high enough for us to see the oil slick on some days. Generally, the field and aerial data were collected synoptically, close to or at the same time as the satellite passes.

3.1.1 UAS

At Ohmsett, Dr. Garcia of Water Mapping developed methods of capturing slick morphology and estimating thickness. Using high-resolution imagery from the HD camera, he created orthorectified mosaics covering the slick extent (Figure 3.1). This data could be used to measure the spatial extent of the surface slick.

Also at Ohmsett, Dr. Garcia developed a method of classifying oil thickness using FLIR thermal IR imagery (Figure 3.2, top) and HD imagery (Figure 3.2, bottom) collected concurrently from a DJI S1000 drone. The thermal IR imagery provides thickness information that cannot be seen in the HD image, based on changes in emissivity. Dr. Garcia orthorectified the images, overlaying the visible and thermal IR, and incorporated thickness data collected from the tank, ultimately creating a figure showing multiple thickness classes for the Ohmsett slick (Figure 3.3).

Dr. Garcia collected UAS data at each of the three field trips to MC20. The drones he flew at MC20 (DJI Phantom Pro and DJI Inspire) did not have sufficient payload to carry the HD camera and the FLIR together. He collected the visible and the thermal IR data separately (Figures 3.4 and 3.5) and, as a result, he did not classify the oil slick into thickness categories using the drone data. However, he did produce imagery available to the researchers on the boat in real time, showing the nature and extent of the slick (Figure 3.4). Images such as the example in Figure 3.4 were collected at nadir and could be used to measure slick extent. Because Dr. Garcia was piloting the UAS from the boat over the slick, we could field-verify the presence of surface oil in real time.

Figure 3.1. Orthorectified mosaic image of the oil slick at Ohmsett, collected using the HD camera mounted on a DJI S1000 drone.

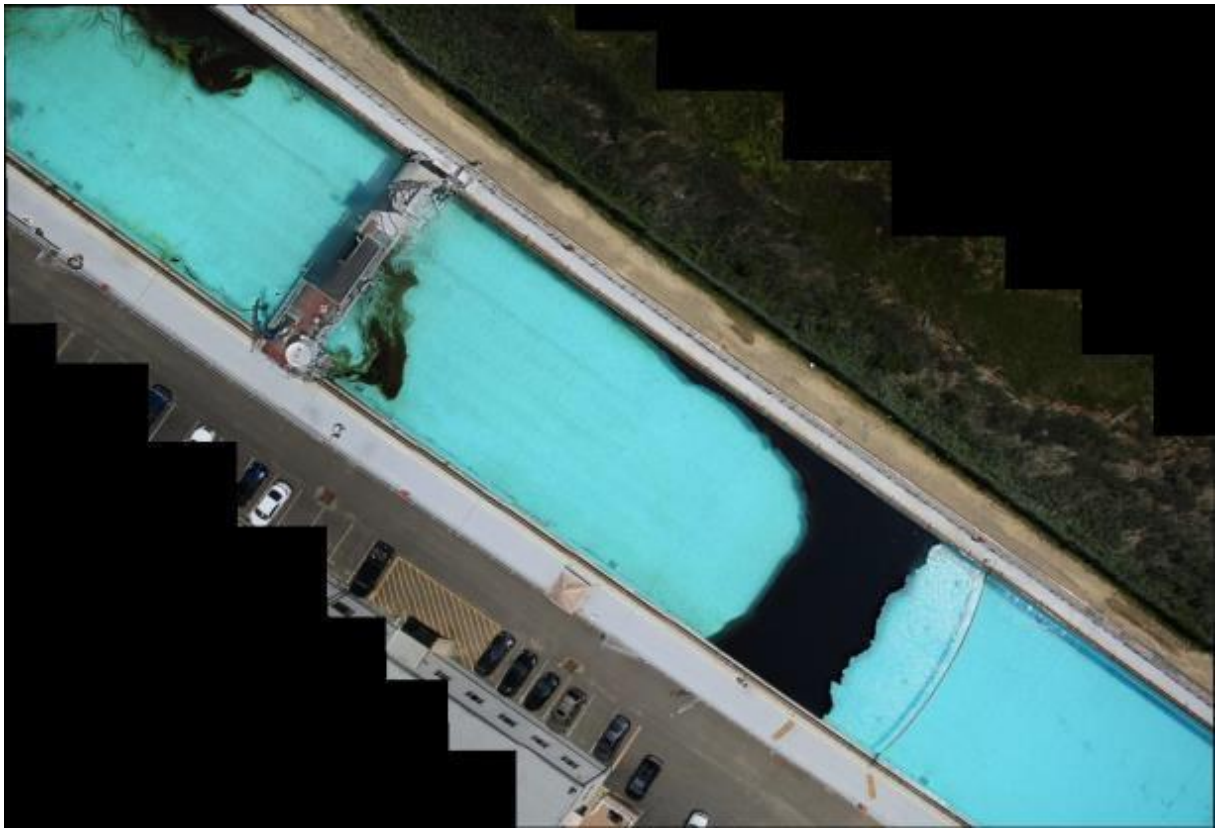

Source: Water Mapping, 2017, Figure 12. See Attachment B.

Figure 3.2. FLIR thermal IR image (top) and HD camera image (bottom) of the oil slick at Ohmsett, taken from a DJI S1000 drone.

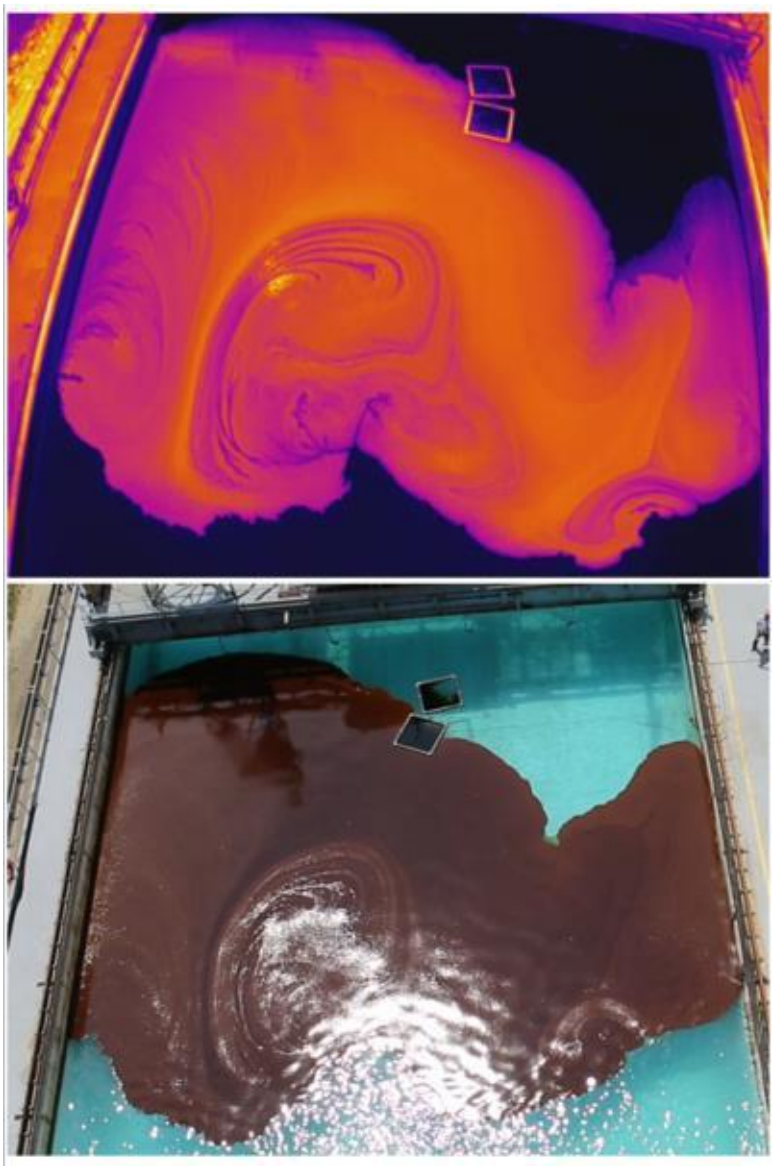

Source: Water Mapping, 2017, Figure 17. See Attachment B.

Figure 3.3. Ohmsett oil slick classified into thickness categories based on HD and FLIR thermal IR imagery. The slick morphology is similar to Figure 3.2, except rotated so that north is up.

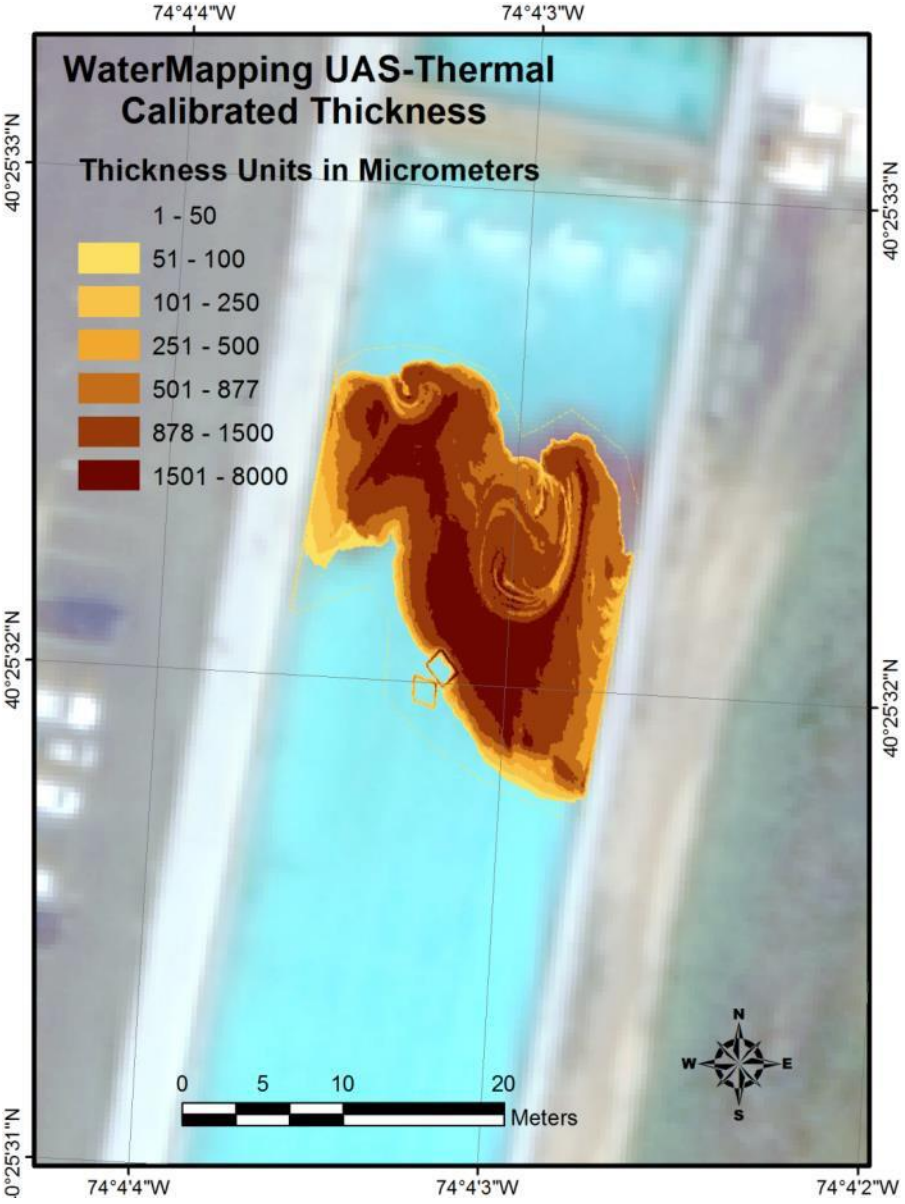

Source: Water Mapping, 2017, Figure 23. See Attachment B.

Figure 3.4. HD image of the MC20 oil slick on November 15, 2016.

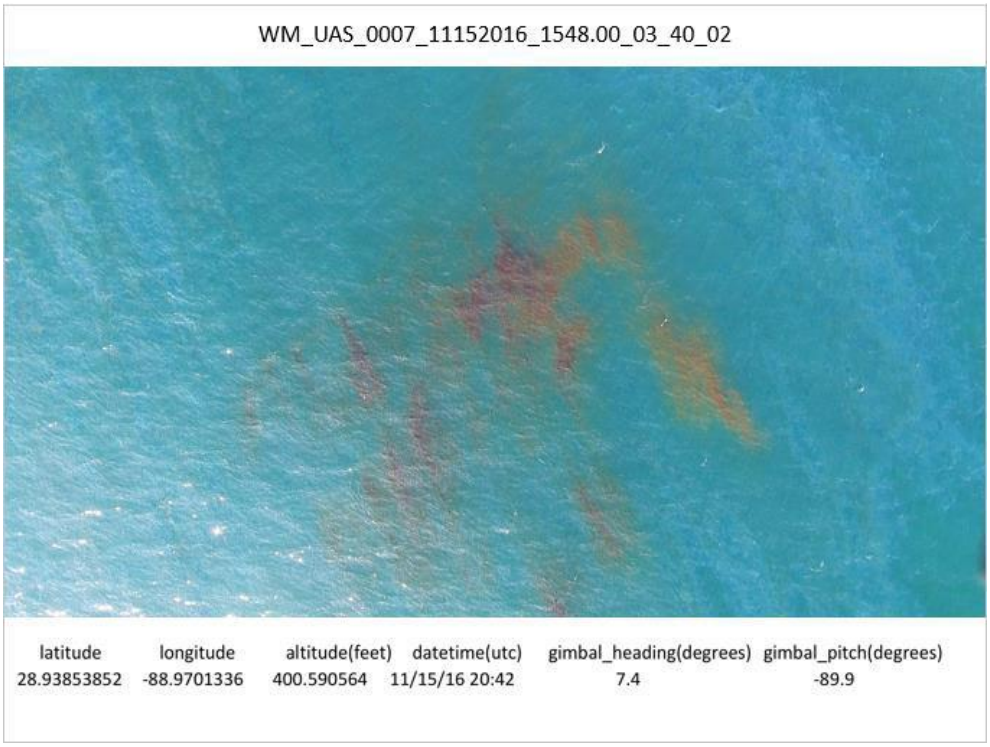

Source: Water Mapping.

Figure 3.5. FLIR thermal IR image of the MC20 oil slick on November 15, 2016. This image was collected shortly after the image in Figure 3.4, at a lower altitude. Thicker oil appears darker.

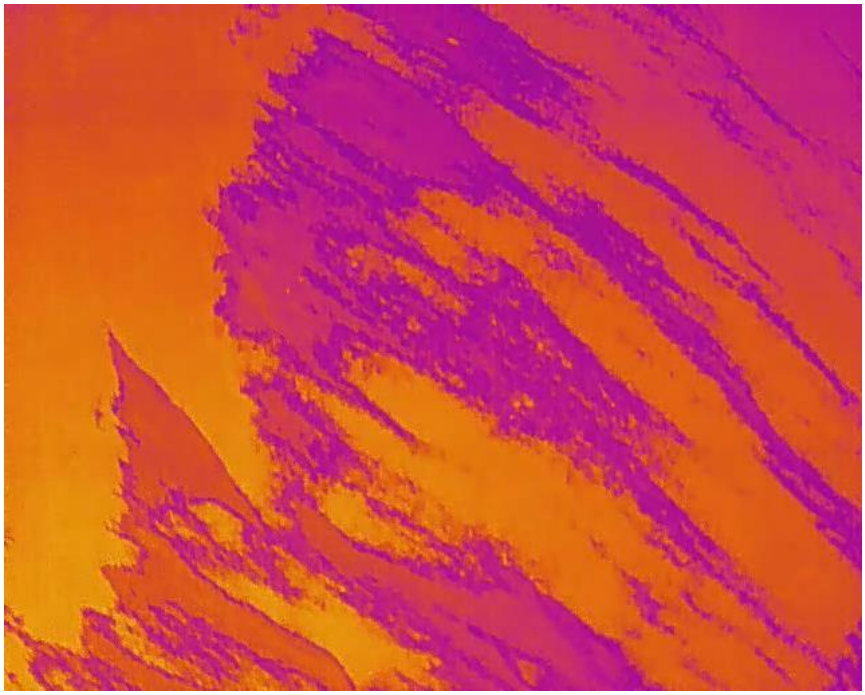

Source: Water Mapping.

3.1.2 TRACS

Ocean Imaging collected multispectral visible bands and thermal IR data using TRACS. They initially refined the data collecting and analysis methods at Ohmsett, with the TRACS instrumentation mounted to a helicopter (see Section 2.3). They classified the thickness categories in the remote sensing imagery using thickness data collected at the water surface from the side of the tank. Details of this method development are provided in Attachment C.

Ocean Imaging's research at Ohmsett included a comparison of multiple sensors as well as the development of a method for estimating approximate volumes of oil per unit area on the surface of the tank. They compared the visible bands from the TRACS multispectral scanner to the visible wavelengths from DigitalGlobe WV-2, in images collected on the same day at approximately the same resolution (Figure 3.6). Both sensors successfully detected the oil slick in the tank. The visible bands from the TRACS multispectral scanner provided more information on slick extent and composition, with less degradation from sun glint, than did WV-2. On the other hand, the WV-2 image verifies that visible satellite imagery on a clear day can detect oil slicks, without mobilizing aircraft.

Figure 3.6. Comparison of WV-2, TRACS visible, and TRACS thermal IR imagery on July 19, 2016 at Ohmsett. The ground sampling distance (GSD) was similar for each image. WV-2 contained less slick detail and more sun glint degradation than the TRACS image.

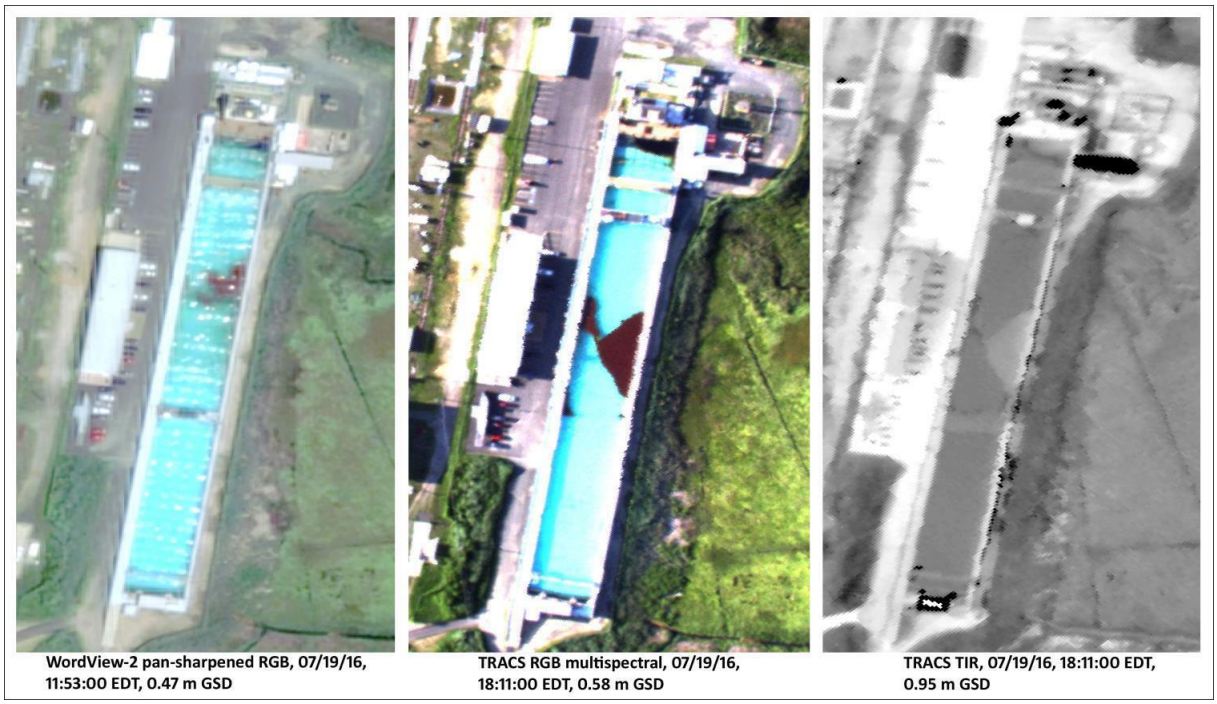

Source: Ocean Imaging, 2016, Figure 7. See Attachment C.

At Ohmsett, Ocean Imaging integrated data collected at the tank surface with their remote sensing data to create a method for classifying remote sensing imagery into classes of oil volume per unit area. They integrated data from HD photographs at the tank surface as well as slick thickness measurements (see Section 3.2) and oil emulsion data to develop this classification (Figure 3.7).

Figure 3.7. Integration of TRACS remote sensing data with surface-collected oil thickness and emulsion data.

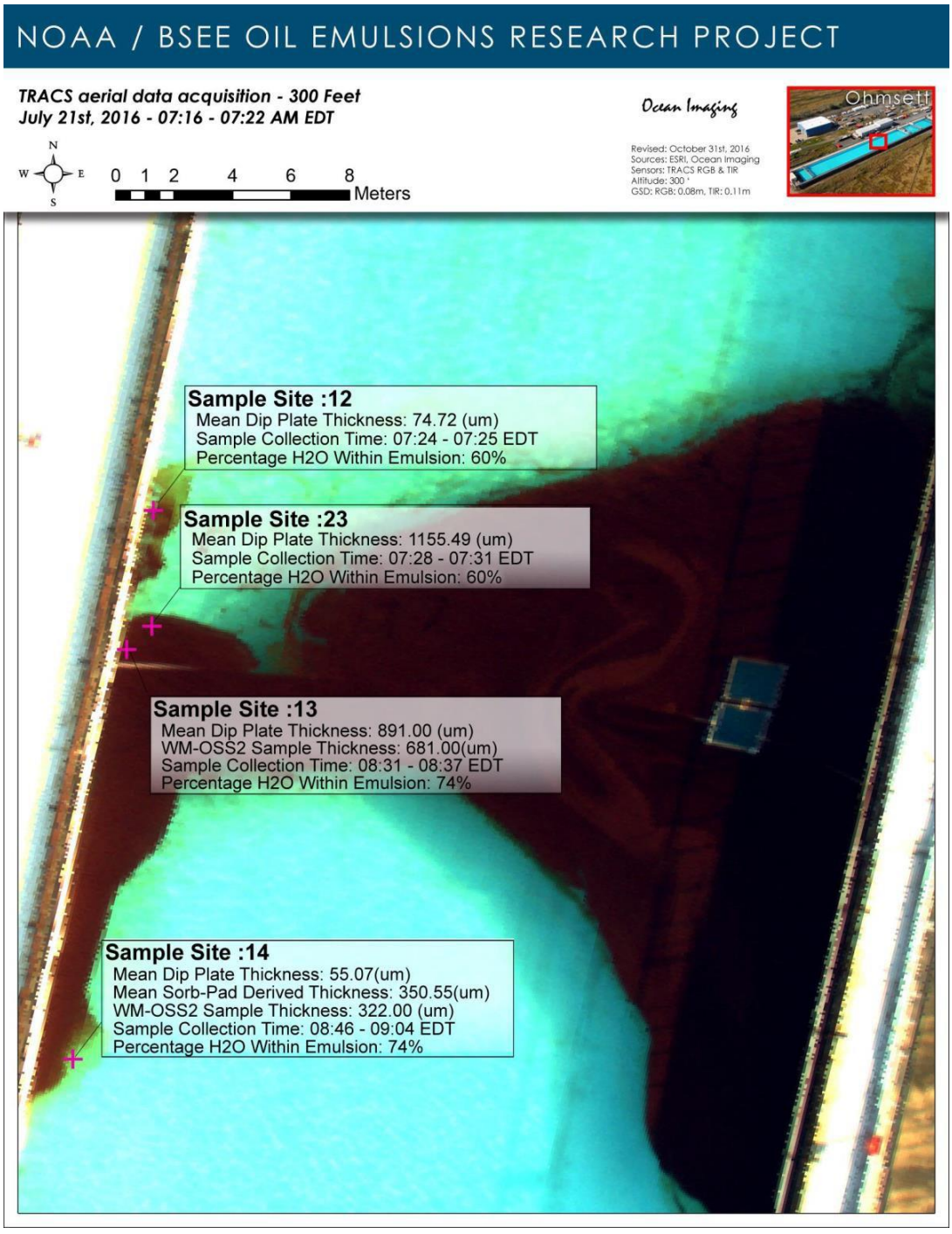

Source: Ocean Imaging, 2016, Figure 16. See Attachment C.

Although not part of their TRACS sensor suite, Ocean Imaging tested a UV sensor at Ohmsett. The results were encouraging (Figure 3.8), clearly outlining the oil slick areas that could be seen in a HD photograph. We have not tested this sensor to assess its ability to discern different slick characteristics. We hope to explore the use of this sensor further in the future.

Figure 3.8. Comparison of HD photograph and UV sensor image of an oil slick at Ohmsett.
Source: Ocean Imaging, 2016, Figure 11. See Attachment C.

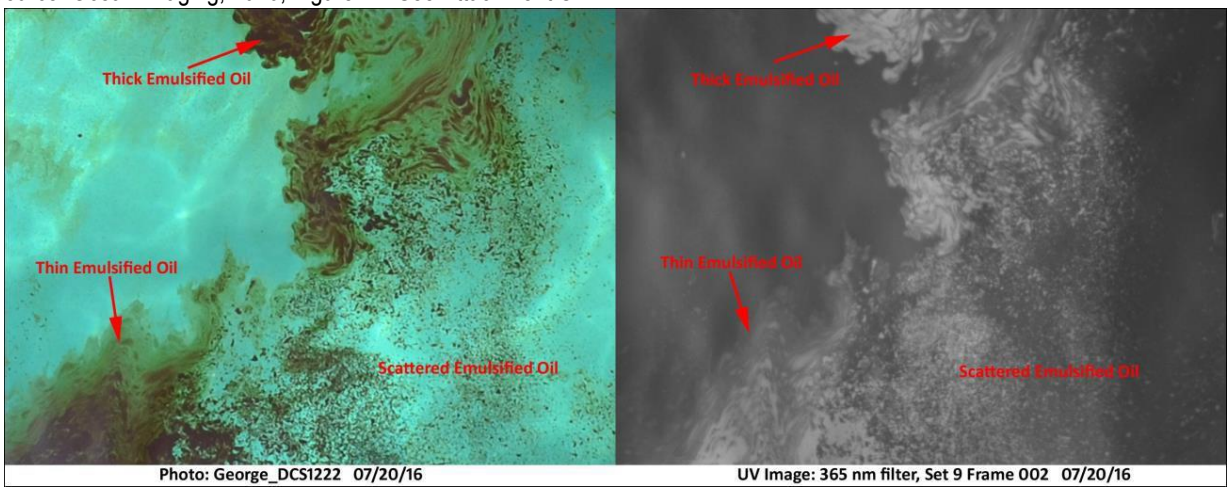

Ocean Imaging field-tested the TRACS multispectral and thermal IR scanners, and the method of classifying imagery integrating remote sensing and field-collected data, at MC20 in November 2016 and April 2017. Here we provide some example Ocean Imaging tools and work products; additional data are provided in Attachments C and F.

On April 25, Ocean Imaging (together with MSRC on the King Air) provided draft mosaics directly to the researchers on the boat via RF (see Section 2.5) within 10–15 minutes of data collection. After receiving the unfiltered imagery aboard the boat, researchers on the boat used Ocean Imaging/MSRC proprietary software to filter the data, enhancing the oil slick features. The resulting product was sufficient to outline the slick near the boat using data from the visible spectrum (Figure 3.9) and to highlight the areas where changes in emissivity (dark pixels in thermal IR) indicated thicker oil (Figure 3.10). This NRT image service provides an important new tool for oil spill response because it gives the boat researchers an immediate picture of the slick extent and the areas of thick oil, which they can sample to ground-truth the remote sensing data and allow for estimates of oil volume per unit area.

Ocean Imaging integrated the slick thickness and emulsion data from MC20 with their TRACS data, as well as data from satellite sensors (SAR and WV-2), to develop estimates of oil volume per unit area, following the method they developed at Ohmsett. As will be discussed in the following section, the oil slick at MC20 was highly heterogeneous; both thickness estimates and oil:water ratio data varied widely over small areas. Because of this reality, Ocean Imaging classified their data into bins of average thickness (volume per unit area), recognizing that these estimates are not precise.

For example, they collated the oil thickness measurements that were collected within two hours of the time that the TRACS imagery was collected on November 17, 2017. Figure 3.11 shows the location of the thickness measurements together with TRACS data for thicker oil and SAR data for sheens. They used the field-collected data to develop their bins of average thickness. The field-collected data clearly validates the ability of TRACS to detect oil slicks and classify the slicks into thickness categories. The data also allow for this initial quantification of the amount of oil on the ocean surface.

Figure 3.9. Draft mosaic of visible imagery at MC20 on April 25, 2017. Ocean Imaging personnel created the mosaic within 10–15 minutes of image acquisition, then pushed the mosaic to a laptop on the boat (visible on the left side) directly from the aircraft via RF connection. These images were collected at an altitude of 6,000 ft.

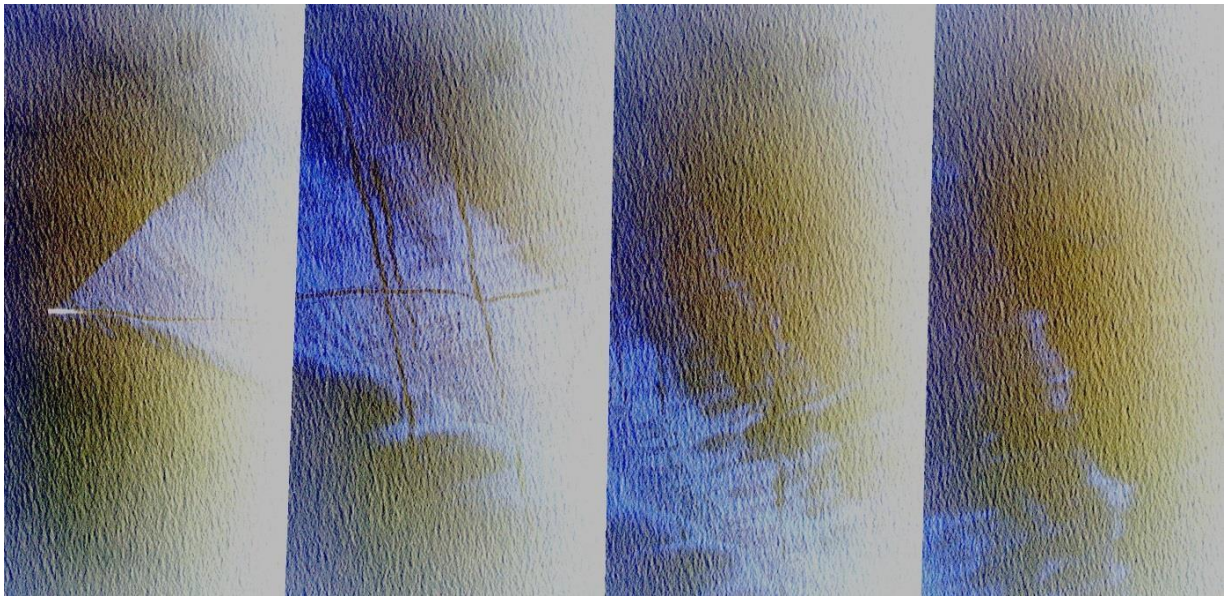

Source: Ocean Imaging/MSRC (see Attachment F).

Figure 3.10. Draft mosaic of thermal IR imagery at MC20 on April 25, 2017. These data were collected concurrently with the data shown in Figure 3.9.

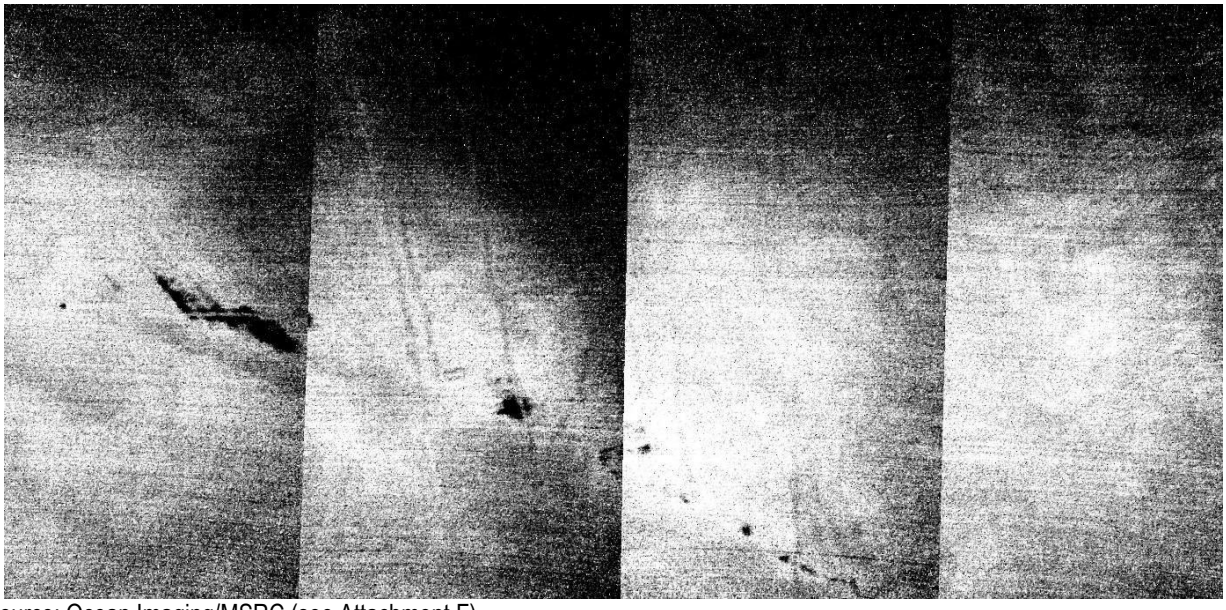

Source: Ocean Imaging/MSRC (see Attachment F).

The oil slick in April 2017 was primarily thin sheen, with few thicker emulsions to classify (Figure 3.12). Bulk oil was difficult to collect from the boat, limiting the oil:water ratio data. Even with these limitations, Ocean Imaging used the data available to classify the slick into multiple thickness categories, and they made an initial estimate of the quantity of oil present on the ocean surface (Figure 3.12).

Figure 3.11. Ocean Imaging's classification of oil thickness ranges at MC20 on November 17, 2016, integrating boat-collected data with remote sensing signatures.

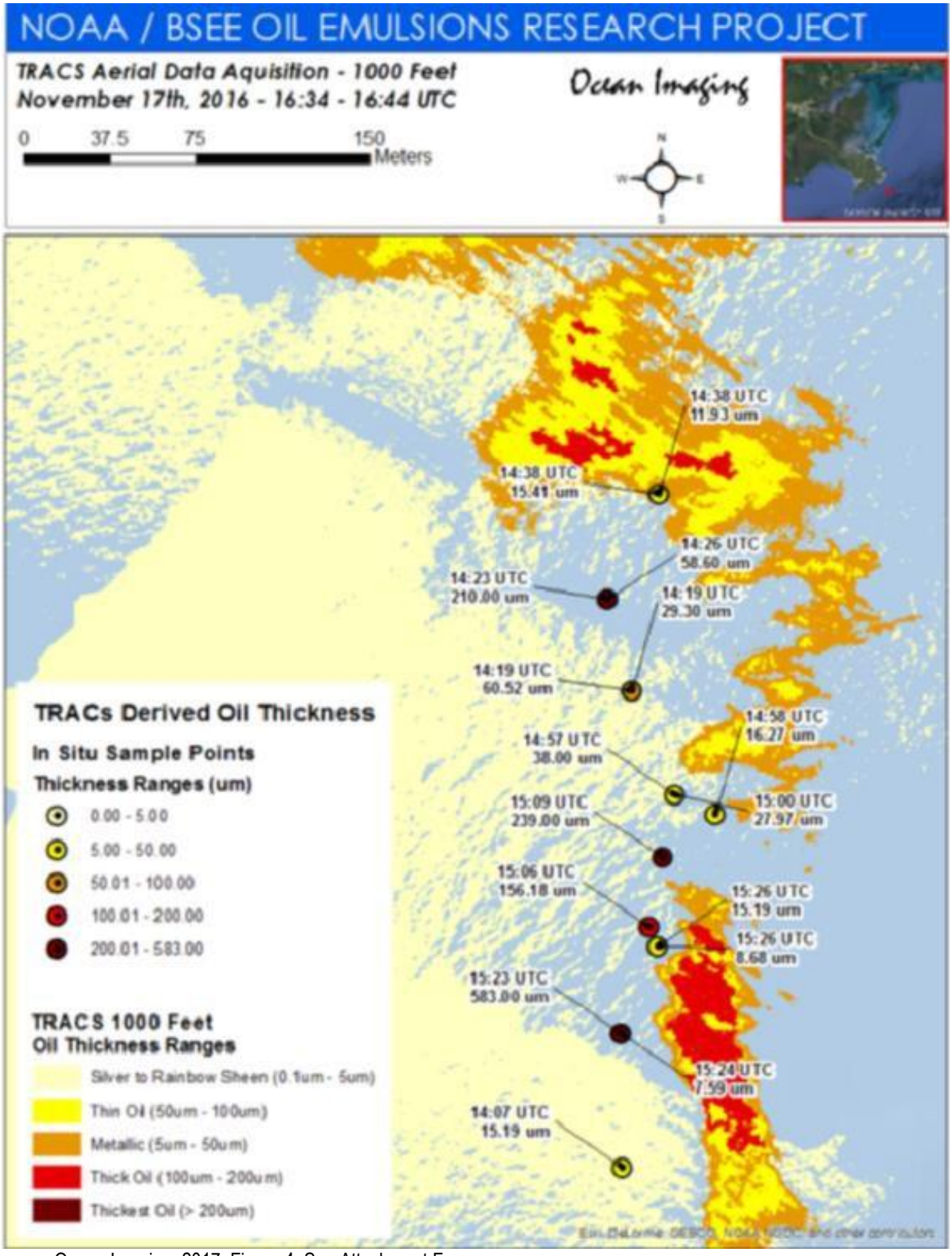

Source: Ocean Imaging, 2017, Figure 4. See Attachment F.

Figure 3.12. Ocean Imaging's classification of the April 25, 2017 oil slick at MC20.

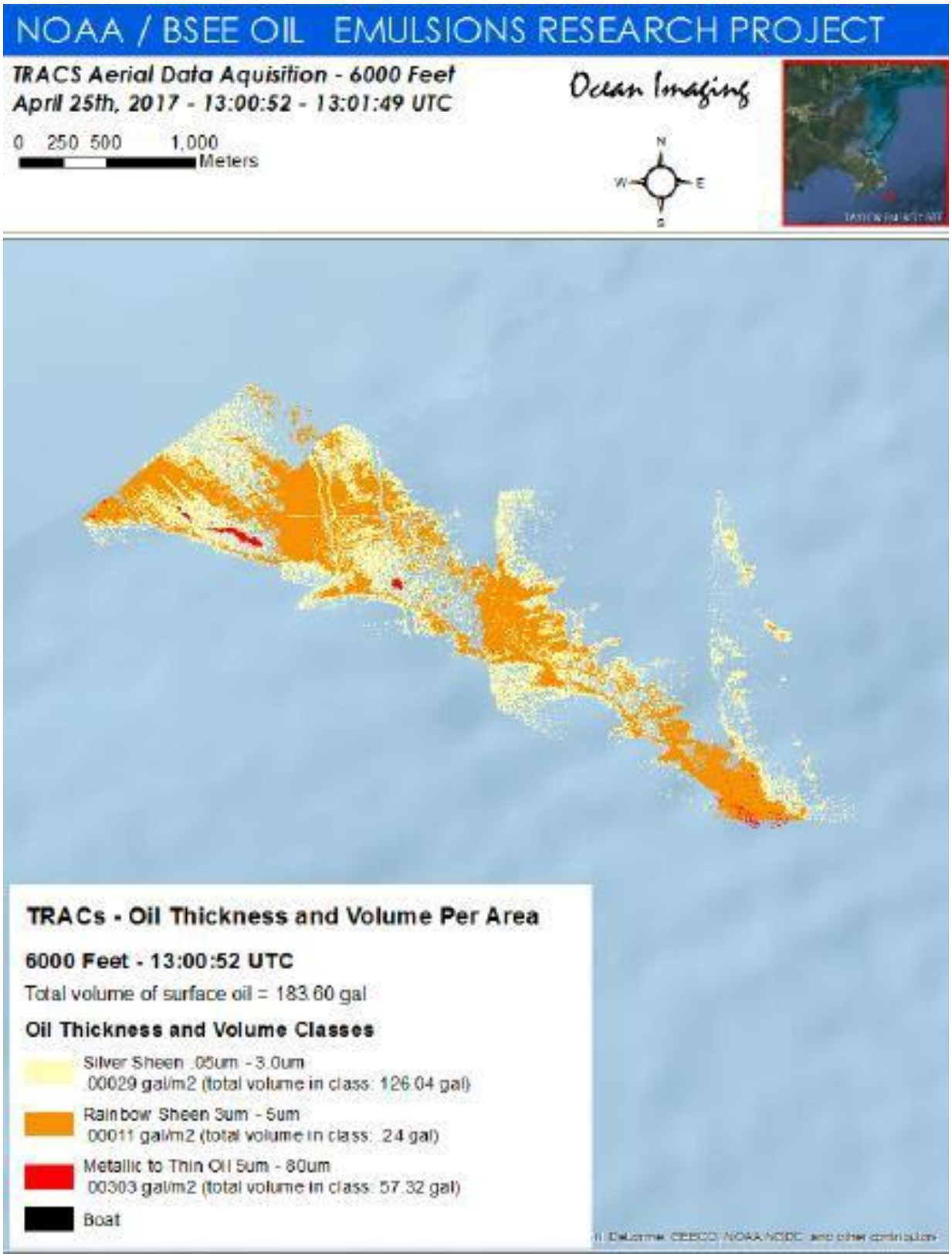

Source: Ocean Imaging, 2017, Appendix B.2 (see Attachment F).

3.1.3 SAR

As noted in Chapter 2, MDA collected high-resolution quad-pole SAR imagery from RADARSAT-2 for each of the field collection events. Researchers in the boat attempted to collect field samples synoptically with the satellite data collection, to the extent practicable. SAR data were analyzed using previously established algorithms, including Dr. Garcia's TCNNA and OEDA algorithms (Garcia-Pineda et al., 2009, 2014).

In addition, MDA tested a rapid-turnaround data service during the April 2017 field event. Using a standard SAR analysis algorithm, MDA produced a compressed SAR image that they emailed to the researchers on the vessel within 45 minutes of data acquisition (Figure 3.13). This NRT transmission of a SAR image is a new and helpful tool, providing the researchers on the boat with an immediate overview of the slick extent. Combined with NRT data from the UAS, TRACS, and the On Wings of Care overflight, a boat crew can devise a field sampling plan that will ensure that ground-truthing data are collected in the areas most critical for quantifying the slick.

Figure 3.13. Compressed SAR image of the MC20 oil slick in the early morning of April 25, 2017. The image was collected shortly before the boat (left of the slick) arrived at the site to collect samples. Researchers on the boat received a Google Earth KML of this image via email 45 minutes after image acquisition.

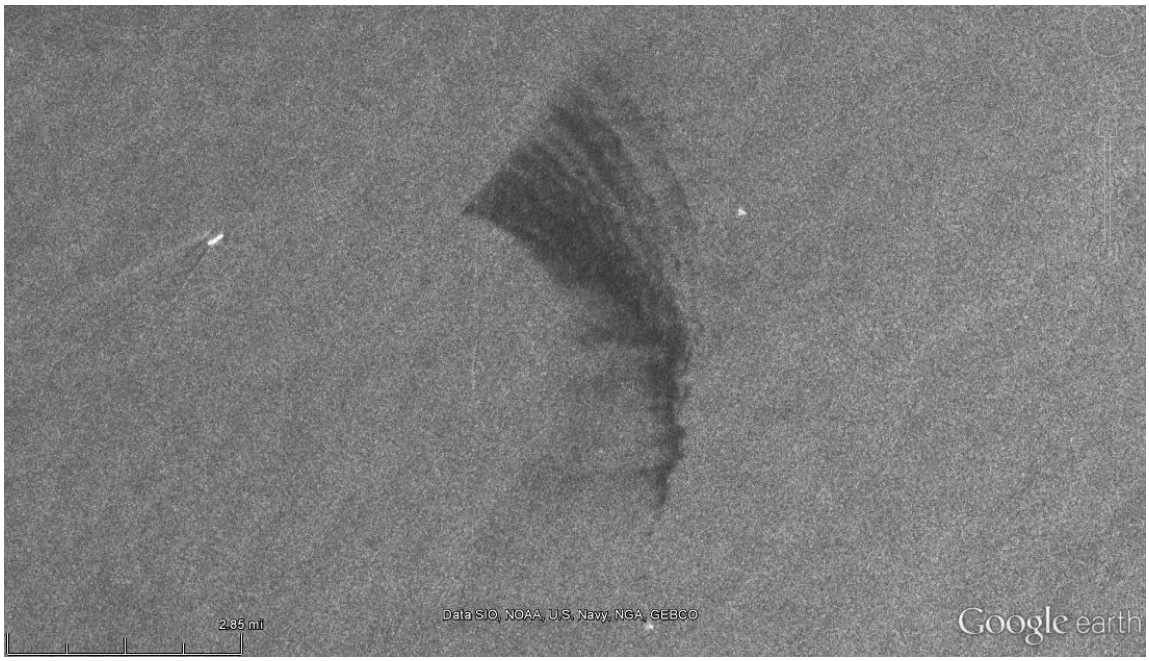

Source: MDA.

Dr. Garcia of Water Mapping reprocessed SAR imagery using TCNNA and, if oil emulsions were present, OEDA. In November 2016, substantial emulsions were present at MC20, allowing Dr. Garcia to classify the RADARSAT-2 image into oil thickness bins, combining overall slick extent (using TCNNA), the extent of detectable emulsions (using OEDA), and slick thickness data collected from the boat (Figure 3.14). With the additional of thickness and emulsion data collected from the boat, Dr. Garcia was able to fully verify that his OEDA algorithm was detecting emulsified oil, and he was able to classify the thickness of those emulsifications using the boat-collected data.

Figure 3.14. Water Mapping's analysis of the thickness of emulsified oil at MC20 on November 17, 2016. The RADARSAT-2 (RS2) data are shown in grey scale, with OEDA-based classifications overlain.

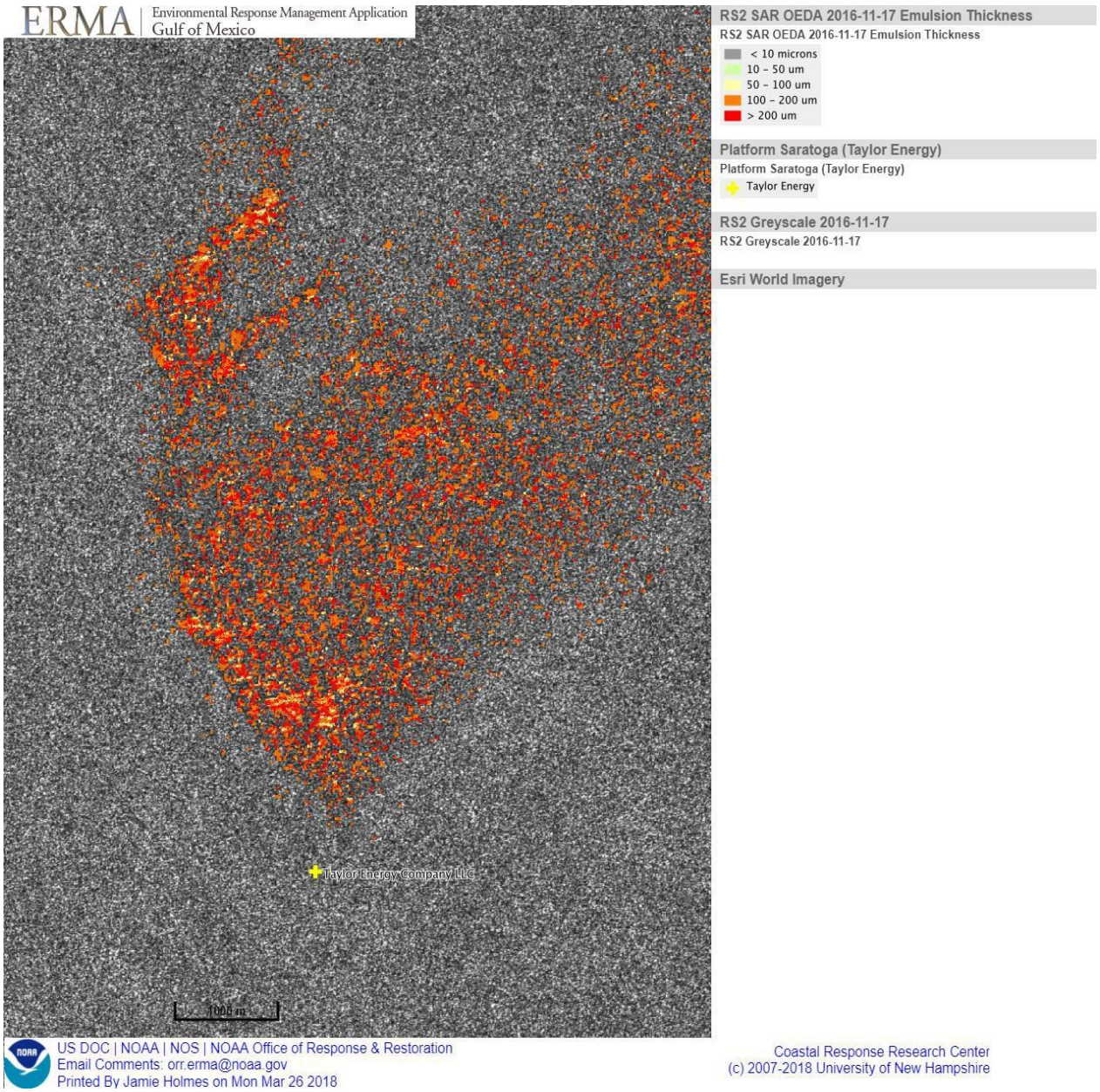

Source: NOAA Gulf of Mexico ERMA.

3.1.4 UAVSAR

NASA JPL collected UAVSAR flight lines during the November 2016 sampling at MC20. By the afternoon of November 16, they provided draft mosaic images of the November 15 flight with radar dark anomalies showing potential oil slicks (Figure 3.15). The SAR anomalies that UAVSAR detected on November 15 covered a larger spatial extent than was evident from aircraft or from the boat. Additional research will be required to determine if oil or some other phenomenon caused those anomalies.

Figure 3.15. Google Earth image of a UAVSAR mosaic showing radar dark anomalies consistent with oil slick in the northern Gulf of Mexico on November 15, 2016.

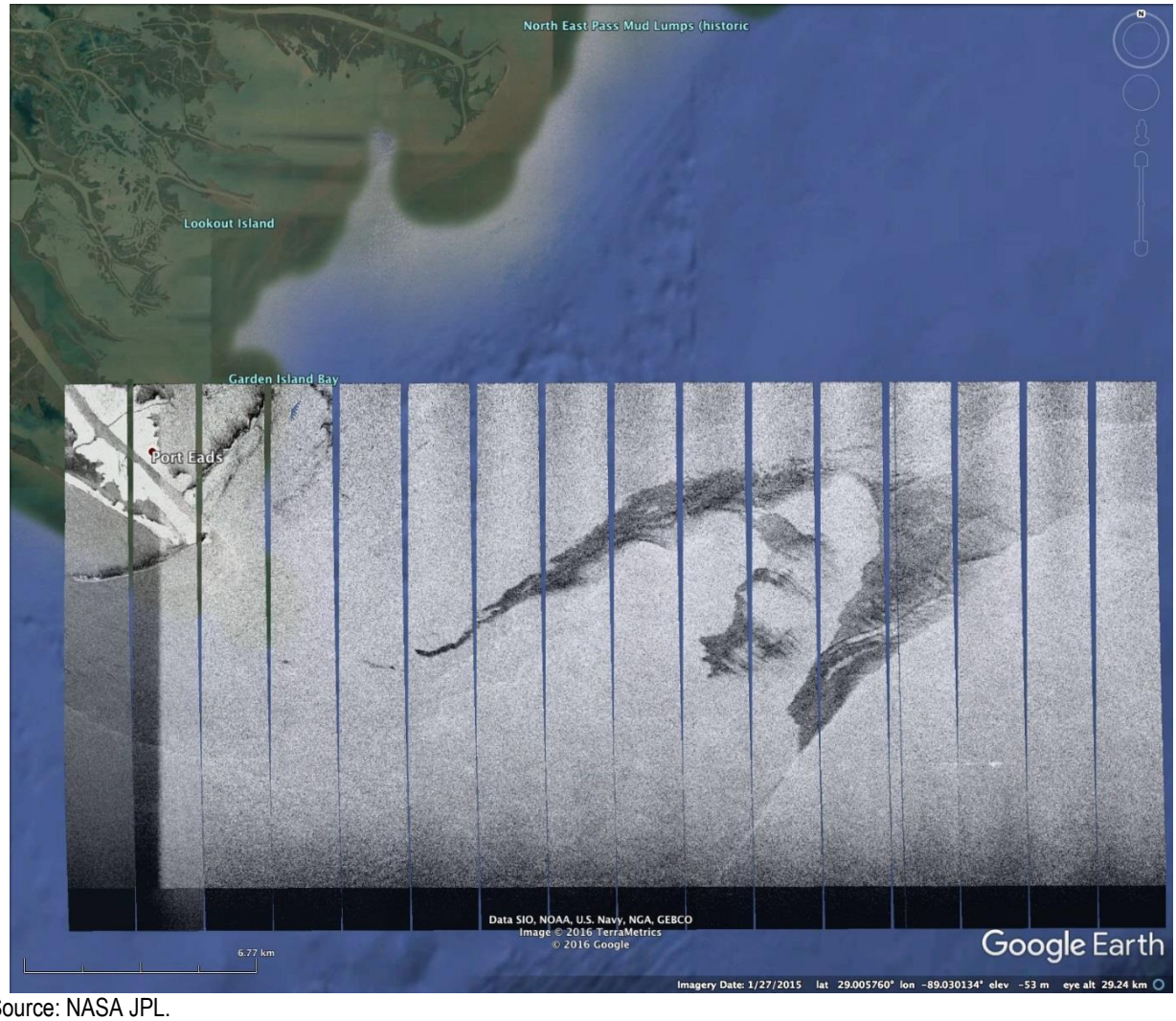

Source: NASA JPL.

As noted in Chapter 2, JPL developed the UAVSAR methods for oil slick detection during the DWH event and has published these methods and data previously (see, for example, Jones et al., 2011, 2012; Minchew et al., 2012). On May 29, 2017, JPL provided ArcMap files of their November 2016 flights, with oil classified into multiple relative thickness categories (Figure 3.16). The areas in the thickest oil categories in UAVSAR correspond well with the areas of emulsions identified in the SAR image using OEDA (see Figure 3.15). JPL collected these data using their own funding sources; they were not able to compare the UAVSAR data to ground-collected data to estimate the approximate slick thicknesses that correspond with the bins shown in Figure 3.16.

Unfortunately, because of scheduling conflicts and maintenance issues, JPL was unable to collect UAVSAR data during the April and August 2017 sampling events.

Figure 3.16. UAVSAR data collected November 17, 2017, classified into relative thickness categories. JPL was not able to compare these data to ground-collected data to provide estimates of oil quantity or thicknesses that would correspond with the relative thickness classes.

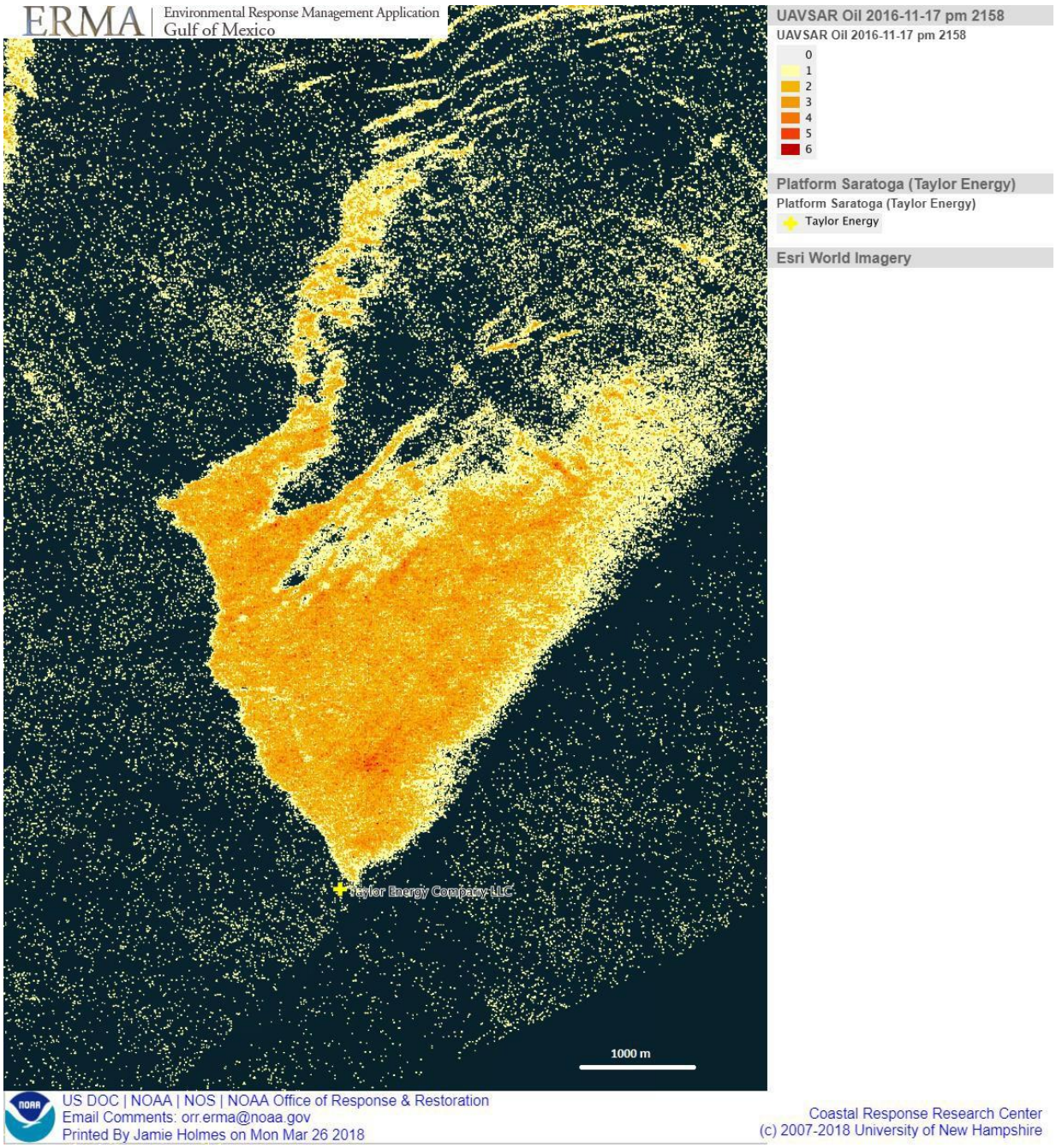

Source: NOAA Gulf of Mexico ERMA.

3.1.5 Fototerra

Fototerra collected data at Ohmsett and at each of the three field sampling events at MC20. They provided preliminary reports for each sampling event (see Attachments H through J). As noted previously, Fototerra operated independently at MC20. Their goals were focused on collecting data using the MEDUSA sensor suite aboard the EMB-110.

3.1.6 Sensor Comparison

Site conditions and logistics limited the synoptic acquisition of remote sensing data from all sensors. UAVSAR was only able to fly in November 2016; poor weather prevented most of the field activities in April 2017, and on the one day of good weather, the oil slick was mostly sheen. Here, we provide comparisons of multiple sensors on November 15, 2016, when we have synoptic data from all sensors; and on April 25, 2017, when all but UAVSAR were present but there was comparatively little oil.

On November 15, 2016, SAR (from RADARSAT-2), UAVSAR, and Ocean Imaging's TRACS all showed a similar oil slick morphology near the MC20 wellhead (Figure 3.17). SAR imagery analyzed by TCNNA is a peer-reviewed standard for estimating oil slick extent. UAVSAR estimated a very similar overall slick extent, with some small areas of relatively thicker oil embedded in the slick. TRACS is higher resolution, and the thermal IR sensor detected thicker oil in the immediately vicinity of the upwelling (Figure 3.17).

Imagery from April 25, 2017 includes data presented previously, such as the TRACS mosaics (Figures 3.9 and 3.10), Ocean Imaging's detailed analysis (Figure 3.12), and the MDA rapid- turnaround SAR image (Figure 3.13). The TRACS data line up well with the SAR data (Figure 3.18).

All of the imagery and remote sensing analyses will be available on the NOAA Gulf of Mexico ERMA COP (https://erma.noaa.gov/gulfofmexico/erma.html). This data will be made publicly available upon official release by BSEE in the near future.

3.1.7 Summary

Synoptic sampling of oil slick data from a boat, a drone, fixed-wing aircraft, and satellites provided a wealth of information for characterizing the oil slick. The research at Ohmsett and MC20 verified that the sensors were successfully discerning the slick extent and thicker oil patches, allowing us to further develop tools for oil spill response.

On the boat, Dr. Garcia of Water Mapping flew drones that provided real-time imagery, allowing the boat captain to position the boat over thicker oil patches, and allowing high-resolution spatial analysis of slick extent. Ms. Schumacher of On Wings of Care provided additional observations of the nature and extent of the oil slick from a Cessna 182, communicating directly with the boat via handheld aviation radio. When positioned near the heaviest oil patches, Dr. Garcia mounted a FLIR thermal IR camera on the drone, providing additional data that helped researchers discern the thicker oil patches at MC20.

Figure 3.17. Ocean Imaging TRACS, UAVSAR, and RADARSAT-2 SAR data collected on November 15, 2016. UAVSAR data were classified into relative thickness categories with no further quantification. SAR imagery was analyzed using TCNNA.

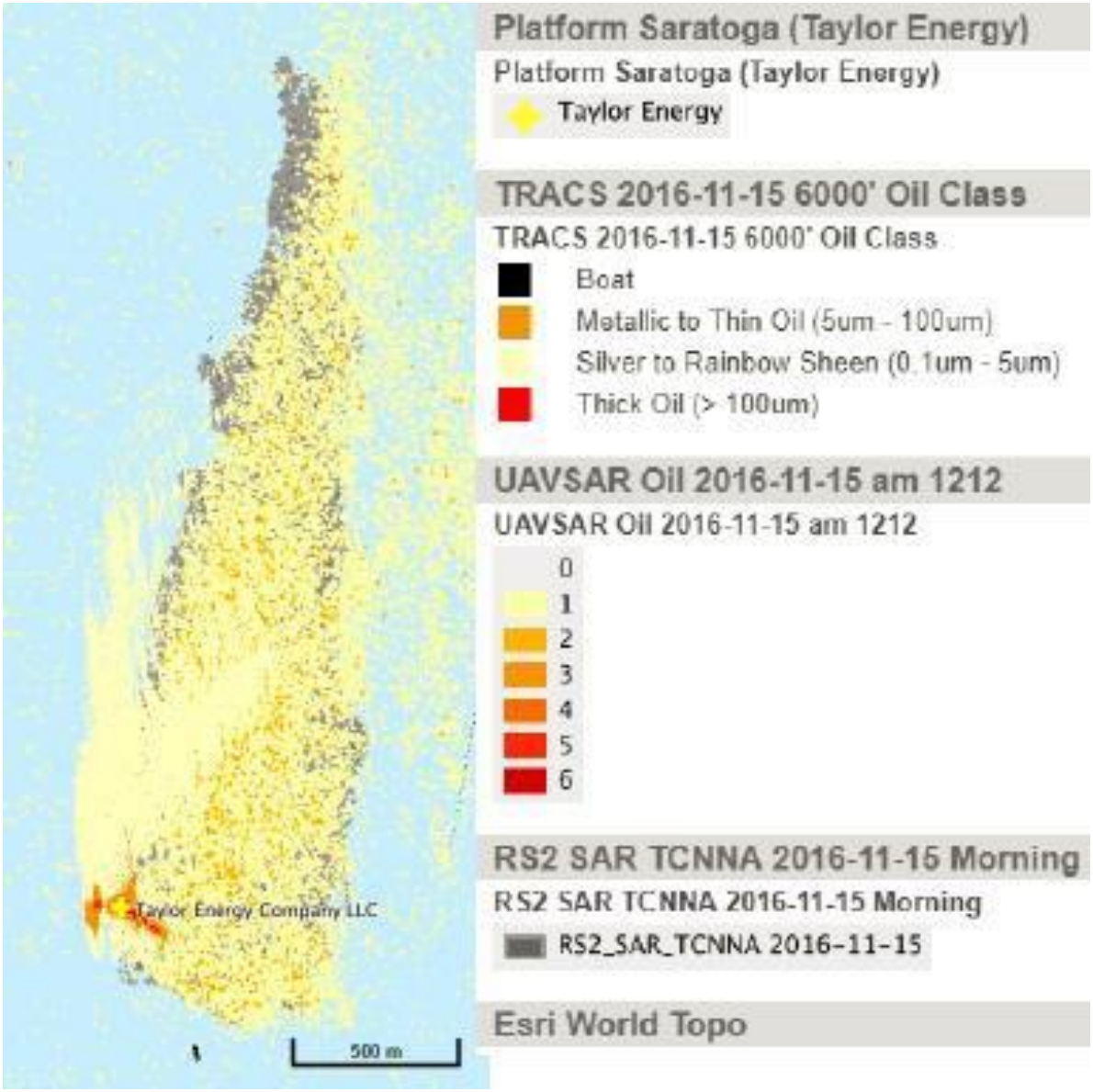

Source: NOAA Gulf of Mexico ERMA.

Ocean Imaging's TRACS, their most recent multispectral scanner and thermal IR sensor package, was one of the more robust sensor packages that we tested. These sensors provide calibrated data that discern spatial extent and thickness data. By overlaying their TRACS data with slick thickness and oil emulsion data collected from a boat as well as SAR and optical satellite data, Ocean Imaging classified the TRACS data into categories of volume per unit area, ultimately leading to approximations of the total volume of oil at surface. In addition, Ocean Imaging demonstrated a new capability of sending visible and thermal IR mosaics of the oil slick directly to the boat from the plane within 15 minutes of data acquisition.

Figure 3.18. RADARSAT-2 SAR analyzed by MDA and TCNNA shows oil slick-related anomalies, compared with slick oil extent from Ocean Imaging's TRACS. TRACS is higher resolution and focused on the areas where thicker slick was likely to be detected. The MDA outline captures most of the slick area that TCNNA detected.

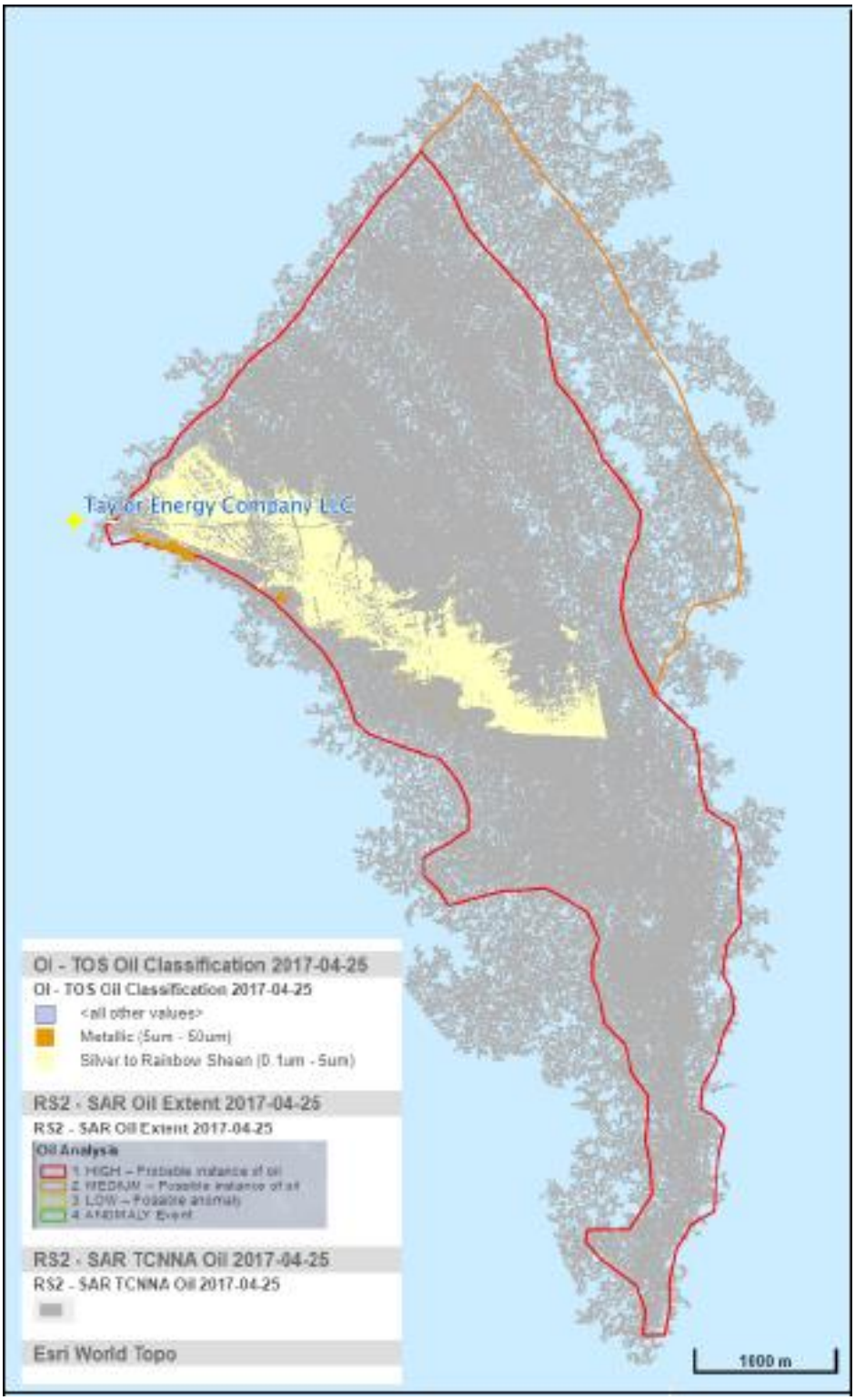

Source: NOAA Gulf of Mexico ERMA.

Similarly, MDA demonstrated a new data service that provided researchers with a compressed SAR image of the oil slick within 45 minutes of data acquisition from RADARSAT-2. Because researchers on the boat had internet connectivity, they received the SAR image while still positioned at MC20. SAR continues to be the most reliable sensor for outlining the extent of oil slicks of any thickness. The TCNNA analysis of the SAR data provides a more detailed picture of the slick extent, after field work is completed. In addition, when substantial emulsions were present in November 2016, Dr. Garcia validated OEDA's ability to discern emulsions in SAR imagery, and he used ground-collected thickness data to classify the OEDA imagery into initial estimated thickness categories.

UAVSAR was previously established as a useful sensor for both detecting and quantifying oil (Jones et al., 2011, 2012; Minchew et al., 2012). UAVSAR data from November 2016 corresponded well with other data sources for depicting the slick near MC20. Areas of thicker oil generally matched the areas outlined in the SAR image using OEDA. Additional research is necessary to determine potential false positives in the UAVSAR imagery near the convergence of the Mississippi River sediment plume with blue water, to compare UAVSAR data to ground-collected data to quantify the thicknesses classified in the imagery. Based on DWH research, we are confident that UAVSAR is another useful tool for detecting and quantifying oil slicks on the open ocean, although with limitations on availability, such as in April and August 2017.

3.2 Slick Thickness

This section provides the a summary of the results from the three slick thickness methods, starting with initial method development at Ohmsett, followed by method validation and refinement at USF and field implementation at MC20. The Ohmsett data and the USF data are presented in more detail in Attachments A and E, respectively. Slick thickness data collected from the boat at MC20 are presented in Attachments K through M.

3.2.1 Ohmsett

A primary purpose of the in situ sampling at the Ohmsett facility was to develop methods for characterizing slick thickness. We tested three different methods for measuring the thickness of oil slicks or sheens: the dip plate, the sorbent pad, and the Water Mapping sampler

Slick thickness measurements in the Ohmsett tank ranged from 3 to 5 µm in the thin sheen that covered most of the tank, up to 8 cm (or 80,000 µm) in the heaviest oil (Figure 3.19). For the three methods that we tested, we saw an increasing trend in the measured thickness as we moved from outside the main slick, to the edge of the main slick, to within the main slick.

At three of the sampling sites, highlighted by grey boxes in Figure 3.19, we collected co-located slick thickness data using the dip plate, sorbent pad, and Water Mapping methods. At these three sites, the co-located thickness measurements varied by 1–2 orders of magnitude. From the photographs of the slicks being sampled (Figures 3.19 and 3.20), we know the slicks were not visually uniform. We also know from previous laboratory research that oil slicks are highly heterogeneous (Cheemalapati et al., 2017). Therefore, the variability we see with the co-located samples is not surprising. It was difficult to separate the variability that was related to uncertainty in the measurement methods versus the heterogeneity of the slick being sampled.

Figure 3.19. Slick thickness measurements taken during in situ sampling at the Ohmsett facility. The dip plate, sorbent pad, and Water Mapping methods were used in the field as well. The U.S. Geological Survey (USGS) tested a separate method at Ohmsett that is not discussed in this report and was not used in any subsequent work.

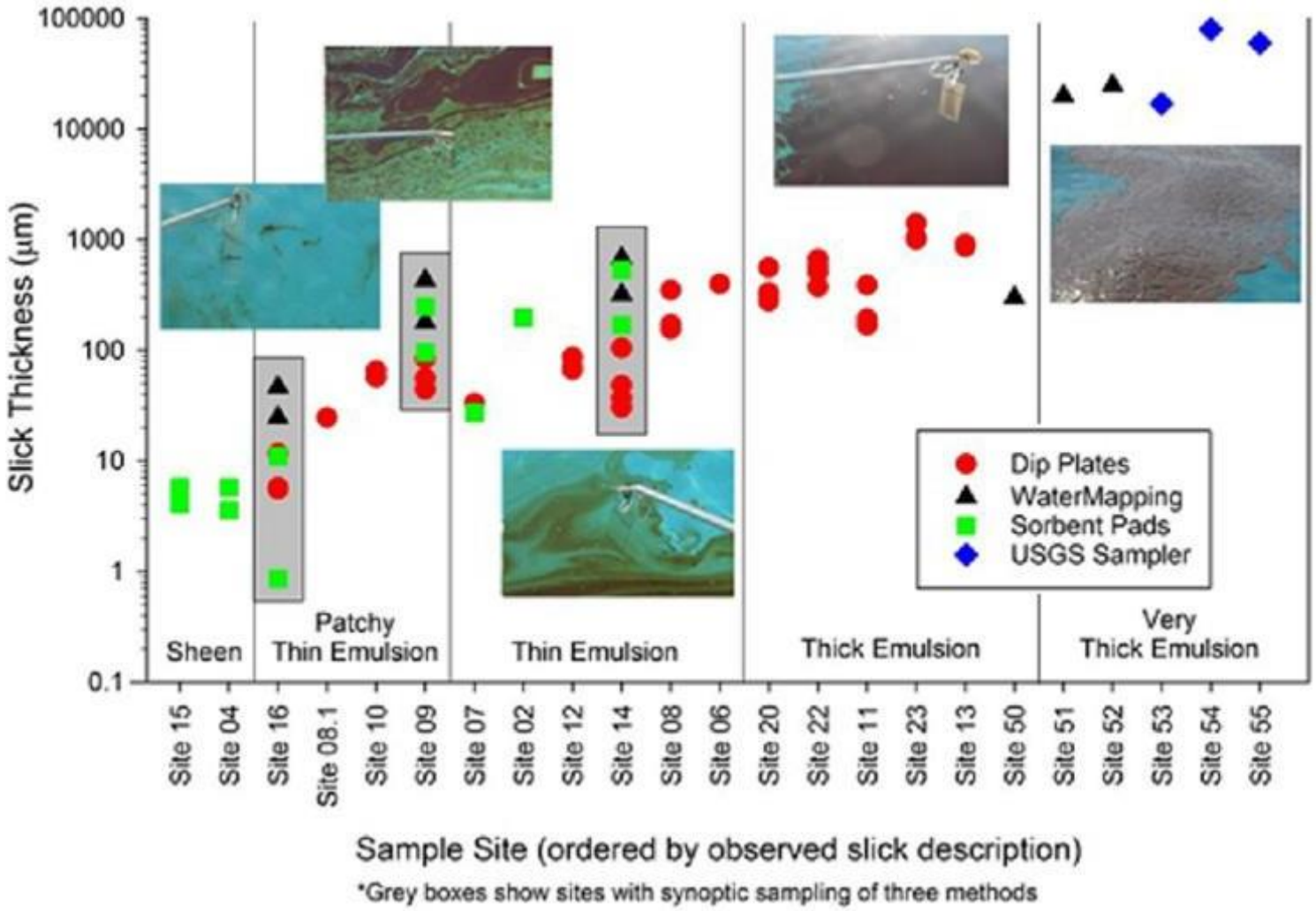

Source: Abt Ohmsett report (Attachment A), Figure 8.

Figure 3.20. Photograph taken underneath the Ohmsett oil slick, demonstrating the heterogeneity of the emulsified oil.

Source: Ohmsett photograph. See Ocean Imaging, 2016, Figure 13 (Attachment C).

3.2.2 USF

Because of the variability of the thickness measurements and the heterogeneity of the slicks, we conducted the controlled laboratory study at USF to assess and validate the three slick thickness methods used in the field. Under more controlled conditions, each of the three methods yielded comparable results. However, the study demonstrated that the Water Mapping method was more accurate when the results were calibrated to an empirically derived calibration curve (Figure 3.21). The results from this study demonstrated that we could apply the calibration curve produced using the Canadian oil sands oil to other oils, including the MC20 oil. We also found that the Water Mapping method also benefited from the addition of a solvent, like gasoline, to the sample tubes to help minimize the amount of oil that adhered to the sides of the tube. With the addition of the solvent and the application of the calibration curve, we found that the Water Mapping method was generally more accurate and precise than the other two methods (Figure 3.22).

Although the USF study occurred after the November 2016 sampling trip to MC20, we re-analyzed the November 2016 data with the calibration curve to determine slick thickness. We were unable to do this for the Ohmsett results because Dr. Garcia changed the sampling design after Ohmsett and the data were not directly comparable with the data used to generate the calibration curve.

Figure 3.21. Water Mapping sampler calibration curve prepared using Canadian tar sands oil.

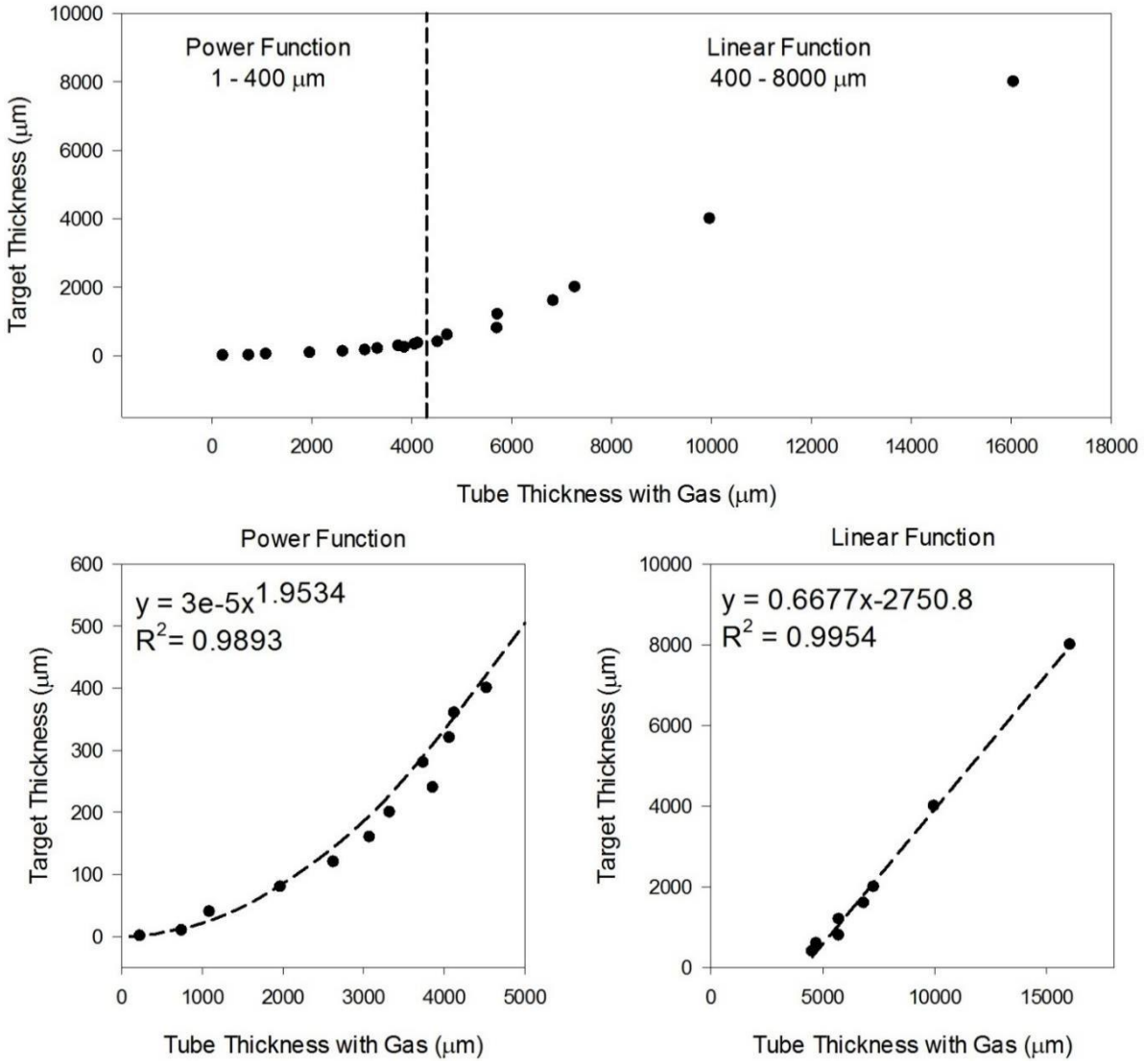

Source: Abt USF data report (see Attachment E), Figure 11.

Compared to our other two methods, the Water Mapping sampler also demonstrated the largest working range, with the ability to measure slicks ranging in thickness from around 10–20 µm to about 10,000 µm (Figures 3.19 and 3.21). However, each thickness measurement requires deploying the sampler with a new sample collection tube, and the analysis requires time-consuming measurements in a laboratory, limiting the number of samples that can be collected and analyzed. In addition, this method provides only the measured thickness of a circle of oil slick less than 4 cm (1.6 in) in diameter, an area that may not necessarily be representative of the thickness of a larger, heterogeneous slick area.

Figure 3.22. Comparison of the three slick thickness measurement methods using different oils across a range of slick thicknesses.
COS = Canadian oil sands crude, WT = West Texas intermediate crude, Tay = MC20 (Taylor Energy) oil, SA = DWH Slick A.

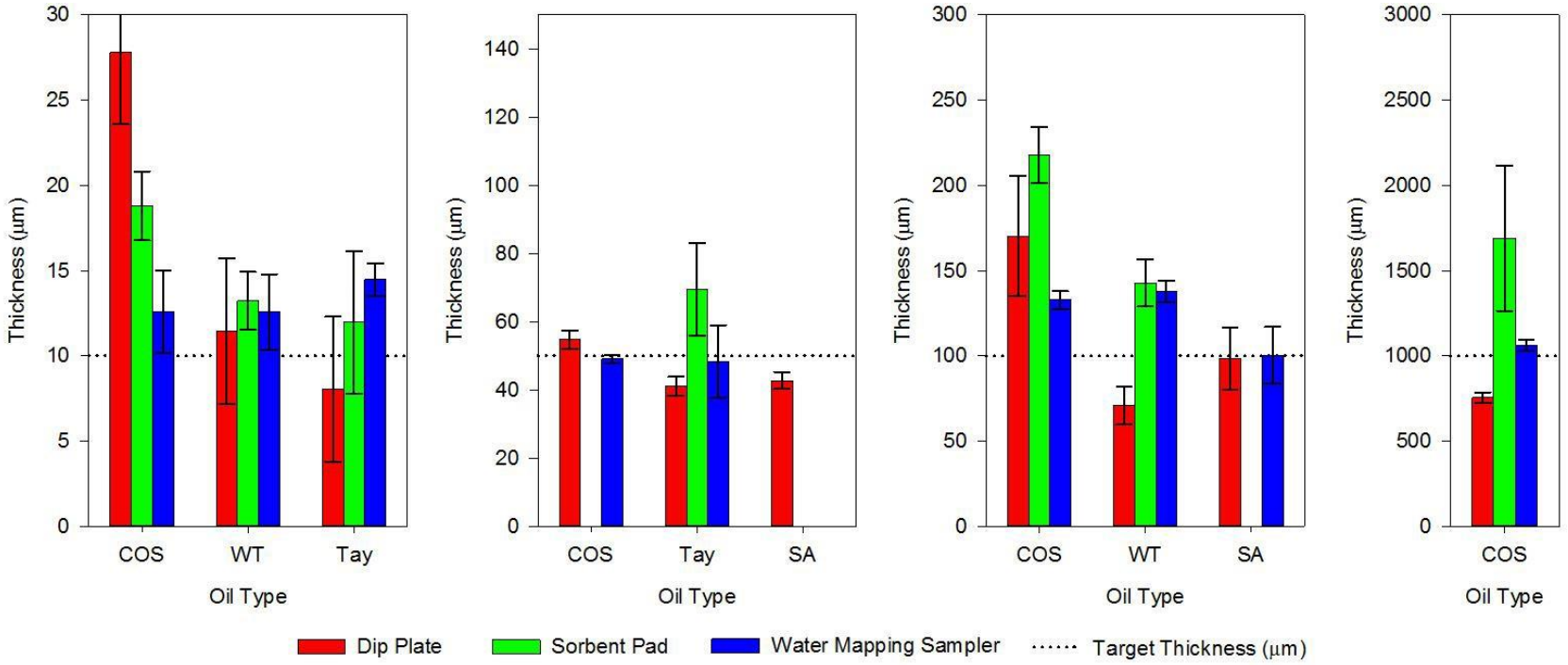

Source: Abt USF data report (see Attachment E), Figure 13.

The sorbent pad method was the least accurate of the three methods (Figure 3.22). The pads overestimated slick thickness across all oil types and volumes. Sorbent pad measurements are also costly, because they require digestion and analysis at a chemical laboratory, which limits the number of samples that can be collected for a project. In addition, the data from the sorbent pad analyses typically take several weeks to be delivered. While there seem to be many disadvantages with the sorbent pad method, it is the most well-established and commonly used method reported in the literature (Parker and Cormack, 1979; Lichtenthaler and Daling, 1985; Daling and Leirvek, 2002). This method also provides thickness estimates for oil sheens, which the other two methods were not able to measure.

Finally, while the dip plate method was generally accurate for many slick thicknesses, the application to unknown slick thicknesses is complicated because of the apparent change in oil adherence that occurred when slicks are 100 µm or greater in thickness (see Attachment E). In addition, the dip plates were limited to a narrower range of thicknesses, with an empirically derived range of about 10-µm to 1,000-µm of slick thickness (Figure 3.22). However, dip plates are the easiest and least-expensive method to deploy, allowing considerably more measurements to be taken compared to the other two methods, and with a much faster turnaround time. Given the heterogeneity of oil slicks in the environment, the ability to collect numerous measurements with higher uncertainty can be more helpful for characterizing overall average slick thickness than collecting a small number of more accurate samples.

3.2.3 MC20: November 2016

We compiled slick thickness measurements from the November 2016 sampling trip, organized by visual slick thickness and separated by waypoint. At several waypoints, we collected co-located samples using one or more of our slick thickness measurement methods. At most of the locations with co-located samples, we found that co-located samples had thickness measurements that differed by orders of magnitude (Figure 3.23). This was similar to the variability we saw between co-located samples collected at the Ohmsett facility. Given the USF study demonstrated that each method was generally accurate within a factor of two, these differences are likely the result of the heterogeneity of the slick being sampled.

To establish detection limits, we also collected dip plate and sorbent pad measurements at one background site (Figure 3.23). For the sorbent pads, the measured oil thickness was well below 0.1 µm. For the dip plate method, however, we measured an average oil thickness (± standard deviation) of 8.0 ± 5.1 µm at the background site. As noted previously, oil sheens in the 10-µm range are below the reliable detection limit for dip plates. These plates may have had residual water that increased the weight of the plate. In subsequent sampling events, we purposefully shook excess water from the dip plate, improving the detection limit reported above. Many slick thickness measurements by dip plate in November 2016 were in rainbow sheen with emulsion not much thicker than 10 µm (Figure 3.23), and thus these data should be used with caution.

Figure 3.23. Slick thickness measurements taken during the November 2016 sampling trip using three different measurement methods. Thickness measurements that were zero are shown as a thickness of 0.01 µm in this plot. Because the dip plate method had positive oil measurements in the reference area (likely caused by water droplets increasing the mass of the dip plate), any dip plate slick thickness measurements near or below 10 µm are unreliable.

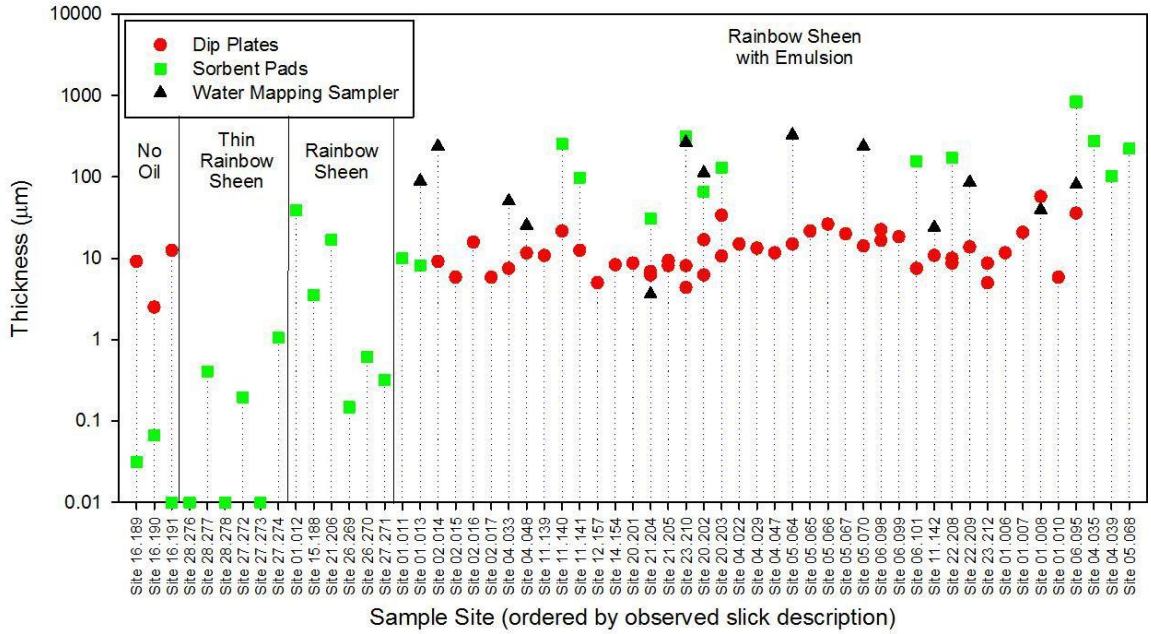

At sites with visible emulsions, the thickest slick measurements were generally 100–300 µm, with one measurement collected at Site 06 as high as 766 µm. At these same sites, the lower range of measured thicknesses was around 5–10 µm. As discussed above, this variability is likely due to the variability of the slick, which has patches of thicker emulsions that were generally up to 300-µm thick, interspersed with rainbow sheen that is only 5–10-µm thick (Figure 3.24).

For sites with only rainbow sheen and no visible emulsion, the measured thicknesses ranged from < 1 to 40 µm; and for sites with a thin rainbow sheen, the measured thicknesses ranged from < 0.03 (not detected) to 1 µm. Overall, these ranges are in line with the thicknesses we would expect to have according to our visible description of the slick and the Bonn Agreement (2009). This not only corroborates our results, but also demonstrates the utility of visual observation for estimating slick thickness (Bonn Agreement, 2009).

Figure 3.24. Heterogeneity of the MC20 oil slick on November 16, 2016, captured by digital camera from the boat.

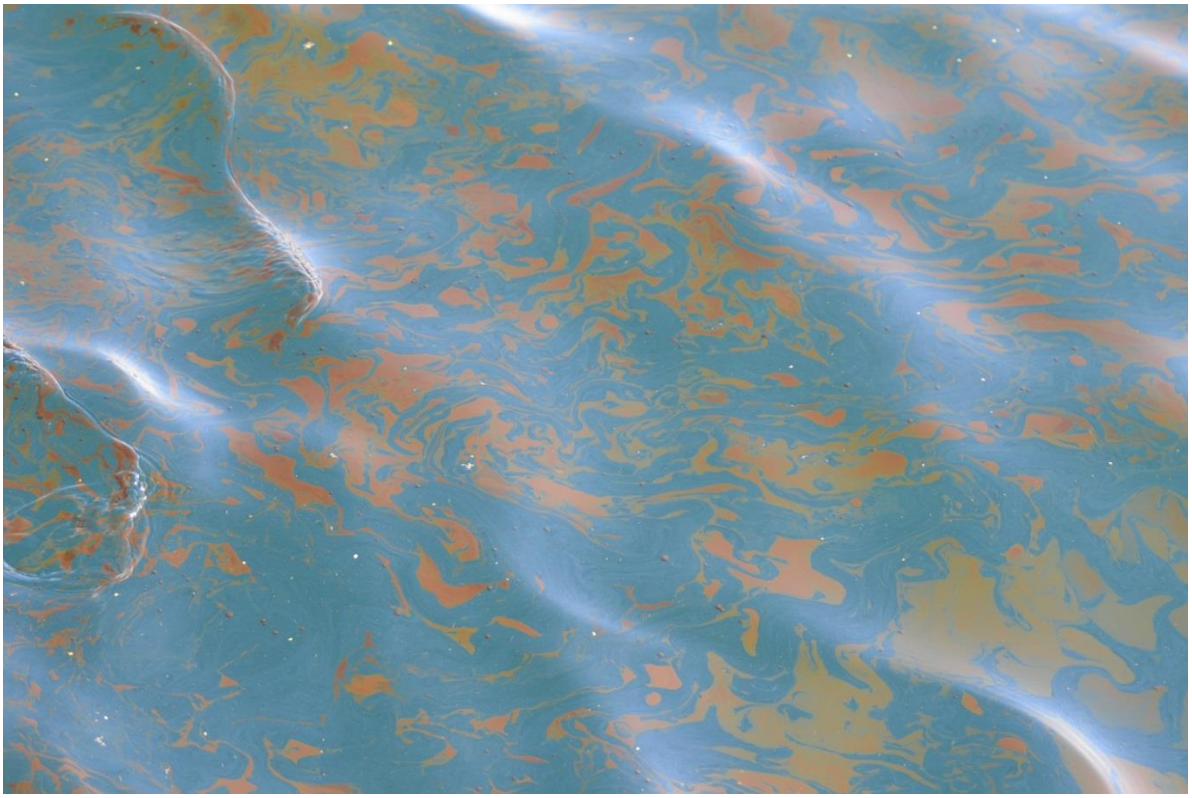

Source: George Graettinger, NOAA.

3.2.4 MC20: April 2017

In April 2017, we sampled one background site and two oiled sites. The measured slick thicknesses at the oiled site with rainbow sheen ranged from < 0.03 µm (below detection) to 30 µm (Figure 3.25). At the site with visible emulsion, the slick thickness measurements ranged from 4 µm to 255 µm (Figure 3.25). We do not have reference area data from April 2017; therefore, based on the November 2016 data, we advise caution when interpreting dip plate data when the slick thickness is near or below 10 µm.

Again, these thickness ranges are consistent with the expected ranges described in the Bonn Agreement (2009). Similar to the November 2016 sampling trip, we saw slick thickness measurements that ranged by more than an order of magnitude at many of the sites where we collected co-located samples.

Figure 3.25. Slick thickness measurements taken during the April 2017 sampling trip using three different measurement methods. Thickness measurements that were zero are shown as a thickness of 0.01 µm in this plot. No reference sites were sampled on this trip, and no sorbent pads were deployed at the rainbow sheen with emulsion sites.

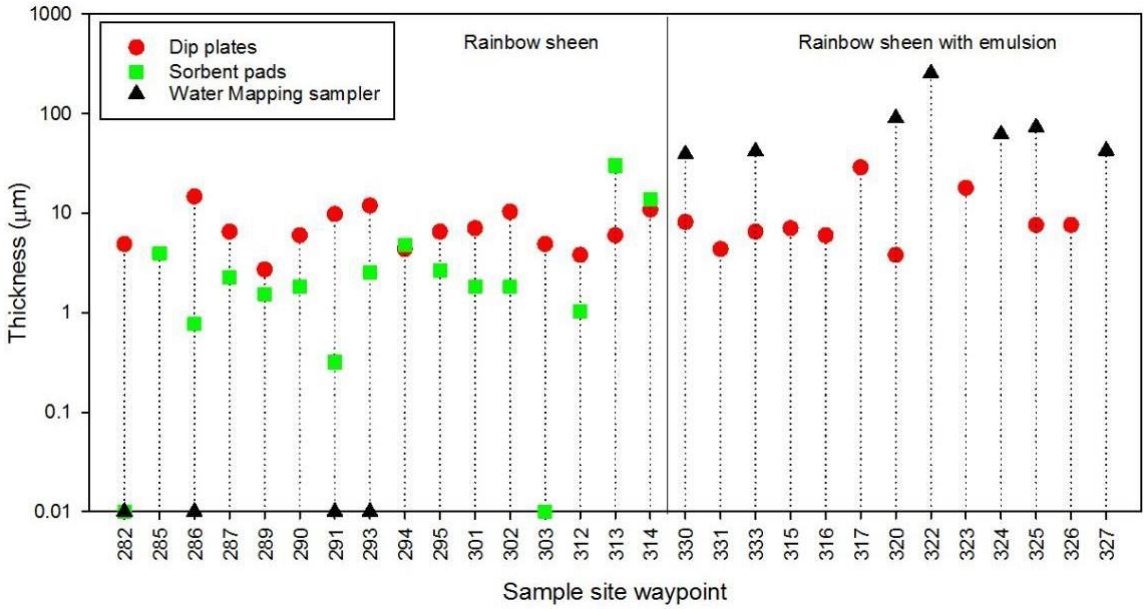

3.2.5 MC20: August 2017

During the August 2017 sampling trip, there were no visible emulsions. The reference site had only a sorbent pad collection. Most oiled sites sampled were described as having a rainbow or metallic sheen. During this trip, the slick thickness measurements ranged from < 0.03 (below detection) to 32 µm (Figure 3.26). Again, co-located samples had thickness measurements that differed by more than an order of magnitude.

Figure 3.26. Slick thickness measurements taken during the August 2017 sampling trip using three different measurement methods. Thickness measurements that were zero are shown as a thickness of 0.01 µm in this plot. No dip plate samples were collected in the reference area.

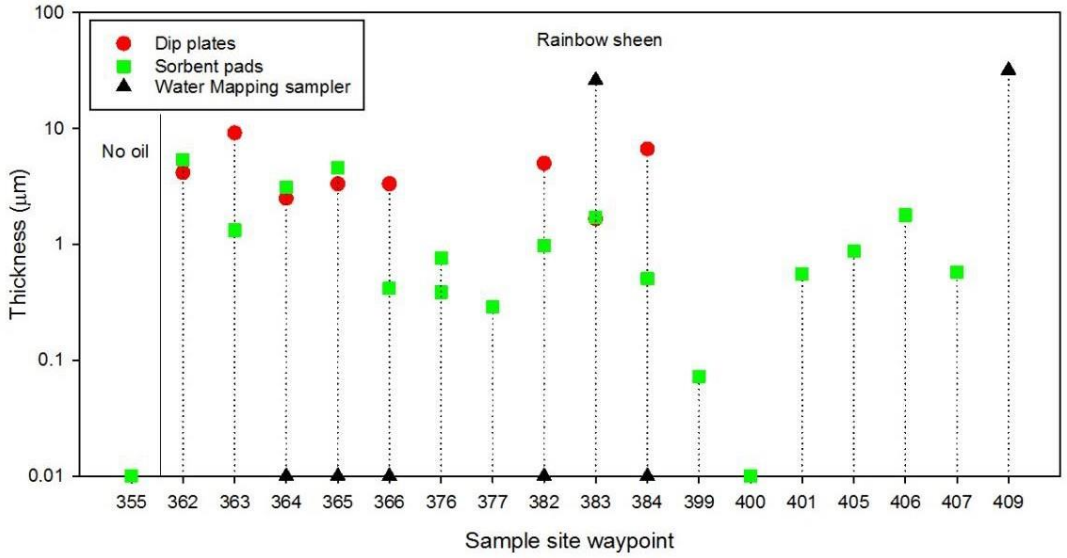

3.2.6 Summary

The dip plate method, the sorbent pad method, and the Water Mapping sampler each had advantages and disadvantages. The Water Mapping method accurately measured a wide range of slick thicknesses at low sample collection and analysis costs. However, only a limited number of samples could be collected in a day, each requiring photographic analysis later, and each measuring only an area of approximately 4 cm in diameter. Thus, the method may not capture an average thickness given the wide variability in slick thickness in the field.

Dip plate measurements were also very low cost and easy to collect. However, the range of thicknesses that the dip plates accurately measured was much narrower than the Water Mapping sampler. The sorbent pad method could more accurately measure the thickness of thinner sheens. However, to determine thickness, the sorbent pads required costly analysis. Furthermore, our laboratory study at USF demonstrated that the sorbent pad method was potentially less accurate and vulnerable to overestimation.

When measuring slicks side-by-side in a controlled laboratory environment, we found that all three methods accurately and precisely measured slick thickness within a factor of two. However, when we used these methods at the Ohmsett facility or in the field, we frequently had thickness measurements that varied by 1–2 orders of magnitude despite being collected at the same time and place. The variability seen in these measurements likely represents the patchiness of the slick being sampled (see, for example, Figure 3.24). The wide range of in situ measurements at coincident locations complicates defining a single slick thickness for a specific location.

Despite these challenges, we did see consistency in the range of thicknesses measured at sites with visually similar slicks. For example, for all three sampling trips, we collected thickness measurements at sites with rainbow sheen. For average thickness measurements from the sites with rainbow sheen for each sampling trip, we obtained a similar average slick thickness of 7 µm, 5 µm, and 4 µm, for November 2016, April 2017, and August 2017, respectively.[1] The range of thicknesses measured at sites with rainbow sheen are similar across the three sampling trips (Table 3.1; see also Figures 3.23, 3.25, and 3.26). Furthermore, our measured thicknesses agree reasonably well with the slick thickness oil appearance categories laid out in the Bonn Agreement Aerials Operations Handbook (Bonn Agreement, 2009). For example, the thickness of a rainbow-colored sheen is expected to fall within the range of 0.3 to 5.0 µm, while a discontinuous true oil color (i.e., what we describe as visible emulsion) is expected to start at 50 µm and the true oil color is expected to become more continuous at 200 µm (Table 3.1).

Whether prepared in a laboratory or found in the field, oil slicks are highly heterogeneous. Consequently, precisely quantifying slick thickness, especially across large areas, is immensely challenging, as our results show. However, even with this degree of variability and uncertainty, slick thickness measurements are a helpful metric for describing an oil slick and relating remote sensing data to water column PAH data.

1. We included data from dip plate and Water Mapping samplers, despite the variability in measuring thin sheens with those methods. The average thicknesses are almost identical if we use only sorbent pad data.

Table 3.1. Bonn Agreement (2009) descriptions of slick thickness by oil appearance compared to visible descriptions and measured thicknesses at MC20

Bonn description of slick appearance	Bonn slick thickness range (µm)	MC20 description of slick appearance	MC20 slick thickness range (µm)
Sheen (silvery/grey)	0.04–0.30	Light sheen	Non detect–0.41
Rainbow	0.30–5.0	Thin rainbow sheen	Non detect–15
Metallic	5.0–50	Heavy rainbow sheen	0.15–39
Discontinuous true oil color	50–200	Rainbow sheen with emulsion	3.6–760
Continuous true oil color	More than 200		

3.3 Water/Oil Sampling

Below we describe the water and bulk oil results from the Ohmsett study and the three sampling trips.

3.3.1 Ohmsett

At the Ohmsett facility, we collected bulk oil samples regularly from the tank to track changes in the slick oil's physical and chemical properties throughout the study. Our results show that both oil density and viscosity increased over time (Figure 3.27). One of the sharpest increases in both oil density and viscosity occurred between the morning and the afternoon of July 18, 2016, just after the wave generators were turned on. This reflects the physical changes to the oil as emulsifications started to form. By that afternoon, the bulk oil already contained 80% water, indicating the rapid formation of emulsified oil.

A high water percentage in the surface oil was maintained throughout the rest of the study, except for a sudden dip on the seventh day (July 20, 2016), after the wave generators had been turned off for several hours. On that day, we saw a corresponding increase in the bulk oil TPH concentration, corroborating the decrease in the water percentage in the surface oil.

Oil droplets started to mix into the water column after the wave generators were started (Figure 3.28). As a result, TPH concentrations in the water increased four-fold between the third day (July 16, 2016), before the wave generators were turned on; and the fifth day (July 18, 2016), just after the wave generators were turned on (Figure 3.29). Water TPH concentrations, along with TPH concentrations estimated from our fluorescence measurements (see Attachment A, Section 3.4), corroborated the observed mixing of oil droplets in the water column (Figures 3.28 and 3.29). In fact, instead of a decrease in concentration with depth, as expected by oil dispersion theory (Delvigne and Sweeney, 1988), we observed an increase. This increase with depth was observed with samples collected both before and after wave generation; however, it was more pronounced after wave generation.

One explanation for this observed increase in concentration with depth could be boundary effects from the tank sides and bottom (i.e., the currents in the tank moved oil to depth because they were constrained from moving laterally). However, the observed increase in concentration started with samples collected from 0.2 m, which is well above the tank bottom, and all samples were collected from the middle of tank, almost 10 m away from the tank sides. It is unlikely that lateral constraints were responsible for increasing the oil concentration below the surface at these locations.

Figure 3.27. Changes in physicochemical properties of slick oil over time.

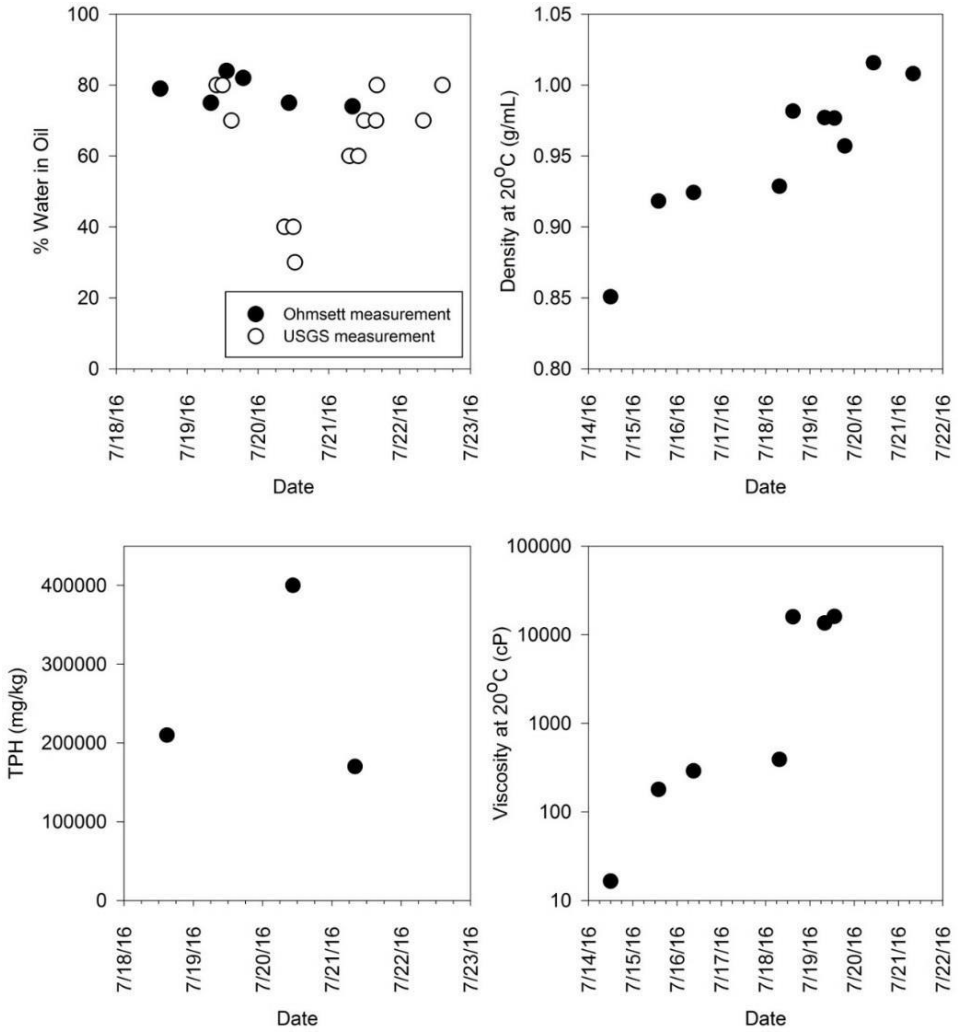

If the Ohmsett tank were a fully mixed system, we would expect to see no change in concentration with depth, however, we consistently see an increase in concentration with depth.

Overall, we found that petroleum hydrocarbons mix into the water column below a slick regardless of whether there is wave action, but the mixing is more pronounced when waves are present. Compared to the literature, the data suggest that mixing in the Ohmsett wave tank may not mimic mixing in the field.

Figure 3.28. Oil droplets mixing into the water column and emulsifying after the wave generators started at Ohmsett. The photograph was taken from an underwater observation window.

Source: George Graettinger, NOAA.

Figure 3.29. Measured and estimated TPH concentrations (µg/L) before and after wave generation versus sample depth (m). Measured TPH concentrations were reported by an analytical laboratory and estimated TPH concentrations were developed from a fluorescence measurement using the regression reported in Attachment A, Section 3.4.

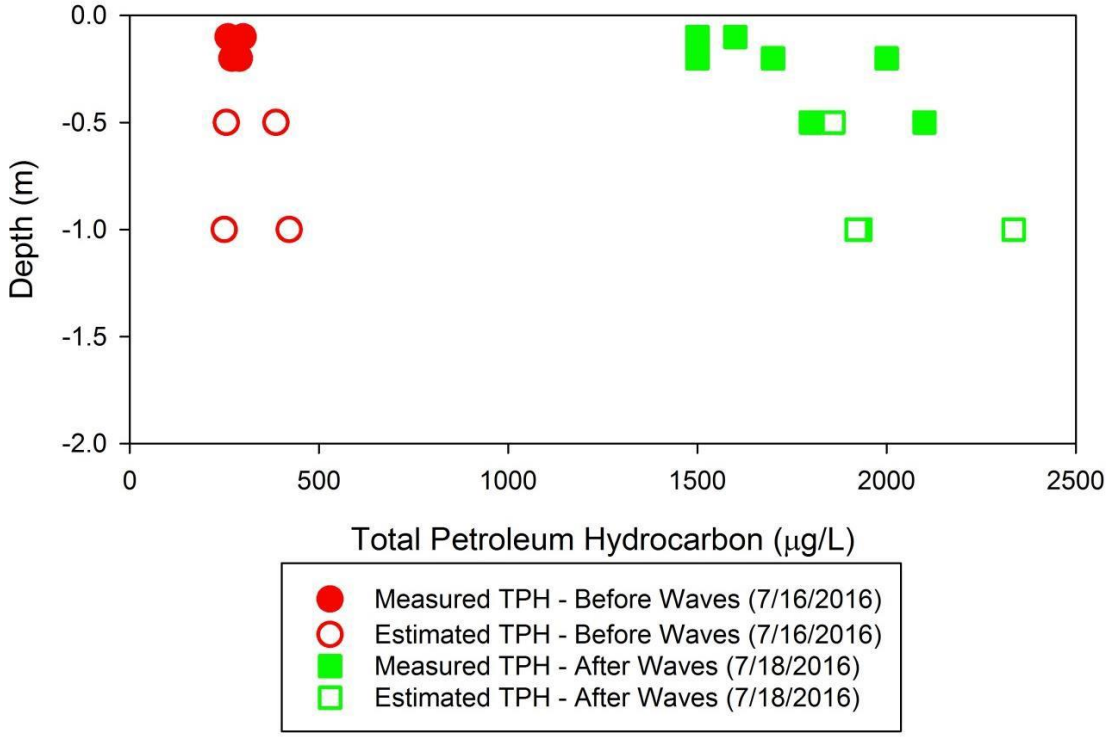

3.3.2 MC20: November 2016

In November 2016, we collected water sample profiles at five oiled sites and a sample at one background site. Figure 3.30 shows photographs of the oil slick at each oil site. The TPH concentrations from the oiled sites ranged from 300 µg/L TPH to 45,000 µg/L TPH. At the background site, the TPH concentration was 470 µg/L TPH.

In addition, we collected two bulk oil samples for physical and chemical characterization, showing lightly emulsified oil (water content below 50%) and PAH profiles similar to oil samples from MC252 (the lease block where the DWH spill occurred). We present this data and other petroleum chemistry data in Section 3.3.5.

Figure 3.30. Photographs of the oil slick at the five oiled sites from the November 2016 sampling trip with measured water profile concentrations.

Photo credits. George Graettinger, NOAA.

3.3.3 MC20: April 2017

In April 2017, we also collected water sample profiles at two oiled sites and one background site. Figure 3.31 shows photographs of the oil slick at each oil site. The TPH concentrations in the oiled samples (290 µg/L to 433 µg/L) were similar to the concentrations in background samples.

In addition, we collected a single bulk oil sample, showing highly emulsified oil (73% water). We present these and additional TPH data in Section 3.3.5.

Figure 3.31. Photographs of the oil slick at the two oiled sites from the April 2017 sampling trip with measured water profile concentrations.

Photo credits: George Graettinger, NOAA.

3.3.4 MC20: August 2017

The oil slicks during the August 2017 sampling trip were too thin to permit bulk oil collection using dip plates or the oil cloth device developed by Dr. Moon. During this trip, we collected water profiles at five oiled sites and one background site. Figure 3.32 shows photographs of three of the oil slick sample sites. Similar to the April 2017 sampling trip, the TPH concentrations in the slick samples were close to background concentrations.

3.3.5 Additional Data and Analysis

The two bulk oil samples collected during the November 2016 sampling trip indicate that the slick oil at the MC20 site was lightly emulsified, with the water content well below 50% (Table 3.2). By comparison, the bulk oil sample collected in April 2017 contained 73% water, suggesting that the slick oil in April was much more heavily emulsified. The differences in water content between the November and April samples were also reflected in the TPH and TPAH50 concentrations of the oil samples, where concentrations of both TPH and TPAH50 were inversely related to water content (Table 3.2).

All three oils demonstrated similar weathering states of around 70% depletion of TPAH51 (TPAH50 + perylene) relative to hopane (Table 3.2). In addition, all three oils had similar PAH compositions, which was similar to the DWH Slick A oil discharged from MC252 (Figure 3.33). The density of the oil samples from the November sampling trip were both near 1 g/mL, while the density of the oil sample from April 2017 was lower at 0.9269 g/mL (Table 3.2).

Figure 3.32. Photographs of the oil slick at three of the oiled sites from the August 2017 sampling trip with measured water profile concentrations.

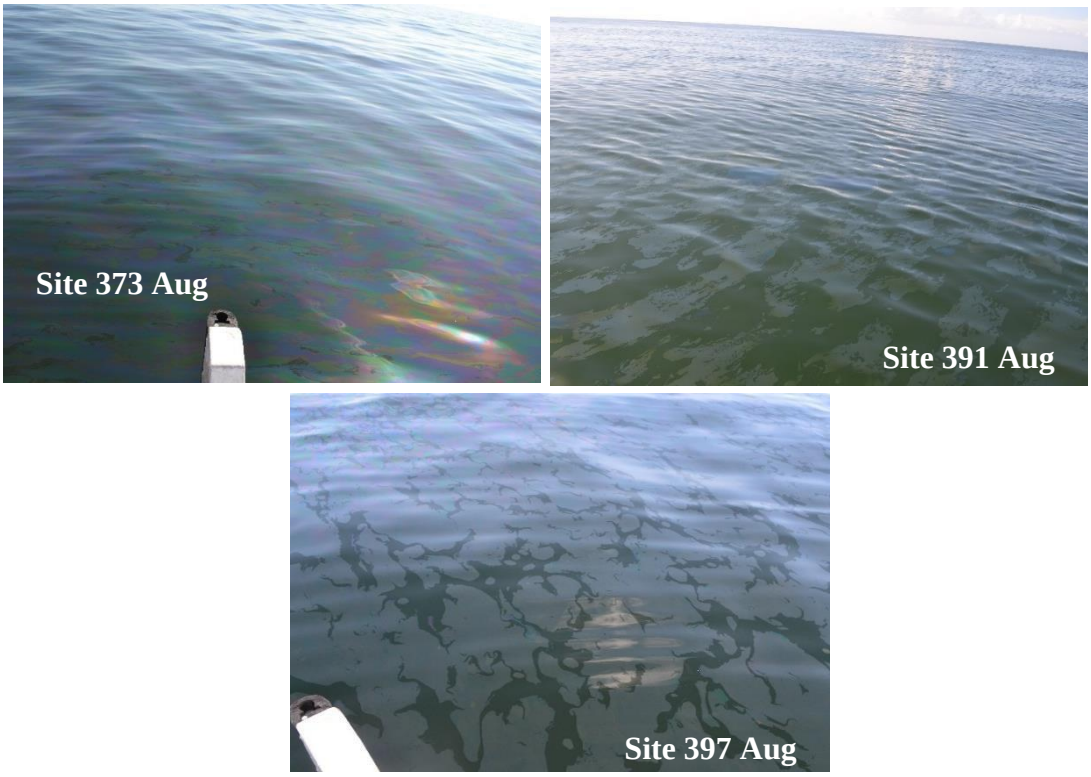

Photo credits: George Graettinger, NOAA

Table 3.2. Bulk oil characterization from November 2016 and April 2017 sampling trips

Sample ID	Date	Latitude	Longitude	Density (g/mL)	Water content (%)	TPH (mg/kg)	TPAH50 (mg/kg)	TPAH50: TPH	%weathered[a]
Taylor-A1115-BO05-07	11/15/2016	28.937219	-88.972446	0.9700	33	500,000	5,001	0.010	69.4
Taylor-A1115-BO06-06	11/15/2016	28.937104	-88.970419	1.004	17	600,000	5,004	0.008	69.4
Taylor-B0425-OL01-01	4/25/2017	28.941282	-88.961985	0.9269	73	260,000	3,812	0.015	72.0

a. % weathered calculation is based on the relative depletion of TPAH50 relative to hopane, using the DWH source oil from MC252 as a surrogate for unweathered MC20 oil.

Figure 3.33. Percent composition of PAHs in the three MC20 (Taylor) bulk oil samples and DWH Slick A oil discharged from MC252.

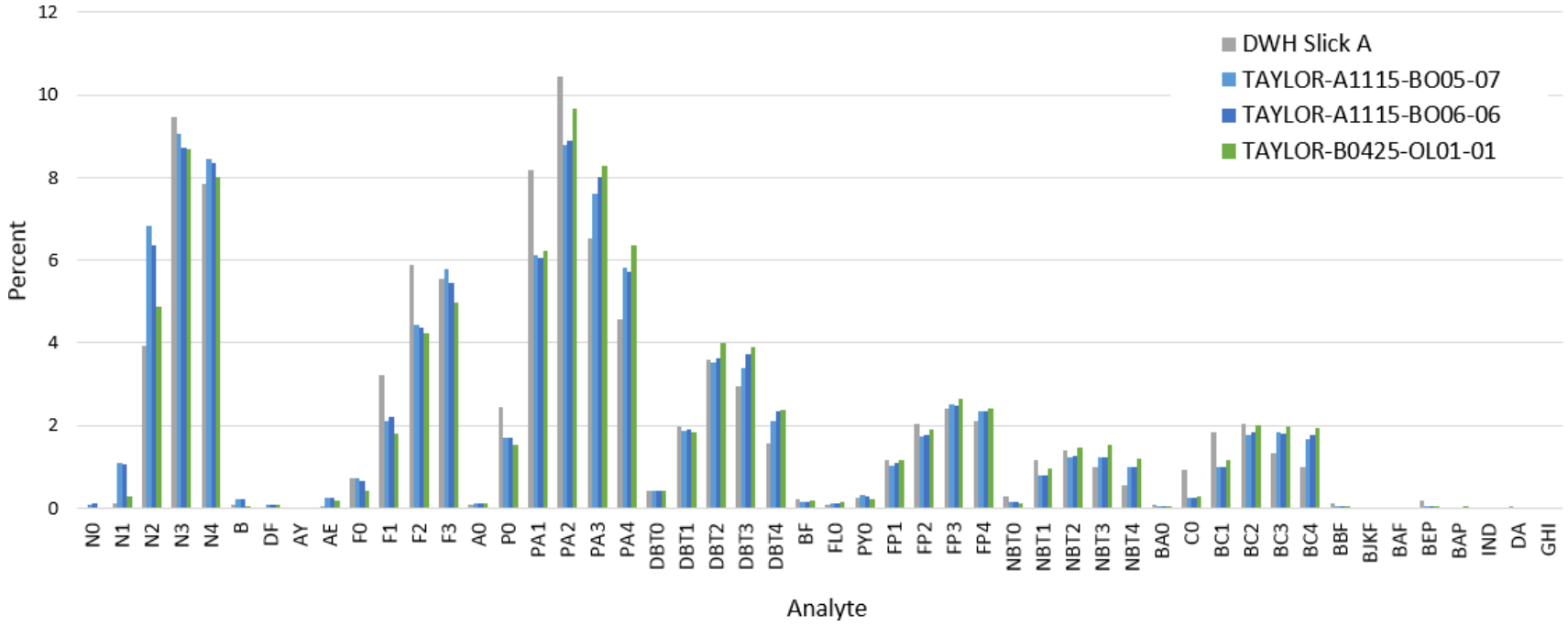

Across the three sampling trips we saw a range in both the amount and extent of dispersed oil in the water column (Figure 3.34). As we would expect from oil dispersion theory (Delvigne and Sweeney, 1988), the differences in observed oil dispersion generally trended with differences in wind intensity and oil slick thickness (Table 3.3). For example, across all trips we experienced the greatest wind speeds during the beginning of the November 2016 sampling trip with a gradual decline in wind speed as the week progressed (Table 3.3; Figure 3.35). The only two sites with TPH concentrations that were elevated compared to background at a depth of 1 m or greater were Sites 03 and 06, which were sampled during the first two days. The highest TPH water concentration measured at a depth of 3 m was collected from Site 03 on the first day, which was the windiest day of the week. By contrast, the sites sampled later that week, as well as all sites sampled in 2017, contained little TPH at depths greater than 1 m.

In the upper water column, we observed elevated TPH concentrations compared to background at all oiled sites sampled during the November 2016 trip; by contrast, TPH concentrations were not elevated in the upper water column under slick-covered sites sampled during either trip in 2017. Again, this trend corresponds to the differences in wind speed, where winds were generally higher throughout the entire week in November compared to wind speeds measured during the two 2017 sampling trips (Table 3.3).

Another influencing factor in the amount of oil dispersed in the water column was slick thickness. The site with the thickest oil (Site 06 from November 2016) had the greatest amount of vertical oil dispersion in the water profile (Figure 3.34). Although the wind intensity was greater during sampling at Site 03 from November 2016, the oil slick was considerably thinner (Table 3.3). Consequently, the concentrations in the uppermost water column were lower at Site 03 compared to Site 06, and the overall amount of oil in the water column across the entire profile was less despite having greater concentrations at deeper depths.

Sites 12 and 15 had relatively thick oil but lower wind speeds compared to Sites 03 and 06. In this case, the measured TPH concentrations in the upper water column from Sites 12 and 15 were similar to the TPH concentrations measured at Sites 03 and 06. However, the oil was not dispersed deeper into the water column (Figure 3.34).

For the 2017 sampling trips, we measured PAH concentrations in addition to TPH in the shallowest water sample from each site. PAHs not only represent one of the most toxic fraction in the oil, but they are also a more selective measure of oil dispersion, with lower overall background concentrations in the water than TPH. For example, while we did not observe any noticeable increase in TPH concentrations in the water column compared to background for the sites sampled in 2017, we did find increased TPAH50 concentrations in the upper water column compared to background at both oiled sites sampled in April 2017 and at one of the oiled sites sampled in August 2017, relative to concentrations at sites with no observed oil (Table 3.4).

PAH concentrations generally varied with both wind speed and slick thickness. For example, across all three trips, the wind speed was the lowest and the sea the calmest during the August 2017 trip, with the second day being calmer than the first day (according to onboard anemometer measurements). Whereas we saw elevated TPAH50 concentrations at both oiled sites in April, we saw elevated TPAH50 concentrations at only one of the five oiled sites sampled during the August trip, and that one site had higher wind speeds than the other four sample sites (Table 3.4). In April, Site 03 had thicker slick oil and greater TPAH50 concentration than Site 01. In August no emulsions or thicker oils were observed and the slick thickness across all sites was generally a thin sheen.

Figure 3.34. TPH concentration in water with depth for the November 2016 (top), April 2017 (middle), and August 2017 (bottom) sampling trips.

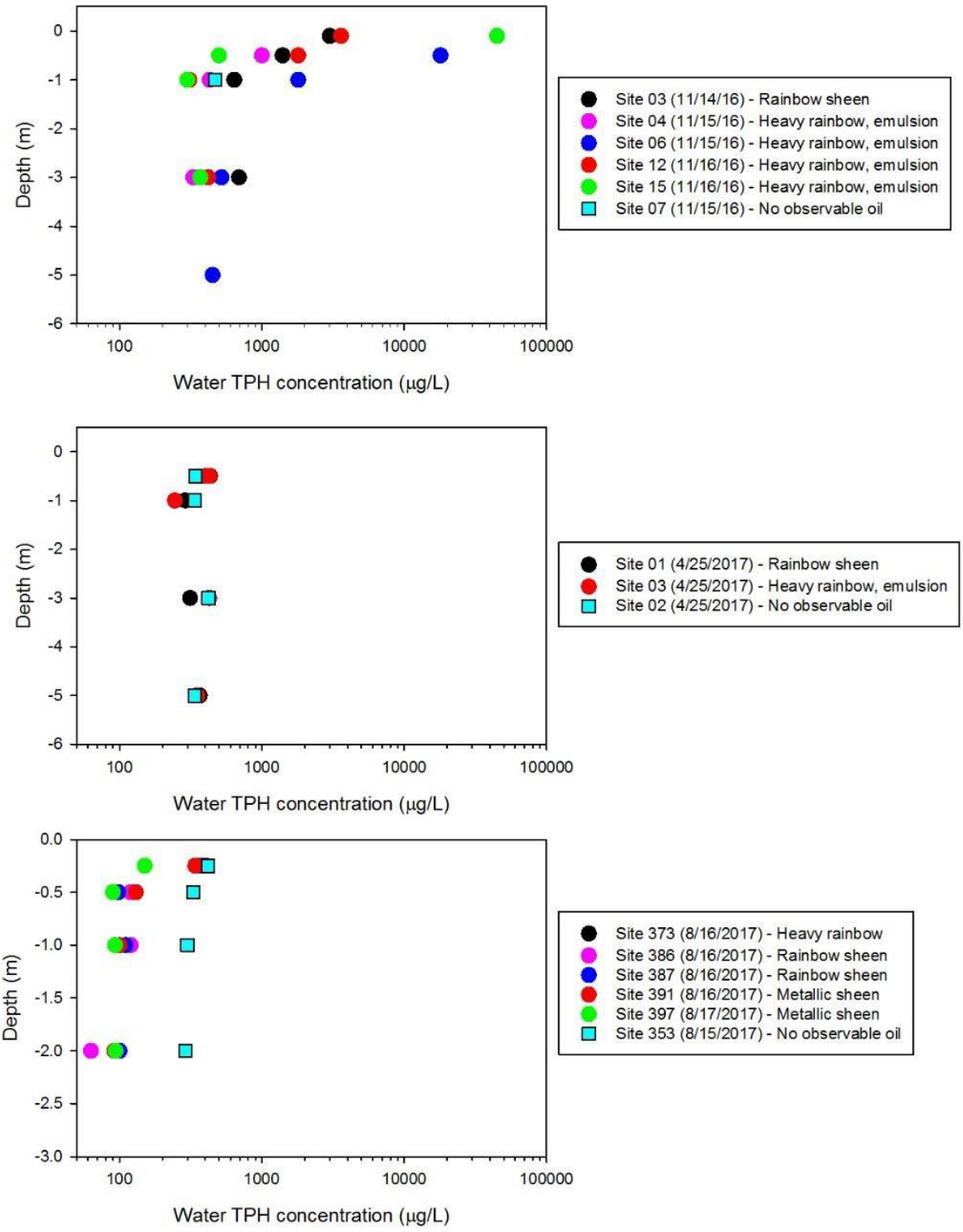

Figure 3.35. Wind speed data from nearby buoys and onboard anemometer measurements from each sampling trip.

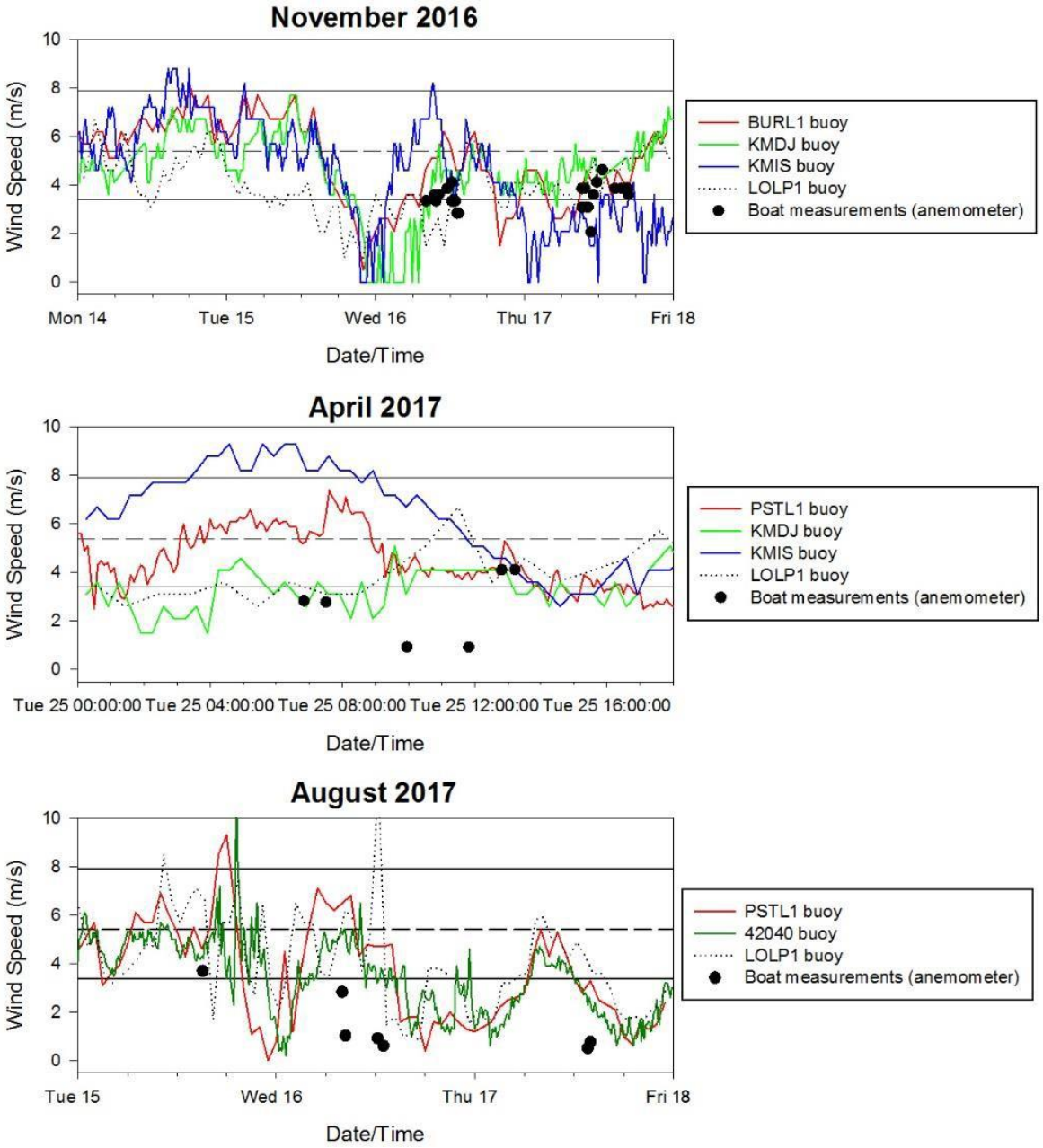

Table 3.3. Wind speed and average slick thickness at water profile sites. Boat wind speeds were determined by averaging handheld anemometer measurements collected on the boat prior to the time of the water sampling at each site. Buoy wind speeds are determined by averaging measurements starting four hours before sampling to the time of sampling at each site.

Date	Time	Site	Boat wind speed (m/s)	KMDJ buoy wind speed (m/s)	KMIS buoy wind speed (m/s)	Average slick thickness (µm)
11/14/2016	12:00	Site 03	NA	5.0	6.3	17
11/15/2016	9:26	Site 04	NA	6.0	5.5	53
11/15/2016	13:49	Site 06	NA	6.8	5.7	136
11/16/2016	12:46	Site 12	3.5	4.3	5.7	44[a]
11/16/2016	13:07	Site 15	3.4	4.4	5.4	44[a]
4/25/2017	9:45	Site 01	2.2	3.1	8.1	4
4/25/2017	12:00	Site 03	1.9	3.6	7	44
8/16/2017	10:00	Site 373	1.9	4.9[b]	5.9[c]	4
8/16/2017	14:00	Site 386	1.6	3.8[b]	4.7[c]	4
8/16/2017	14:16	Site 387	1.6	3.8[b]	4.7[c]	4
8/16/2017	15:50	Site 391	1.4	3.4[b]	3.2[c]	4
8/17/2017	11:50	Site 397	0.5	4.0[b]	4.3[c]	5

a. Due to the lack of measurements at Sites 12 and 15, slick thickness was determined using measurements at Site 11, which had a visually similar slick.

b. There were no records from the KMDJ buoy for the August 2017 sampling trip, so the 42040 buoy measurements are reported instead.

c. There were no records from the KMIS buoy for the August 2017 sampling trip, so the BURL1 buoy measurements are reported instead.

Table 3.4. TPAH50 and TPH concentrations from uppermost sample of each water profile collected during the April and August 2017 sampling trips. TPAH50 concentrations in the water column were higher under slick areas compared to areas with no observed oil, whereas TPH concentrations were not.

Date	Time	Site	Slick description[a]	TPAH50 (µg/L)	TPH (µg/L)
4/25/2017	11:09	Site 02	No observed oil	0.082	342
8/15/2017	17:20	Site 352	No observed oil	0.050	420
4/25/2017	9:45	Site 01	Rainbow sheen	0.172	420
4/25/2017	12:00	Site 03	Heavy rainbow, emulsion	0.286	420
8/16/2017	10:00	Site 373	Heavy rainbow sheen	0.221	400
8/16/2017	14:00	Site 386	Rainbow sheen	0.035	360
8/16/2017	14:16	Site 387	Thin rainbow sheen	0.066	380
8/16/2017	15:50	Site 391	Silvery sheen	0.061	340
8/17/2017	11:50	Site 397	Silvery sheen	0.070	150

a. A visual description of the slick based on site photos.

3.4 Fluorometry

3.4.1 Cyclops

During the November 2016 and the April 2017 sampling trips, we used a handheld Turner Cyclops-7 fluorometer with a crude oil-specific sensor to estimate oil concentrations in the water column. We collected transect and profile data to characterize oil dispersion under the oil slicks. In addition, we collected contemporaneous fluorescence data during all water sampling events to help calibrate the fluorometer.

Profiles

We tested two different methods for collecting profile data using the Turner Designs Cyclops fluorometer. For the first method we started at a specific depth (e.g., just below the water surface) and slowly lowered/raised the fluorometer to the target depth, collecting fluorescence data continuously as the sensor was lowered or raised. We then noted the record number at the start and finish of the profile as well as the starting and ending depths. For the second method, we collected fluorescence data at several discrete depths, collecting continuous data for at least one minute at each depth.

Figure 3.36 shows profiles collected from two background sites, one from within the Mississippi River discharge plume and another in blue waters. Figure 3.37 shows fluorescence profiles collected from six different oiled sites. To compare the two different profiling method, in Figure 3.37 we present data from both the continuous profiling method and the discrete depth profiling method, including two sites where we used both methods.

At the MC20 site, the oil slick typically straddles the Mississippi River plume, made up of organic-rich water from the Mississippi River, and the clear blue water of the Gulf of Mexico. Colored Dissolved Organic Matter (CDOM) and crude oil have overlapping fluorescence spectra, which can complicate the interpretation of fluorescence data (Conmy et al., 2014). We saw the effects of CDOM on background fluorescence at our two background sites, where the background fluorescence within the Mississippi River plume was more than two-fold higher than the background fluorescence in blue water. In addition, within the plume, there was a small but distinct decrease in fluorescence with depth. This behavior is similar to what we would expect to see with the fluorescence signal at a site with oil dispersed beneath a slick, further complicating the data interpretation.

Without additional methods for distinguishing these two sources of fluorescence, the sensitivity, selectivity, and accuracy of fluorometry in detecting and quantifying oil in water can be limited. Newer, more advanced in situ fluorometers are working to better tune their excitation and emission wavelengths to enhance discrimination between crude oil and other interfering fluorophores in the environment such as CDOM. Unfortunately, the Cyclops 7 used during this project encountered significant interference within the plume. To combat this problem, we used a site-specific background fluorescence to determine if the fluorescence signal under the slick was elevated.

Figure 3.36. Fluorescence profiles collected at two background sites.

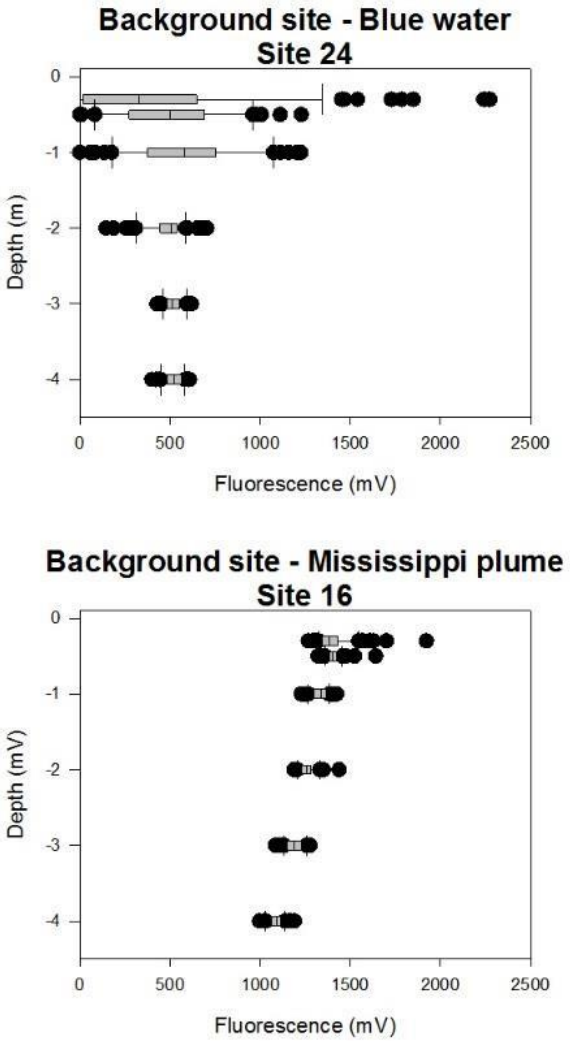

Despite the potential limitations of the Cyclops 7, we saw clear evidence of a crude oil hydrocarbon signal in several of the fluorescence profiles collected during the November 2016 sampling trip. Similar to TPH water profiles described in Section 3.3, the fluorescence profiles show a relationship between wind intensity, slick thickness, and the extent and amount of oil dispersed in the water column. For example, sites with thicker slicks, like Sites 03, 10, 12, 14 and 15 (Figure 3.37), generally demonstrated elevated fluorescence under the slick.

Figure 3.37. Fluorescence profiles collected under different slick conditions. Box plots show data from profiles collected at discrete depths and red squares show profiles where fluorescence data were collected continuously as the fluorometer was raised and/or lowered into the water column. The solid vertical line shows the site-specific background fluorescence. Note X-axis scale change for Site 12.

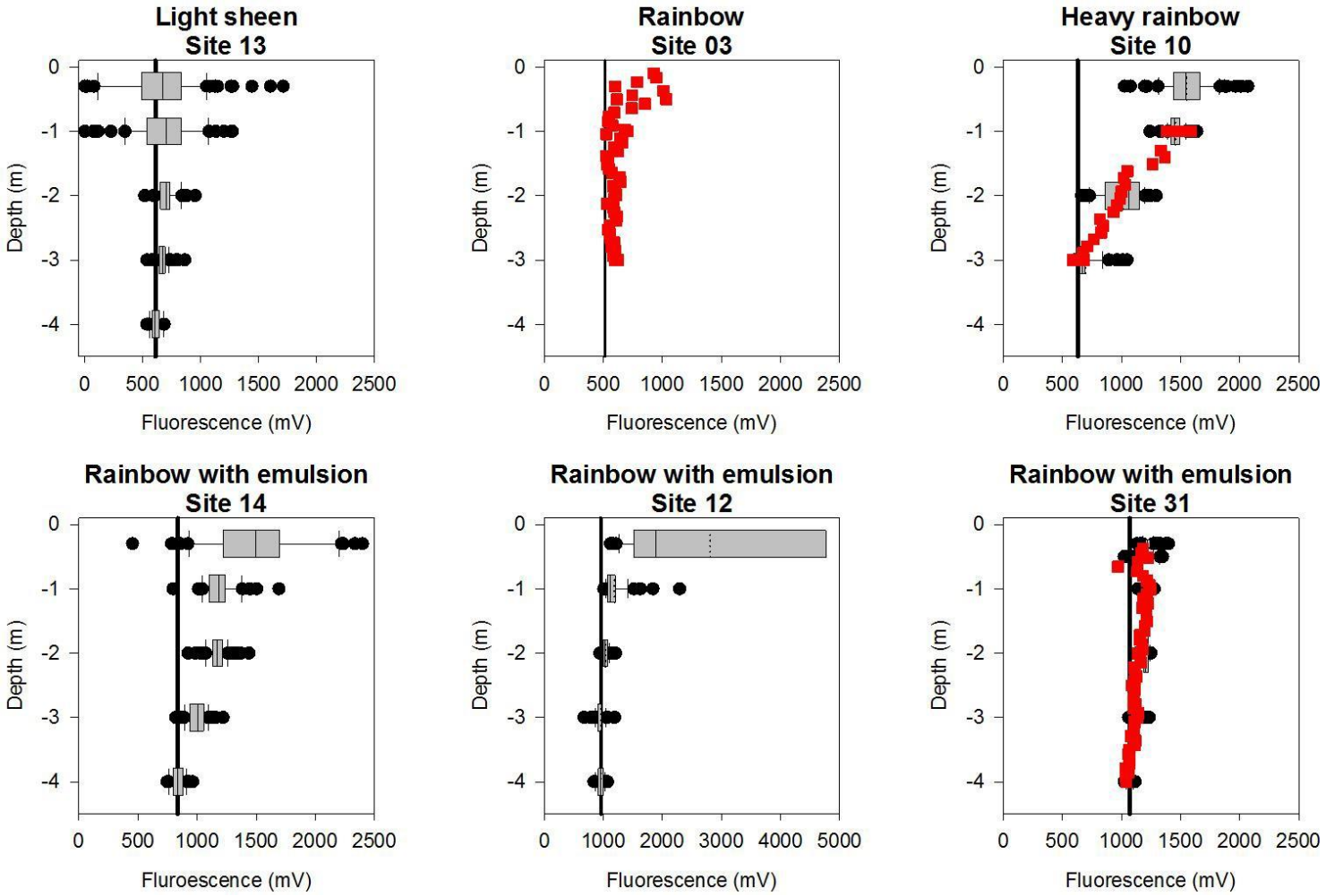

On the other hand, for the fluorescence profile at Site 13 (Figure 3.37), which had a thin sheen, there was little to no increase in fluorescence above the site-specific background, and the profile was similar to the fluorescence profile collected at our background site in blue water. In addition, both sites displayed an interesting increase in the scatter of the fluorescence data at the shallowest depths. Despite having a shade cap over the fluorometer sensor, we hypothesize that this scatter is related in some way to sunlight, given we only saw this behavior at the shallow depths in blue water, where light penetration is greatest. We did not see this behavior at the background site within the Mississippi River plume or sites with thicker oil slicks, both of which would reduce sunlight penetration. Even with the increased noise and scatter in the data at these sites, the median and mean fluorescence concentration of these shallow depths were similar to the fluorescence concentrations measured at deeper depths.

Finally, while the profile at Site 31 was collected under a thicker slick, it was conducted at the end of the last day of the week after several days of declining wind speeds when the sea was relatively calm (see Figure 3.35). Consequently, despite the thicker slick at the surface, we see no evidence of oil dispersion in the water column (Figure 3.37).

Transects

In addition to profiles, we also used the Cyclops-7 fluorometer to collect transects at a number of sites. To collect transect data, we would set the fluorometer at a single depth (typically 1 m) and maneuver the boat into and out of the slick. To mark when we entered or exited different slick areas, we would set GPS waypoints.

Figure 3.38 shows an example of a fluorescence transect from Site 04. In this transect, elevated fluorescence is associated with thicker slicks overhead. However, the spatial extent of the subsurface plume does not exactly match the spatial extent of the overhead slick. We see this in the last panel of Figure 3.38, where our waypoints indicate we have entered a thicker surface slick with emulsion, but there is not a corresponding elevation in the fluorescence signal.

Overall, we conclude that the fluorescence data can provide sufficient information to map the spatial extent of a subsurface oil plume.

TPH versus Fluorescence

During the November 2016 sampling trip, we also recorded spot measurements from the Cyclops-7 fluorometer at the same depths and at the same time that we were collecting water samples. Using these spot measurements and the corresponding TPH concentrations, we plotted fluorescence versus TPH concentration for each site. Generally, we found a linear relationship between fluorescence and TPH concentration when regressed across all sites (Figure 3.39).

Figure 3.38. Fluorescence transect collected at Site 04 on 11/15/2016. Arrows show where we marked waypoints during the transect and provide waypoint description.

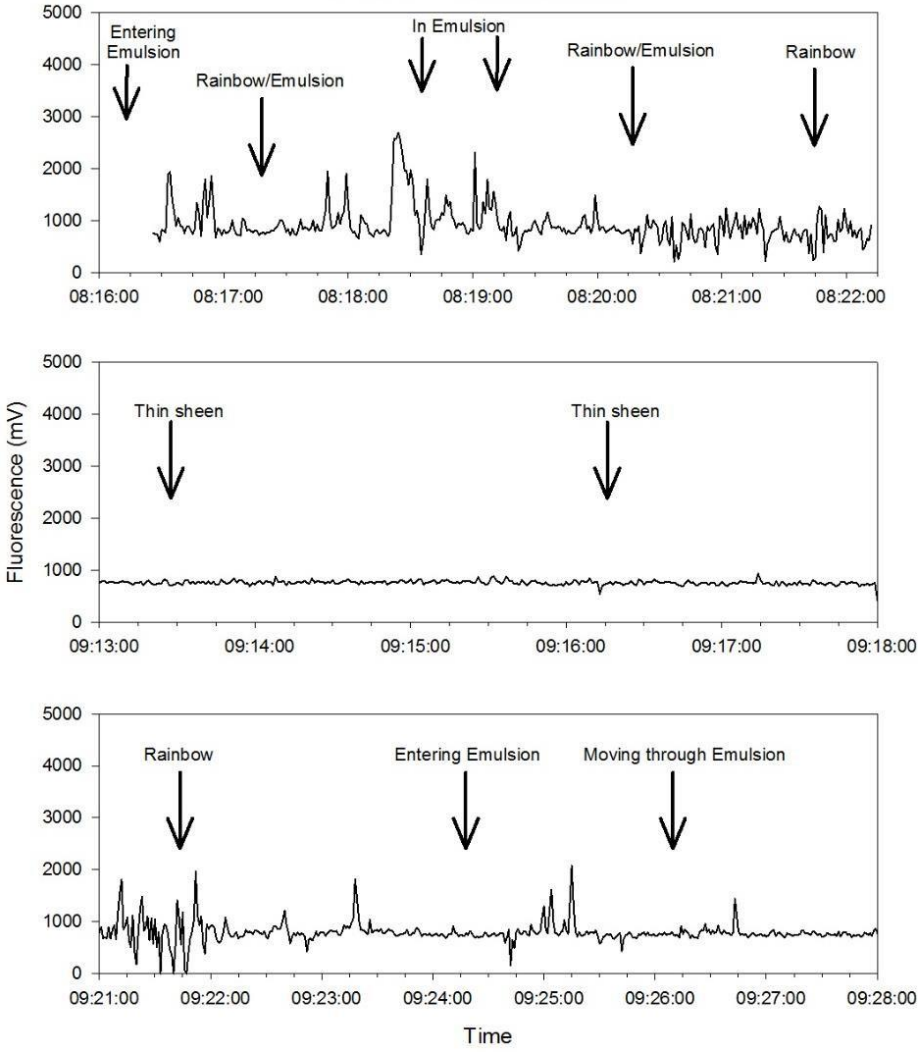

However, when looking at each site individually, while overall the slopes appeared the same, the different sites appeared to have different intercepts.

We hypothesize that this offset between the sites was due to differences in the background fluorescence at each site. To normalize for this difference, we subtracted a site-specific background fluorescence from each spot reading and refit the data. To estimate the site-specific background fluorescence, we used transect data from the site collected from outside the slick area. If this was not available, we used the fluorescence signal collected from 4 m or deeper.

After normalizing the fluorescence data for differences in background fluorescence, we obtained a considerably better fit between fluorescence and TPH concentration (Figure 3.40).

Figure 3.39. TPH concentration versus raw fluorescence signal from contemporaneous measurements. Black solid line represents the regressed trend line and blue solid lines show the 95% confidence intervals.

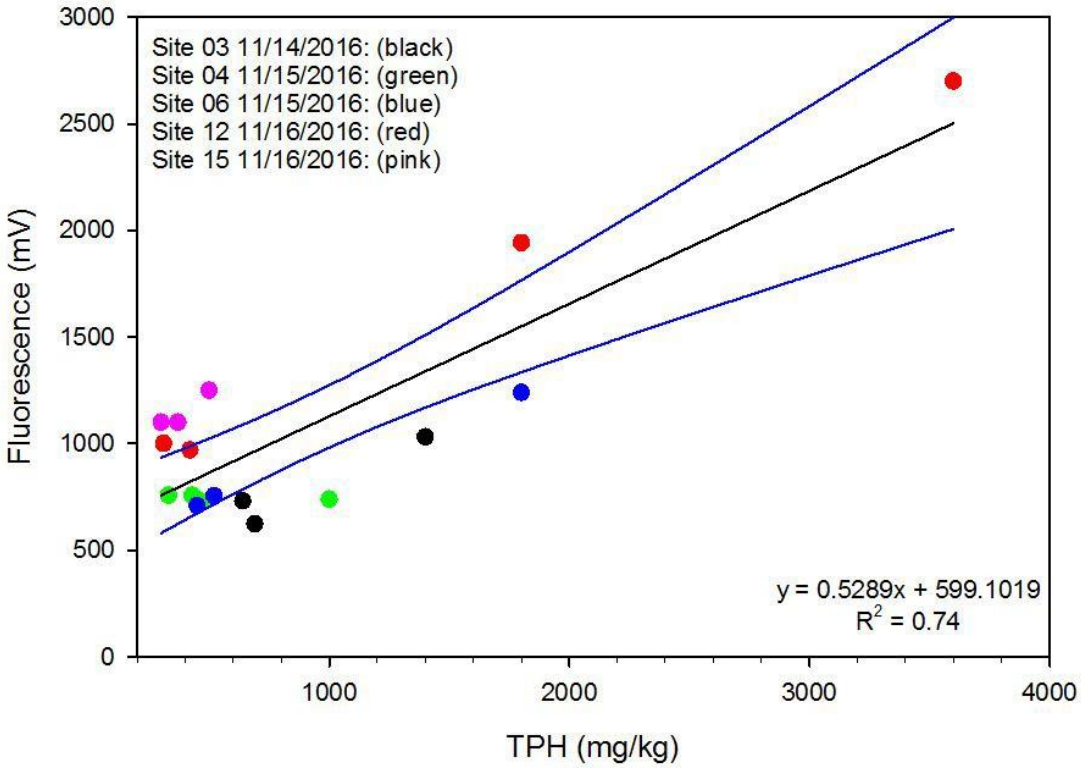

Figure 3.40. TPH concentration versus site-specific background subtracted fluorescence signal from contemporaneous measurements. Black solid line represents the regressed trend line and blue solid lines show the 95% confidence intervals.

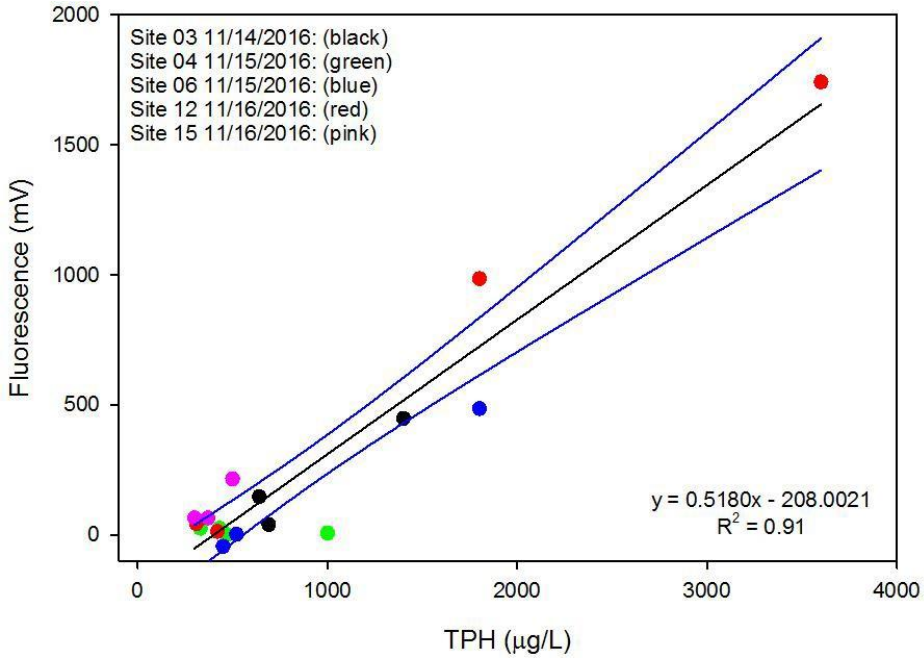

Figure 3.41. Fluorescence profiles and corresponding profiles of measured TPH concentrations (black dots) and TPH concentrations estimated from fluorescence (red triangles) for three sampling sites. Note the change in scale for Site 03.

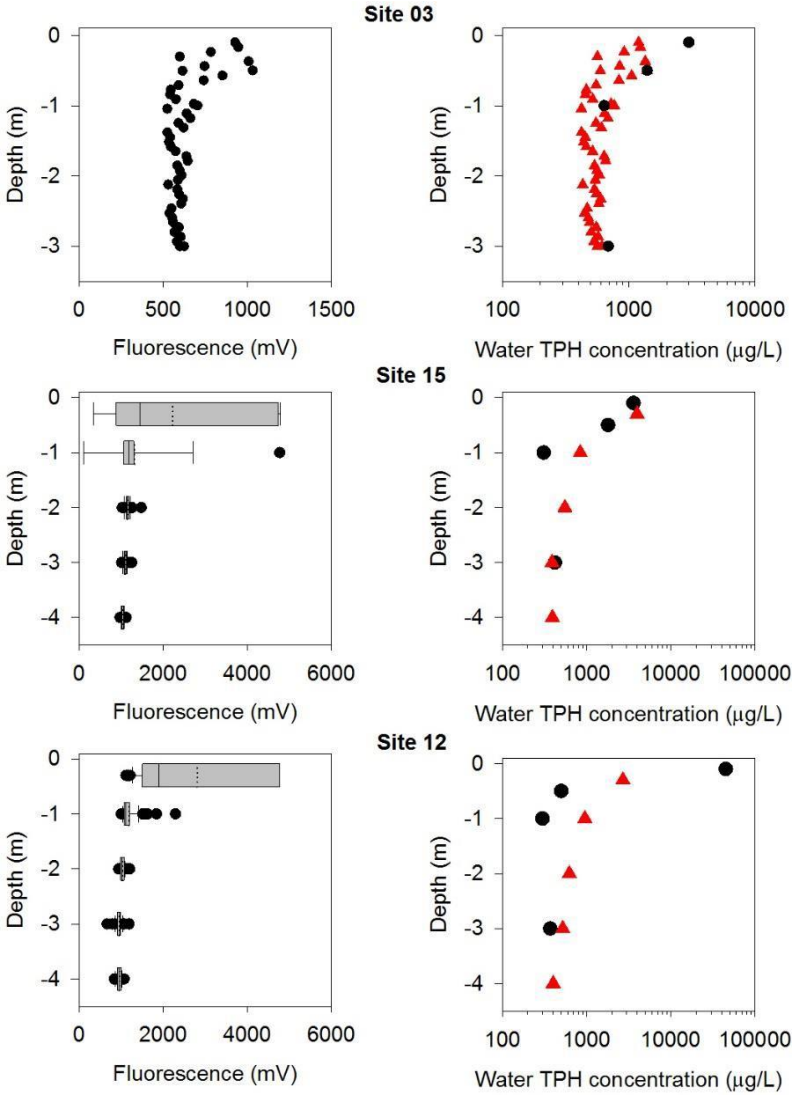

Figure 3.41 provides a comparison of the fluorescence profiles collected at a site with profiles of measured TPH concentrations. Using the regression in Figure 3.41, we also present TPH concentrations estimated from the average fluorescence at each depth. For all three sites, we found reasonable agreement between the measured TPH concentrations and the TPH concentrations estimated from fluorescence. Sites 12 and 15 from the November 2016 sampling trip were collected from the same general location, back to back, and capture the potential variability in a water profile collected under similar conditions.

Ultimately, our results show that fluorescence spectroscopy, paired with water sampling, can be a useful tool for estimating dispersed oil concentrations in the water column. Fluorescence spectroscopy also offers the added benefit of collecting continuous measurements, providing far greater spatial and temporal resolution of a dispersed oil plume than can be determined by

grab sampling alone. In addition, fluorescence data can provide real-time feedback on the presence of dispersed oil, which can be used to guide sampling efforts.

3.4.2 REMUS 100

The REMUS 100 measured fluorescence on programmed transects in August 2017. Data were collected at multiple depths. The data confirm that oil droplets and dissolved oil fluoresce, allowing field staff to identify and track the subsurface plume.

At the time of this writing, the REMUS data analyses were not completed. A draft presentation of REMUS 100 data is provided in Attachment N.

3.5 Air Sampling

3.5.1 HDS and PUF Samplers

During the November 2016 sampling trip, we conducted air sampling using HDS passive samplers for BTEX and active air pumping through PUF sorbent tubes for PAH. Overall the measured BTEX and PAH concentrations were relatively low. However, when compared to background concentrations, we saw elevated concentrations of BTEX at all oiled sites, and elevated PAH concentrations at two of the three oiled sites (Figure 3.42). We also found that concentrations were generally higher near the water surface and decreased rapidly with height at oiled sites (with the exception of an anomalous reading at Site 8), suggesting that the source of the contamination was at the water surface and that there was significant mixing within the air column near the water surface.

To avoid potential contamination due to fumes from a running boat motor, for all sites except Site 25, we turned the boat off and drifted during sample collection. However, since the boat drifted faster than the slick oil, it was a challenge to maintain our position within the slick. We found the boat would typically drift out of the slick area within minutes, which meant a majority of our 15-minute sample collection time was conducted over clean water. As a result, our measured air concentrations likely underestimated the actual air concentrations directly above the slick.

To address this problem, for Site 25, we used the boat to help maintain our position in the slick. At Site 25, BTEX concentrations were considerably higher (Figure 3.42). We did not see a corresponding increase in the TPAH16 concentrations, which were similar to the TPAH16 concentrations measured at Site 06. We investigated whether the motor exhaust may have contaminated the air samples at Site 25. However, a comparison of this site's BTEX composition to the BTEX composition from the other oiled sites where the motor was shut off suggests there was no contamination due to the boat's motor.

Another challenge we faced during air sampling was determining where to sample. Like the subsurface oil plumes, elevated air concentrations above slicks were seemingly heterogeneous (based on the UltraRAE data – see the following section). While this is not surprising, it means that air concentrations above slicks are difficult to characterize with a small number of grab samples. However, given the complexity and time needed to conduct air sampling, the number of samples is always going to be limited. Pairing data from a continuous monitor, like the UltraRAE, with discrete grab samples could help improve the spatial and temporal resolution of an air sampling program.

Figure 3.42. BTEX and total PAH based on 16 parent PAHs (TPAH16) at four sample sites in November 2016.

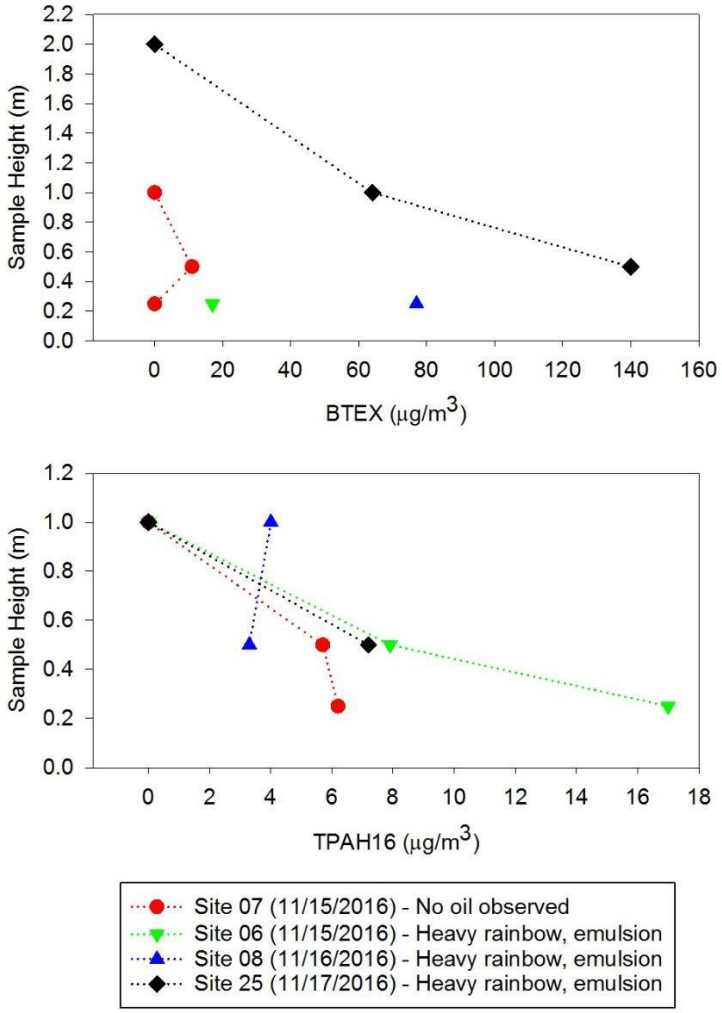

Finally, we lost several samples because of equipment malfunction and error, which left a number of data gaps and reduced data quality. While improved sampling design, such as better housing units for the HDS samplers and PUF air pumps, could address many of these problems, air sampling is ultimately complex and will likely require a concerted effort to further develop and significantly improve sampling logistics and success rates. However, our preliminary data indicate that the concentration of BTEX in the air just above an oil slick is likely a major data gap that cannot be adequately addressed by the typical air sampling conducted onboard a boat or research vessel that is often many meters above the water surface.

3.5.2 UltraRAE

On all three sampling trips, an UltraRAE VOC gas detector was onboard as part of the HSP to continuously monitor the VOC concentrations in the air. Figure 3.43 presents spot readings collected during the November 2016 sampling trip. When compared to the slick thickness data, we find that the highest, most-consistent VOC concentrations come from those sites with the thick oil (e.g., Site 06 and Site 04). However, thick oil does not necessarily equate to high VOC concentrations (e.g., Site 05).

Figure 3.43. Spot readings of VOC concentrations from the UltraRAE gas detector by site.
Grey bars show coincidental air sampling by HDS and PUF sorbent tube.

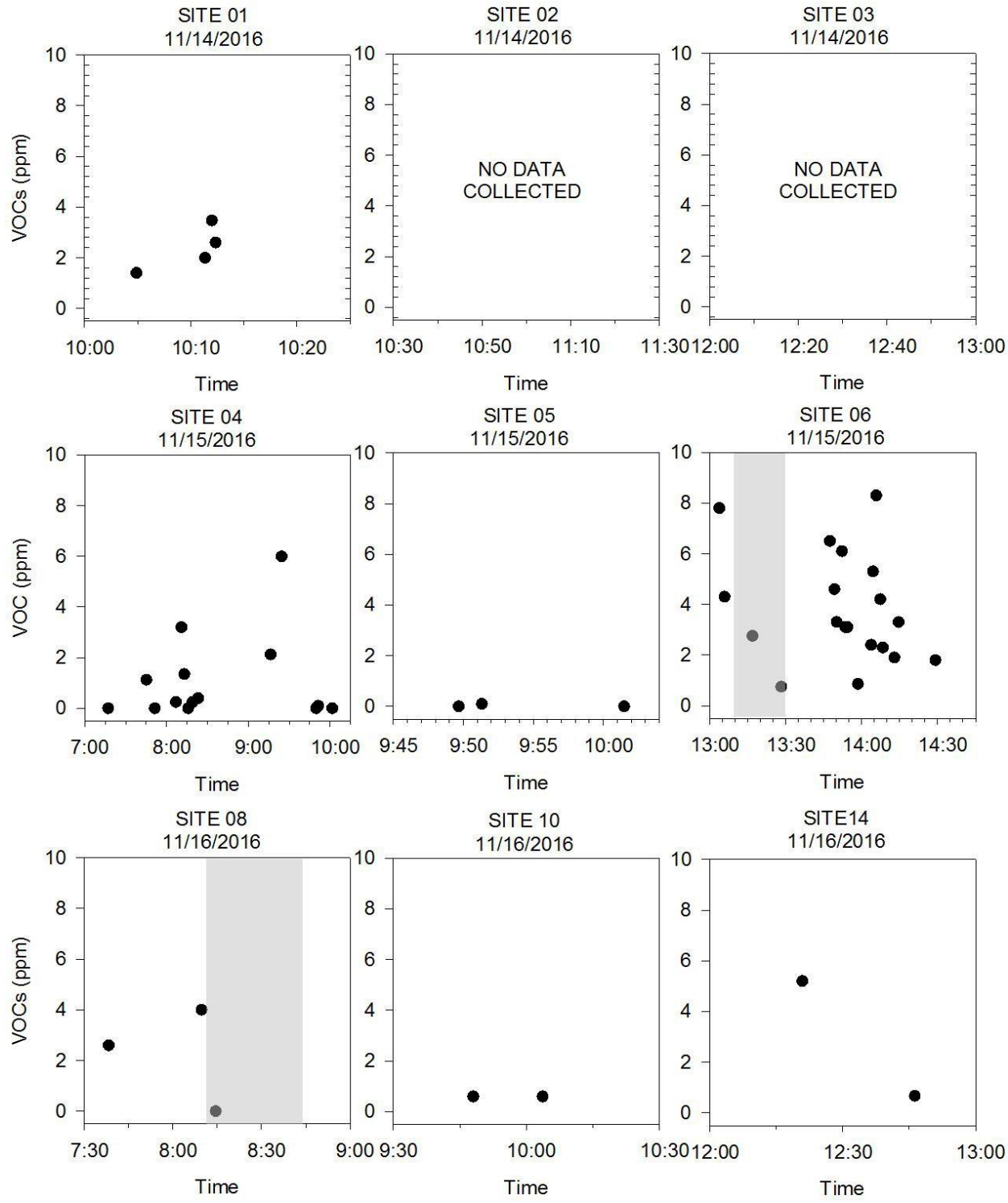

No spot readings were collected on November 17, 2016. Since recording spot readings from the UltraRAE monitor was not part of our original sampling plan, we did not record measurements on a regular schedule and instead tended to only capture measurements when the monitor alarm was sounding. The alarm sounded at 1 ppm, which is the Occupational Health and Safety Administration (OSHA) 8-hour exposure limit for benzene. Therefore, the lack of measurements on the last day is likely because the VOC concentrations were generally low, and thus the monitor alarm did not trigger us to collect measurements.

There are no UltraRAE data from the April 2017 sampling trip.

For the August 2017 sampling trip, we set up the UltraRAE to continuously log readings at 1-second intervals. Because of equipment malfunction, we did not record UltraRAE data for the first two days of the August 2017 sampling trip. For the last day (August 17, 2017), readings were generally low, with no readings above the OSHA 1 ppm total VOCs limit for a maximum 8-hour exposure. This was anticipated, given that the slick at MC20 was almost entirely light sheen at the time.

3.6 UV and Visible Light Penetration

During the April 2017 trip, we measured UV light penetration into the water column and calculated attenuation in an area outside of the oil slick. Offshore UV penetration into clear areas with blue water can often reach 25–30 m [Lay et al., 2015a; Bridges et al., In review (a)]. As noted previously, MC20 is close to the mouth of the Mississippi River, which can reduce water clarity compared to blue-water areas further offshore.

We used a specially designed protective housing to reduce oil exposure to the Biospherical radiometer used to measure light intensity. Although the lid on this housing was UV-transparent, it still attenuated some light. As a result, the measurements we collected were sufficient to estimate relative attenuation and changes in UV light under different scenarios during our trip, but the raw light intensity values cannot be directly compared to other data collected without this protective housing. Near MC20, the depth at which only 10% of the surface UV light (380 nm) was still present, the Z10 depth was approximately 1.4 m (Figure 3.44).

We also measured the Secchi disk depth at the same location where we measured this light profile in the water column. The Secchi depth at this site was 1.7 m.

In addition, we measured light penetration at a fixed depth as the boat was drifting from outside of the slick to within the slick over a 15-minute period beginning at 1:45 PM on April 25, 2017. We attached the radiometer to the side of the boat, which logged light intensity values every 0.2 seconds at depths that ranged from 1.3 to 1.5 m (Figure 3.45). The protective housing that enclosed the radiometer caused the meter to record some anomalous values due to shadows the housing created and other apparent interferences. Therefore, values for UV light (380 nm) displayed in Figure 3.45 are a subset of these data containing no anomalous values.

Figure 3.44. UV light (380 nm) penetration into the water column away from the MC20 surface slick on April 25, 2017, at approximately 11:30 a.m. The upper and lower asymptotes of this dataset were removed to estimate the UV light extinction coefficient [slope of this line (16.4)] and subsequent Z10 depth (1.4 m). This profile was measured down to a maximum depth of approximately 3 m.

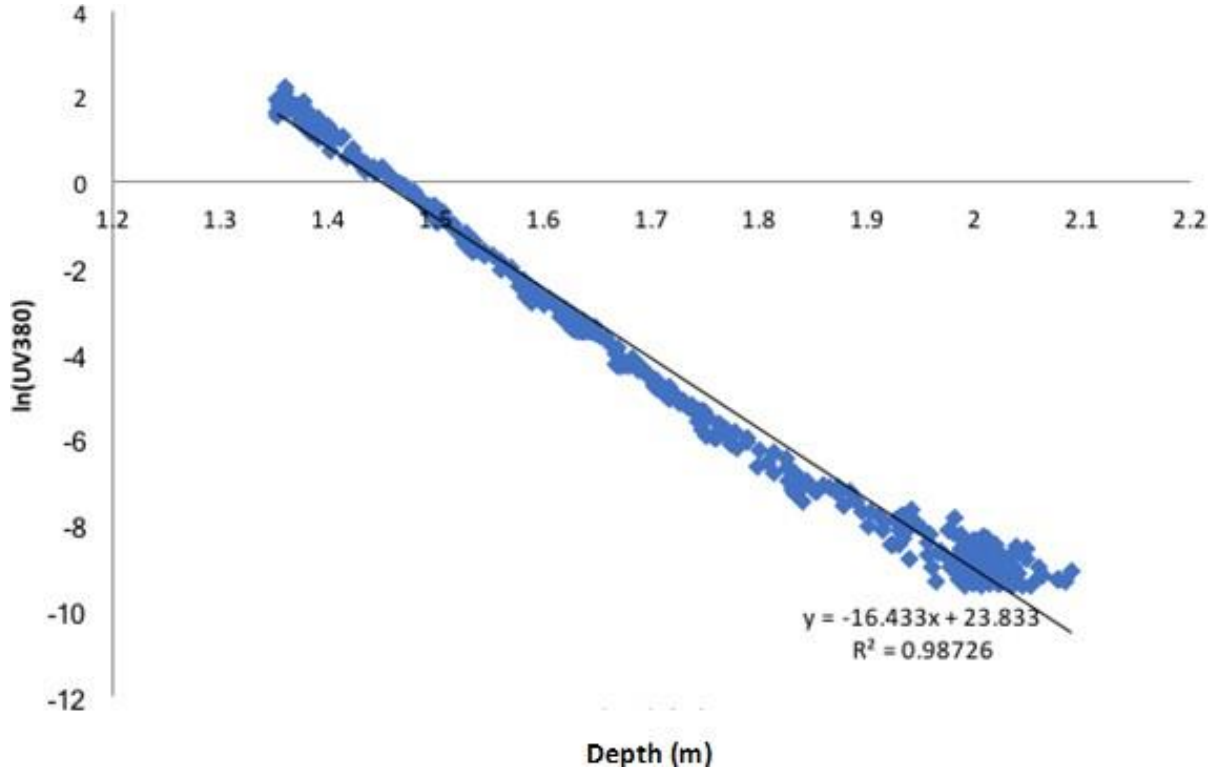

During the August 2017 trip, we used HOBO light sensors attached to our water sampling raft to measure light attenuation. These sensors measured light across a broad spectrum, between approximately 150 and 1,200 nm. We used these sensors to determine relative changes in light intensity just under surface slicks by comparing the data from one sensor that was out of the water on the top of our sampling raft to two additional sensors attached to arms extending out from either side of the raft to a depth of about 15 cm (Figure 3.46). The average light attenuation of the two submerged sensors at our reference site on August 15, 2017 was 59% of surface irradiation (i.e., 59% of the surface irradiation was no longer measured at a depth of 15 cm into the water column). We collected similar readings in areas with visible surface slicks at six locations on August 16 and three locations on August 17, 2017. The attenuation values at these sites ranged from 47% to 71% on August 16, and from 55% to 87% on August 17. Thus, at some slick sites, the attenuation was no different than at reference sites, and at some sites the attenuation was considerably higher.

Figure 3.45. UV light penetration to 1.3–1.5 m on April 25, 2017 beginning at 1:45 p.m. The Biospherical radiometer (submerged white container in photograph) measured light intensity at various wavelengths, while contained in a protective housing with a UV-transparent lid. The radiometer was deployed upwind of the surface slick and attached to the side of the boat at a fixed depth as the boat drifted into the slick. The photograph, showing the radiometer below the surface sheen, was taken approximately 10 minutes and 23 seconds into the drift (dashed vertical line on plot). Waypoint (WP) numbers are also shown on the plot to mark the beginning of the sheen and other observations regarding slick thickness or boat shadows that were observed during the transect. The protective housing caused shadows and other interferences; therefore the data presented here represent a trimmed subset that did not contain these anomalous values.

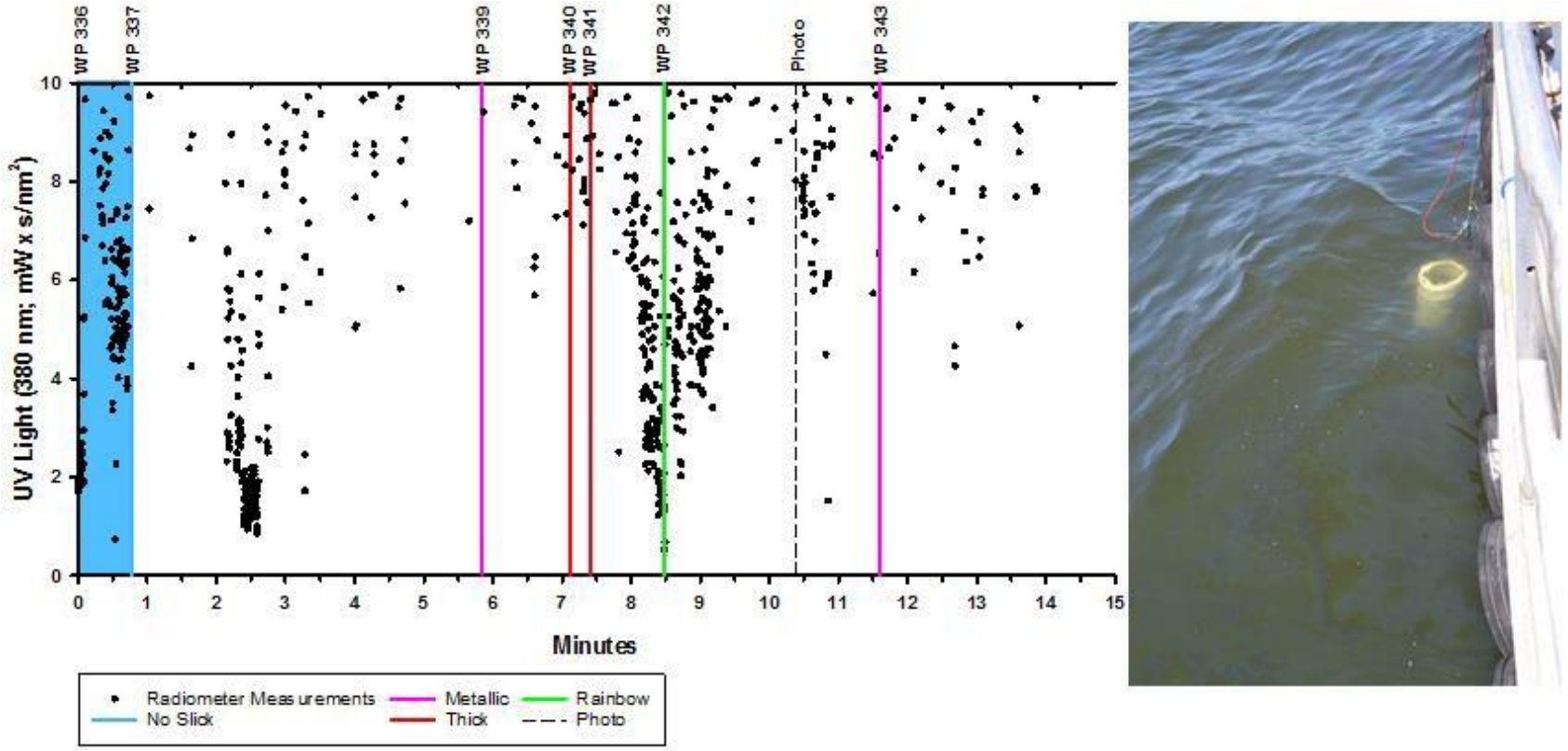

Figure 3.46. Water sampling raft deployed with HOBO light sensors at the reference site on August 15, 2017 (A) and a site with visible sheen on August 17, 2017 (B). The average light attenuation in the water at a depth of 15 cm at the reference site was 59%, and the average attenuation at the visibly oiled site was 87%.

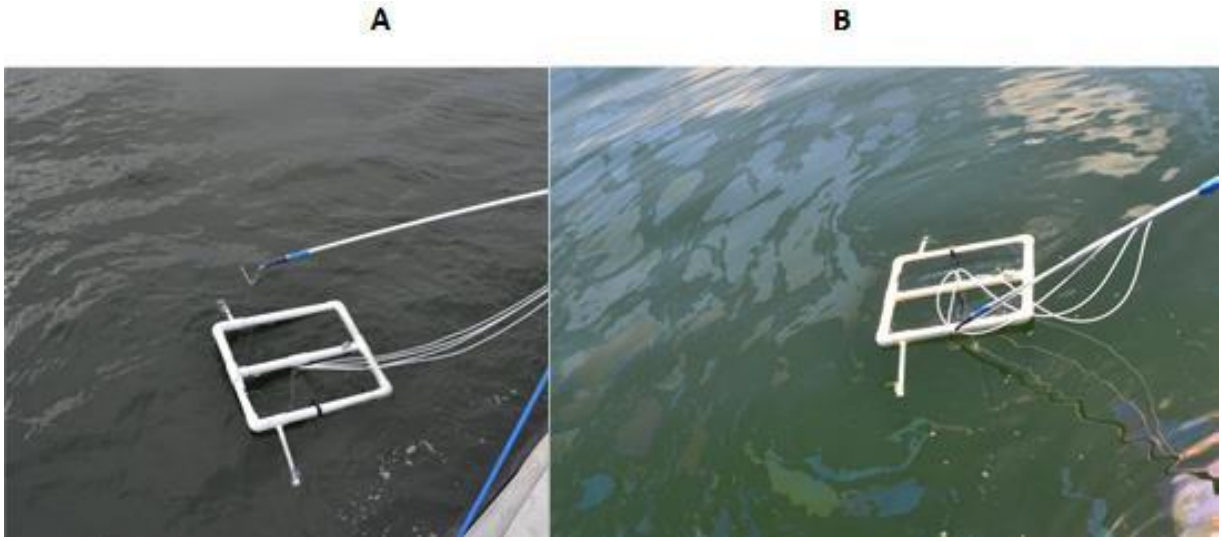

3.7 Datasonde

During the August 2017 trips we used a YSI EXO1 datasonde to collect water quality measurements (e.g., temperature, pH, conductivity, turbidity, dissolved oxygen) at various depths. These measurements generally coincided with water sample or surface slick collection activities.

We collected one profile at the reference area on August 15 (Figure 3.47) and from locations with visible surface oil on August 16 (three sites) and August 17 (three sites; for example, see Figure 3.48). Although we attempted to collect measurements during the April trip, the auto-logging feature of the sonde was not configured correctly and no field data were collected.

Although the data are uncalibrated and noisy, in general the water quality parameter changes with depth were similar between the reference areas and the control sites.

Figure 3.47. Water parameter profiles collected with the YSI datasonde from the reference area on August 15, 2017 at 3:05 p.m. The sonde recorded continuously as it was lowered to a depth of about 5 m and then brought back up to the surface.

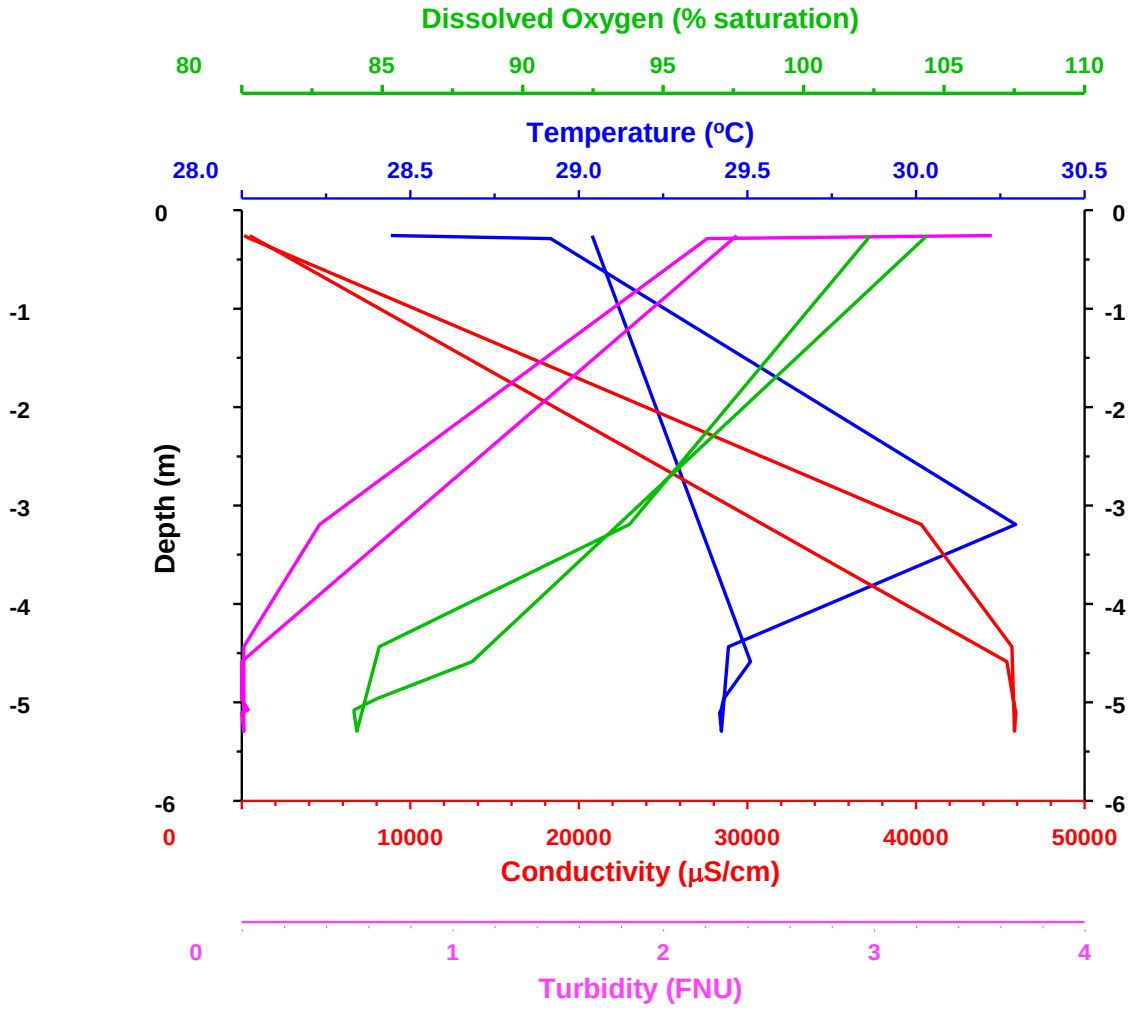

Figure 3.48. Water parameter profiles collected with the YSI datasonde near MC20 on August 17, 2017 at 12:26 p.m. The oil sheen is visible on the surface while a sorbent pad is used to collect oil at the same time. The sonde collected data continuously as it was lowered to a depth of about 17 m and then brought back to the surface.

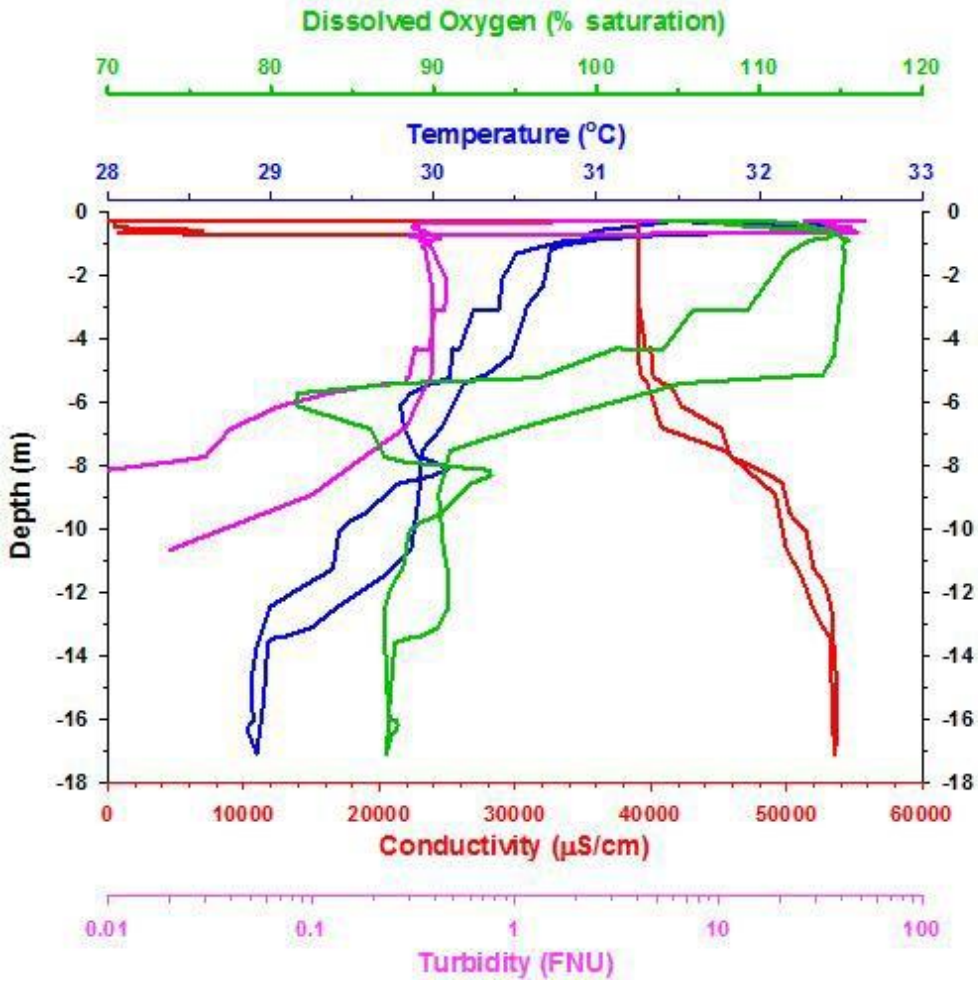

3.8 Toxicity

As discussed previously, the PAH composition of MC20 oil collected in November 2016 and April 2017 was very similar to the Slick A surface oil discharged from MC252 during the DWH spill (see Figure 3.33). Additionally, the percent depletion of TPAH51 (TPAH50 + perylene) relative to hopane was also similar for the three samples compared in Figure 3.33: DWH Slick A – 68% (e.g., Forth et al., 2017a); MC20 November 2016 – 69.4%; MC20 April 2017 – 72.0% (see Table 3.3).

Understanding the influence of UV light on toxicity is very important in habitats with UV exposure [Lay et al., 2015a; Bridges et al., In review (a)]. Exposure to UV light can increase the toxicity of oil by 10–100 times in WAF exposures [Lay et al., 2015b; Morris et al., 2015b; Alloy et al., 2017; Sweet et al., 2018; Damare et al., 2018; Bridges et al., In review (b)] as well as thin surface sheens (Morris et al., 2015a).

Not surprisingly, when larval mysid shrimp were exposed to MC20 and DWH Slick A oils and exposed to 8 hours of UV light (see Chapter 2), the photo-induced toxicity of the two oils were very similar. There was no significant difference, based on their overlapping 95% confidence intervals (CIs) of the lethal concentrations (LCs). The 24-hour LC20 and LC50 values[1] for the MC20 oil were 8.5 µg/L TPAH50 (95% CI: 6.13, 11.3) and 19.4 µg/L TPAH50 (95% CI: 15.3, 24.7), respectively (Figure 3.49A). Similarly, the 24-hour LC20 and LC50 values for the DWH Slick A oil were 7.7 µg/L TPAH50 (95% CI: 5.8, 9.9) and 15.5 µg/L TPAH50 (95% CI: 12.6, 19.1), respectively (Figure 3.49B).

These bioassays were conducted using HEWAFs prepared with either of the oils and exposure to eight hours of UV light in the laboratory. The integrated UV dose over eight hours was approximately 1,450 $mW \cdot s/cm^2$. This level of UV exposure is very similar to the average UV (380 nm) exposure in the Gulf of Mexico during the DWH spill [1,550 $mW \cdot s/cm^2$; Lay et al., 2015a; Bridges et al., In press (a)].

We also conducted exposures of larval mysid shrimp to control and high concentration HEWAF solutions without UV exposure. The TPAH50 concentrations for the MC20 and DWH Slick A HEWAFs were 101 and 110 µg/L, respectively. The 24-hour mean mortality rates (n = 5) in the control, MC20, and DWH Slick A HEWAF exposures without UV were 2.2%, 0%, and 4%, respectively. The 48-hour mean mortality rates in the control, MC20, and DWH Slick A HEWAF exposures without UV were 2.2%, 34%, and 16%, respectively. Thus, the toxicity of the MC20 oil was significantly higher ($p = 0.005$) than the DWH Slick A oil after 48-hour of exposure. However, unlike with photo-enhanced toxicity tests where effects often manifest within the first 24–48 hours, the toxicity of these HEWAFs in the absence of UV should be evaluated over a longer timeframe (e.g., 96 hours), with a range of exposure concentrations to determine the dose-response relationship and compare the relative toxicity between these two oils.

1. LC20 is the calculated concentration lethal to 20% of the organisms, and LC50 is the calculated dose lethal to 50% of the organisms.

Figure 3.49. Dose-response curves and LC20 and LC50 estimates for 24-hour bioassays conducted with larval (72 hours post-hatch) mysid shrimp. Shrimp were exposed to HEWAFs prepared using surface oil collected from MC20 in April 2017 (A) or DWH Slick A oil (Forth et al., 2017a, 2017b). These bioassays included an 8-hour exposure to UV light (380 nm) using indoor lighting that resulted in an integrated UV (380 nm) exposure of approximately 1,450 mW·s/cm^2.

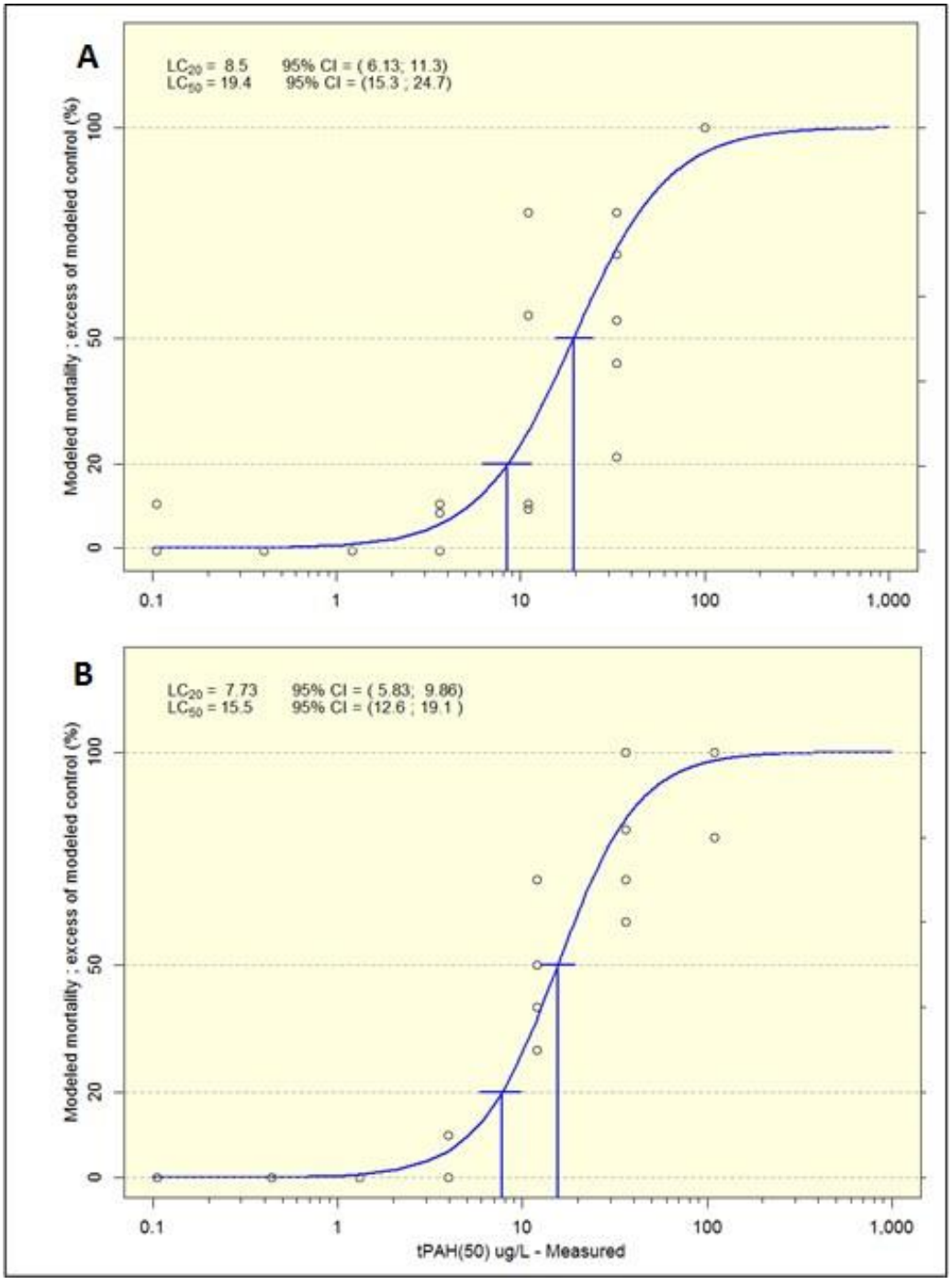

3.9 Other Data

NOAA has a comprehensive dataset of the work described herein. Data will be uploaded to ERMA (the NOAA COP) and/or DIVER, a NOAA data repository as most appropriate. These supplemental data include photographs and videos of field activities.

GoPro underwater videos are included in the supplemental dataset. The video camera was attached to the water sampling raft. Some videos show surface oil (Figure 3.50A) and subsurface oil droplets (Figures 3.50B and 3.51).

Figure 3.50. Surface oil (A) and subsurface oil droplets (B) taken with GoPro camera on April 25, 2017. These droplets were apparently being re-submerged due to wave action and did not have obvious gas bubbles associated with them. The thicker surface oil in A (white circles) is typical of the type of bulk oil sample we collected for chemical analysis and toxicity testing.

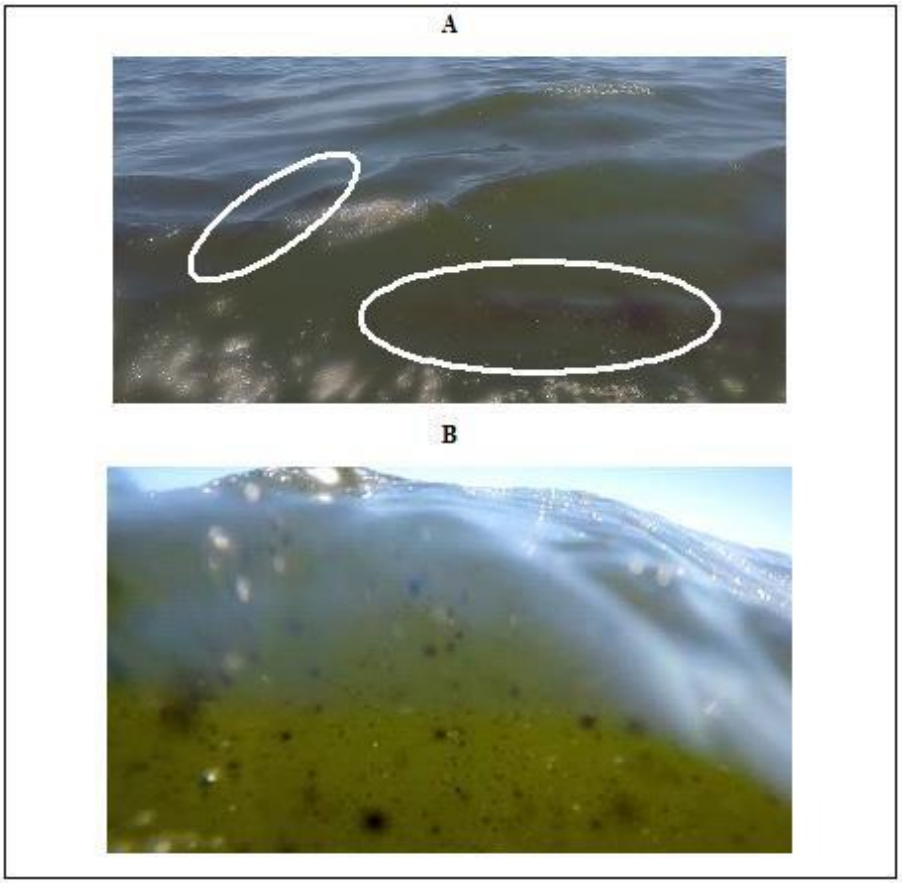

Figure 3.51. Frame from a GoPro video showing the underwater view of the water surface (looking up) from August 17, 2017 at approximately 12:15 p.m. near the source of the MC20 oil. Dark dots near the surface (e.g., red circle) are oil droplets attached to gas bubbles that were rising (e.g., black circle) to the surface where they floated around and eventually popped (e.g., white circle). Immediately after the droplets popped, they quickly expanded out into thinner slicks (rusty color). One of the subsurface HOBO light sensors attached to the water sampling raft is visible in the foreground. Surface conditions during this video were very calm and droplets were not being re-submerged as in the Figure 3.50.

4. Summary and Recommendations

Natural resource trustees, oil spill responders, and regulators all have need to identify and quantify oil slicks on the open ocean. Trustees assessing natural resource damages need to estimate the exposure of natural resources (including marine mammals, sea turtles, fish, flora, and other fauna). Responders need to identify "actionable" oil at the surface, or oil of sufficient quantity that responders can feasibly collect, burn, disperse, or otherwise reduce the amount of oil in the oil slick. Regulators need estimates of the quantity of oil released when addressing Clean Water Act penalties.

With methods developed at Ohmsett and USF, and implemented at MC20, we have taken great strides in expanding methods and tools for identifying and quantifying oil slicks in the open ocean. The "oil on water" group developed several innovative methods of analyzing remote sensing data, correlating satellite data covering a broad area of slick with low-altitude aircraft data that provided considerably greater detail over a small area of the slick. However, this group had no corresponding field data collected synoptically from a boat.

The studies described here help to fill that data gap, with synoptic data collected from below the ocean surface, on the ocean surface, a few hundred feet above the ocean surface (UAS), 1,000 to 6,000 ft above the ocean surface (fixed-wing aircraft), and from space. This provides oil slick information across many spatial scales.

As noted previously, all of the data collected in support of this project will be available in the NOAA Gulf of Mexico ERMA COP (https://erma.noaa.gov/gulfofmexico/erma.html) and/or DIVER (https://www.diver.orr.noaa.gov/). This data will be made publicly available upon official release by BSEE in the near future.

4.1 Data Summary

The following sections summarize the data collected and strengths and weaknesses of different methods employed as part of this research.

Remote Sensing

From the research discussed here, we conclude the following about the ability of specific sensors to detect and quantify oil:

- SAR satellite imagery can detect the spatial extent of the oil slick as well as detect areas of thick, emulsified oil.
- Post-processing of the Ocean Imaging data, combining TRACS reflectance and emissivity values with data collected synoptically from satellites and aboard the ship, provides a more defensible estimate of the quantity of oil at the ocean surface than was available for DWH.
- Post-processing of UAS data can provide a higher-resolution estimate of the quantity of oil over a small area.
- Visible satellite imagery can detect oil slicks during the day, when cloud cover and sun glint are minimal.

Remote sensing data continue to be important for assessing and quantifying an oil slick. Each of the sensors used in this research has advantages and disadvantages, depending on the spatial resolution, the overall size of the slick, and the cost of mobilization. The collection of ground-truth data provides critical validation to these systems. However, as noted previously, the oil thickness/volume data are variable and imprecise on any scale, including from a boat. Additional aerial, ground, and subsurface data will need to be acquired to address these challenges.

The approximate quantification of oil thickness and/or volume from remote sensing data can be accomplished with this extensive synoptic sampling of oil thickness, oil:water ratios, and other ground validation data. Remote sensing data provide invaluable threshold information, allowing responders and damage assessment professionals to prioritize operational decisions and assess natural resource damage to trust resources. However, a precise quantification of oil thickness and/or volume is currently beyond the reasonable expectations of remote sensing technologies.

Sensor Comparison

Most of the sensors evaluated in this study detected reflectance/emissivity anomalies that were consistent with each other and with ground verification measurements collected from the boat. SAR and multi-spectral sensor data collected synoptically with in situ samples generally agree and support the use of multiple remote sensing platforms in the absence of control data. While the use of remote sensing data without ground-truthing can provide excellent relative thresholding information, these data must be used with caution. They are excellent for risk-based, operational decision-making (such as identifying actionable oil), but they provide only relative quantification information. Given the three-dimensional heterogeneity of oil slicks, aerial remote sensing data currently provide only one piece of the oil volume equation.

In Situ Oil Thickness Measurements

Measuring oil thickness from a ship helps to calibrate remote sensing data. However, oil is inherently heterogeneous on any scale, and thus many thickness samples are required to provide the range of oil thicknesses over a given area. The three methods tested as part of this research have different advantages and disadvantages:

- The dip plate method of measuring thickness is fast and inexpensive; however, the method has a limited range of thicknesses for which it is accurate.
- The sorbent pad method of measuring thickness provides the most accurate estimate of slick thickness for thin sheens. It is less accurate in thicker oil, and the need for laboratory analysis of the pads makes it relatively slow and expensive to obtain data.
- The Water Mapping method is the most accurate of the three methods. However, sampling using this method is time-consuming, as the sampler can collect only one sample covering a small area, and each sample requires the addition of a solvent, a photograph in a laboratory setting, and a manual pixel-based measurement to estimate thickness.

Despite the drawbacks of oil thickness measurement methods, the information gathered from this activity is an important step in ground-truthing the remote sensing data.

Subsurface Oil

- Oil at MC20 is not entirely at the ocean surface. Underwater camera imagery and fluorescence data from boat-based instruments and the REMUS 100 detected numerous subsurface oil droplets.
- This research confirmed that windy days (such as in November 2016) produce waves that mix surface oil several meters below the ocean surface. In addition, on calm days (such as in August 2017), oil droplets encased in gas bubbles often remain just below the ocean surface for some period of time, before the bubbles burst and the oil becomes a surface slick.
- UV light attenuates faster under oil slicks. This is important for estimating potential photo- induced toxicity.

Quantifying subsurface oil is important both for estimating the exposure of natural resources such as fish that are below the ocean surface, and for quantifying the total volume of oil released into the ocean.

Toxicity Testing

- The result of this research demonstrated consistent toxicity between oil discharged from MC252 during the DWH spill and oil discharged from MC20.

Establishing the toxicity of the oil is an important step in assessing potential natural resource injuries and damages.

4.2 Tools Developed

The research presented in this report has led to the development of many new tools that will assist oil spill responders, NRDA practitioners, and regulators with the assessment of oil slicks. Here we present a list of the some of these tools and their importance.

NRT Data Transmission and Data Services

One of the issues that plagued the DWH oil spill response and NRDA community was the lag time providing data to Incident Command, and the lack of data dissemination to the broader community. With the work conducted as part of this study, we have developed methods for NRT communications between remote sensing experts and the boat crew collecting samples for field verification, and we have developed new methods of providing data services to ERMA, NOAA's COP. Specific examples include the following:

- The crew on the boat successfully tested multiple methods of transmitting and receiving data via the Internet while at sea in the northern Gulf of Mexico. Affordable and practical Internet connectivity from a small vessel on the ocean is important because it allows the crew to download imagery collected from above, and it allows the crew to upload NRT data to the COP.

- MDA successfully introduced a new data service that provides an initial estimate of oil slick extent in SAR imagery within 45 minutes of data collection; during DWH, the SAR imagery was often not available until the following day.
- Ocean Imaging successfully developed methods of creating draft mosaics of visible oil and thicker oil while still flying, stitching images collected with their TRACS sensor mounted to a fixed-wing aircraft at low altitude. They also successfully sent the data directly to researchers on the boat while the plane was overhead, with no Internet connection required.
- Dr. Garcia of Water Mapping successfully collected real-time visible and thermal IR imagery from a UAS launched from the boat in the open ocean. This data are highly useful for guiding the ship to areas with the thickest oil, ensuring that the researchers on the boat quantify oil thickness and chemistry in the most heavily oiled areas.

Remote Sensing Analysis

This research is leading to the development of new tools for analyzing remote sensing data. After refining his TCNNA and OEDA algorithms for the semi-supervised classification of SAR imagery to determine slick extent and emulsions (respectively), Dr. Garcia has developed a toolkit (Attachment G) that allows other researchers, such as those at the NOAA NESDIS, to implement these algorithms. His toolkit includes tools for the enhanced analysis of oil in visible satellite imagery as well.

Slick Thickness

The research at Ohmsett, USF, and MC20 all led to refinement of the collection and analysis of slick thickness for three separate methods. The sorbent pad method is the likely tool of choice for measuring the thickness of thinner sheens, which the other methods do not measure well. The dip plate method is the tool of choice for slicks that are approximately 10- to 1,000-µm thick, when collecting many samples quickly and inexpensively is more important than precision. The Water Mapping method is still in development; once completed, this device will be another tool that responders can use for measuring thickness with more accuracy and precision than the other two methods.

Subsurface Oil

As noted previously, this research demonstrated that a substantial portion of an oil slick is below the sea surface, particularly if winds are creating wave action that mixes the oil to depth. Basic tools for recording this phenomenon include waterproof underwater cameras such as a GoPro.
More advanced tools include boat-mounted fluorometers such as the Cyclops-7 and UAV-mounted fluorometers such as the one on REMUS 100. Although further development of these tools is necessary to quantify subsurface oil, the work presented in this research shows the promise of these developing tools.

UV Attenuation

The Hobo light meter provides a simple and inexpensive method for collecting UV light attenuation data, which are important for determining the toxicity of the subsurface oil. These

meters can be added to the toolkit of oil spills responders and NRDA scientists on boats; deployment is easy, and the devices log their own data.

4.3 Recommendations for Future Work

Future research can further improve the tools and methods for quantifying oil slicks. One recommendation is to attempt additional collections at MC20 at times when more emulsified oil is present, and/or collect samples at other known oil slick locations such as Santa Barbara, California.

The oil slicks at MC20 are highly variable. On some occasions, there is a large quantity of oil with heavy emulsions. At other times, such as in August 2017, the slick is almost entirely sheen, and bulk oil samples cannot be collected. The interpretation of remote sensing data would benefit from additional bulk oil samples and quantification of the oil:water ratios to help discern the quantity of oil on the surface.

The close examination of oil slicks in the laboratory, in a tank, and in the open ocean showed the highly heterogeneous nature of these slicks. Future research for quantifying average slick thickness (or oil volume per unit area) could focus on methods that allow researchers to collect and analyze many samples in a short timeframe. Multiple samples with less precision may be preferable to a small number of precise samples over a very confined area.

As noted previously, this research demonstrated the importance of subsurface oil slicks. Future research could include the development of additional methods, models, and devices that can help to quantify the subsurface oil quantity and PAH concentrations. UAVs with fluorometers can help provide a three-dimensional image of a rising plume of gas and oil droplets. Subsurface photography can help to quantify oil immediately below the ocean surface (oil that generally is not detected with remote sensors). Methods of collecting and analyzing data over a spill area need additional development.

Finally, this research demonstrated the ability to collect oil samples from the field and rapidly set up tests to demonstrate the potential toxicity of the oil. Future research could include the development of a toxicity assessment toolkit, including potentially running in situ toxicity tests in the open ocean, and developing methods for rapidly scaling up laboratory toxicity tests using site-collected oil and water shortly after collection.

References

Alloy, M., T.R. Garner, K. Bridges, C. Mansfield, M. Carney, H. Forth, M. Krasnec, C. Lay, R. Takeshita, J. Morris, S. Bonnot, J. Oris, and A. Roberts. 2017. Co-exposure to sunlight enhances the toxicity of naturally weathered *Deepwater Horizon* oil to early lifestage red drum (*Sciaenops ocellatus*) and speckled seatrout (*Cynoscion nebulosus*). *Environmental Toxicology and Chemistry* 36(3):780–785.

Bolker, B. and R Development Core Team. 2013. bbmle: Tools for General Maximum Likelihood Estimation. R package version 1.0.15. Available: http://CRAN.R-project.org/package=bbmle. Accessed 3/13/2018.

Bonn Agreement. 2009. Bonn Agreement Aerial Operations Handbook, 2009. Part 1: General. Available: https://www.bonnagreement.org/site/assets/files/1081/ba-aoh_revision_2_april_2012- 1.pdf. Accessed 3/13/2018.

Bridges, K., C.R. Lay, M.M. Alloy, M.L. Gielazyn, J.M. Morris, H.P. Forth, R. Takeshita, C. Travers, J.T. Oris, and A.P. Roberts. Estimating incident ultraviolet (UV) radiation exposure in the Northern Gulf of Mexico during the *Deepwater Horizon* oil spill. In review (a).

Bridges, K., M. Krasnec, J.T. Magnuson. J.M. Morris, M.L. Gielazyn, J.R. Chavez, and A.P. Roberts. Influence of UV and PAH exposure duration on survival of red drum (*Sciaenops ocellatus*) larvae. In review (b).

Cheemalapati, S., H.P. Forth, H. Wang, K.R. Konnaiyan, J.M. Morris, and A.L. Pyayt. 2017. Measurement of thickness of highly inhomogeneous crude oil slicks. *Applied Optics* 56(11): E72–E76.

Conmy, R.N., P.G. Coble, J. Farr, A.M. Wood, K. Lee, W.S. Pegau, I.D. Walsh, C.R. Koch, M.I. Abercrombie, M.S. Miles, and M.R. Lewis. 2014. Submersible optical sensors exposed to chemically dispersed crude oil: Wave tank simulations for improved oil spill monitoring. *Environmental Science & Technology* 48(3):1803–1810.

Daling, P.S. and F. Leirvik. 2002. BONNEX 2002, June 17th–19th: Oil Film Thickness Measurements and Pictures Taken from Sampling Boats – Data Report. SINTEF Report # STF66 F02084.

Damare, L., K. Bridges, T. Curran, B. Soulen, M. Alloy, H. Forth, C. Lay, J. Morris, J. Stoeckel, and A. Roberts. 2018. Photo-induced toxicity in early life stage fiddler crab (*Uca longisignalis*) following exposure to *Deepwater Horizon* oil. *Ecotoxicology*. In press. doi: 10.1007/s10646-018- 1908-6.

Delvigne, G.A.L. and C.E. Sweeney. 1988. Natural dispersion of oil. *Oil and Chemical Pollution* (4):281–310.

DWH Trustees. 2016. *Deepwater Horizon* Oil Spill: Final Programmatic Damage Assessment and Restoration Plan and Final Programmatic Environmental Impact Statement. Available: http://www.gulfspillrestoration.noaa.gov/restoration-planning/gulf-plan. Accessed 3/13/2018.

Faraggi, D., P. Izikson, and B. Reiser. 2003. Confidence intervals for the 50 per cent response dose. *Statistics in Medicine* 22:1977–1988.

Forth, H.P., C.L. Mitchelmore, J.M. Morris, and J. Lipton. 2017a. Characterization of oil and water accommodated fractions used to conduct aquatic toxicity testing in support of the *Deepwater Horizon* oil spill natural resource damage assessment. *Environmental Toxicology and Chemistry* 36(6):1450–1459.

Forth, H.P., C.L. Mitchelmore, J.M. Morris, C.R. Lay, and J. Lipton. 2017b. Characterization of dissolved and particulate phases of water accommodated fractions used to conduct aquatic toxicity testing in support of the *Deepwater H*orizon natural resource damage assessment. *Environmental Toxicology and Chemistry* 36(6):1460–1472.

Fototerra. 2016a. Draft Report (Ohmsett Test). Prepared by Fototerra Aerial Survey LLC, Richmond, TX. August 2.

Fototerra. 2016b. Taylor Energy Site – Offshore Oil Spill Remote Sensing Test. Preliminary Report. Prepared by Fototerra Aerial Survey LLC, Richmond, TX. December 1.

Fototerra. 2017a. Taylor Energy Site 2nd Campaign – Offshore Oil Spill Remote Sensing Test. Preliminary Report. Prepared by Fototerra Aerial Survey LLC, Richmond, TX. May 2.

Fototerra. 2017b. Taylor Energy Site 3rd Campaign – Offshore Oil Spill Remote Sensing Test. Preliminary Report. Prepared by Fototerra Aerial Survey LLC, Richmond, TX. September 12.

Garcia-Pineda, O., B. Zimmer, M. Howard, W. Pichel, X. Li, and I.R. MacDonald. 2009. Using SAR images to delineate ocean oil slicks with a texture-classifying neural network algorithm (TCNNA). *Canadian Journal of Remote Sensing* 35(5): 411-421. doi: 10.5589/m09-035.

Garcia-Pineda, O., I.R. MacDonald, C. Hu, J. Svejkovsky, M. Hess, D. Dukhovskoy, and T. Moorey. 2014. Detection and mapping of floating oil emulsions with synthetic aperture radar. *Oceanography* 26(2):124–137.

Jones, C., B. Holt, and B. Minchew. 2012. *Deepwater Horizon* Oil Slick Characterization with UAVSAR. Presented at SPIE Remote Sensing 2012. Available: https://trs.jpl.nasa.gov/bitstream/handle/2014/43103/12-4512.pdf. Accessed 3/5/2018.

Jones, C.E., B. Minchew, B. Holt, and S. Hensley. 2011. Studies of the *Deepwater Horizon* oil spill with the UAVSAR radar. In *Monitoring and Modeling the Deepwater Horizon Oil Spill: A Record Breaking Enterprise*, Y. Liu, A. MacFadyen, Z-G. Ji, and R.H. Weisbery (eds.). Geophysical Monograph Series 195. American Geophysical Union. pp. 33–50.

Lay, C.R., J.M. Morris, R. Takeshita, H.P. Forth, C.L. Travers, A.P. Roberts, M. Alloy, T.R. Garner, and K. Bridges. 2015a. Incident Ultraviolet (UV) Radiation and Extinction Coefficients in the Northern Gulf of Mexico during the *Deepwater Horizon* Oil Spill. Technical Report. Prepared by Abt Associates, Boulder, CO and University of North Texas, Denton, TX, for National Oceanic and Atmospheric Administration Assessment and Restoration Division, Seattle, WA. December 16. Available: in Section 5.12.2 Technical Reports: https://www.doi.gov/deepwaterhorizon/adminrecord.

Lay, C.R., J.M. Morris, R. Takeshita, H.P. Forth, C.L. Travers, A.P. Roberts, M. Alloy, T.R. Garner, and C. Overturf. 2015b. The Effect of Ultraviolet (UV) Radiation on the Toxicity of *Deepwater Horizon* Oil. Technical Report. Prepared by Abt Associates, Boulder, CO and University of North Texas, Denton, TX, for National Oceanic and Atmospheric Administration Assessment and Restoration Division, Seattle, WA. December 16. Available: in Section 5.12.2 Technical Reports: https://www.doi.gov/deepwaterhorizon/adminrecord.

Leifer, I., W.J. Lehr, D. Simecek-Beatty, E. Bradley, R. Clark, P. Dennison, Y. Hu, S. Matheson, C.E. Jones, B. Holt, M. Reif, M., D.A. Roberts, J. Svejkovsky, G. Swayze, and J. Wozencraft. 2012. State of the art satellite and airborne marine oil spill remote sensing: Application to the BP

Deepwater Horizon oil spill. *Remote Sensing of Environment* 124:185–209. doi: 10.1016/j.rse.2012.03.024.

Lichtenthaler, R.G. and P.S. Daling. 1985. February. Aerial application of dispersants – comparison of slick behavior of chemically treated versus non-treated slicks. In *International Oil Spill Conference 1985.* American Petroleum Institute. pp. 471–478.

Minchew, B., C.E. Jones, and B. Holt. 2012. Polarimetric analysis of backscatter from the *Deepwater Horizon* oil spill using L-band synthetic aperture radar. IEEE Transactions on Geoscience and Remote Sensing 50(10):3812–3830.

Morris, J.M., H.P. Forth, C.R. Lay, R. Takeshita, and J. Lipton. 2015a. Toxicity of Thin Floating Oil Slicks to Fish and Invertebrates. Technical Report. Prepared by Abt Associates, Boulder, CO, for National Oceanic and Atmospheric Administration Assessment and Restoration Division, Seattle, WA. August 31. Available: in Section 5.12.2 Technical Reports: https://www.doi.gov/deepwaterhorizon/adminrecord.

Morris, J.M., M.O. Krasnec, M.W. Carney, H.P. Forth, C.R. Lay, I. Lipton, A.K. McFadden, R. Takeshita, D. Cacela, J.V. Holmes, and J. Lipton. 2015b. *Deepwater Horizon* Oil Spill Natural Resource Damage Assessment Comprehensive Toxicity Testing Program: Overview, Methods, and Results. Technical Report. Prepared by Abt Associates, Boulder, CO, for National Oceanic and Atmospheric Administration Assessment and Restoration Division, Seattle, WA. December 16. Available in Section 5.12.2 Technical Reports: https://www.doi.gov/deepwaterhorizon/adminrecord.

Nichols, C.L.D., T.R. Garner, M.M. Alloy, K.N. Bridges, B.K., Soulen, J.L. Gnau, A.M. Wormington, L.E. Sweet, J.M. Morris, and A.P. Roberts. Factors affecting photo-induced toxicity in mysid shrimp (*Americamysis bahia*) with oil collected from the *Deepwater Horizon* spill. In prep.

Ocean Imaging. 2016. *Deepwater Horizon* Lessons Learned Studies: Detection of Oil Thickness and Emulsion Mixtures Using Remote Sensing Platforms. Phase 1 Report. Prepared for Abt Associates Inc. and National Oceanic and Atmospheric Administration. Ocean Imaging Corp., Littleton, CO November 23.

Ocean Imaging. 2017. *Deepwater Horizon* Lessons Learned Studies: Detection of Oil Thickness and Emulsion Mixtures Using Remote Sensing Platforms. Final Report. Prepared for Abt Associates Inc. and National Oceanic and Atmospheric Administration. Ocean Imaging Corp., Littleton, CO. August 30.

Parker, H.D. and D. Cormack. 1979. Evaluation of Infrared Line Scan (IRLS) and Side-looking Airborne Radar (SLAR) over Controlled Oil Spills in the North Sea. Report No. LR 315 (OP). Warren Spring Laboratory, Stevenage.

Ritz, C. 2010. Toward a unified approach to dose – response modeling in ecotoxicology. *Environmental Toxicology and Chemistry* 29(1):220–229.

Ritz, C. and J.C. Streibig. 2005. Bioassay analysis using R. *Journal of Statistical Software* 12(5).

Robbe, N. and T. Hengstermann. 2006. Remote sensing of marine oil spills from airborne platforms using multi-sensor systems. In A. Brebbia and J.S. Antunes do Carmo (eds.), *Water Pollution VIII: Modelling, Monitoring and Management*. *WIT Transactions on Ecology and the Environment.*

Svejkovsky, J. and J. Muskat. 2006. Real-Time Detection of Oil Slick Thickness Patterns with a Portable Multispectral Sensor. Minerals Management Service, Final Report for Project #0105CT39144.

Sweet, L.E., A.T. Revill, J. Strzelecki, S.E. Hook, J.M. Morris, and A.P. Roberts. 2018. Photo- induced toxicity following exposure to crude oil and ultraviolet radiation in two Australian fishes. *Environmental Toxicology and Chemistry*. In press. doi: 10.1002/etc.4083.

U.S. EPA. 2013. Benchmark Dose Software (BMDS). Version 2.4 R70 [Build: 04/01/2013]. U.S. Environmental Protection Agency, National Center for Environmental Assessment. Available: http://www.epa.gov/NCEA/bmds/index.html. Accessed 3/7/2018.

Venzon, D.J. and S.H. Moolgavkar. 1988. A method for computing profile-likelihood-based confidence intervals. *Applied Statistics* 37:87–94.

Water Mapping. 2017. *Deepwater Horizon* (DWH) Lessons Learned Studies: Detection of Oil Thickness and Emulsion Mixtures Using Remote Sensing Platforms. Interim Technical Report for Abt Associates. Revised July 31. Water Mapping LLC, Gulf Breeze, FL.